Development of enhanced techniques for aerodynamic monitoring using pressure-sensitive-paint (PSP)

A dissertation submitted for the degree of
Doctor of Philosophy

by

Jan Hradil
M.S. (Charles University, Prague)

Supervisors: Prof. Brian MacCraith
Dr. Colette McDonagh
School of Physical Sciences
Dublin City University
Dublin, Ireland

July 2005

I hereby certify that this material, which I now submit for assessment on the programme of study leading to the award of *Doctor of Philosophy* is entirely my own work and has not been taken from the work of others save and to the extent that such work has been cited and acknowledged within the text of my work.

Signed: .....

ID No.: 50152624

Date: 18. 7. 2005

Contents

Chapter 1

Introduction and theoretical background

1.1 Introduction to pressure-sensitive paint (PSP) measurements

1.1.1 Current techniques for aerodynamical testing

Aerodynamical testing, which is carried out in order to improve the design of aircraft and automotive vehicles, is traditionally performed on specially prepared scale models in wind tunnels. This involves making air pressure measurements across the surface. Pressure measurements are taken from hundreds or even thousands of points, called pressure taps, located at the surface. From each pressure tap a small pipe runs from the inside of the model to the manometer(s) located outside of the wind tunnel, where the actual reading is taken. The production of models is very expensive and the test surface is not continuous due to the presence of the taps. Furthermore, the rigidity of the model is affected. Alternatively pressure can be registered by a series of pressure transducers attached to the surface of the model.

Both methods require modification of the surface, which, on its own can change airflow properties above the surface, especially at subsonic and transonic speeds (Mach numbers $M < 1$ and $M > 1$, respectively, see table 1.1). To avoid this, the number of measured points is a compromise between the required accuracy (density of readings) and the impact on the aerodynamics.

With rapid improvements in Computational Fluid Dynamics (CFD), the need for accurate and detailed pressure data has become even more urgent so that new codes can be adequately verified and tested before they are used in the design processes. Conventional

Test regime	**Mach no.**	**speed** [m/s]	α †	β ‡	**# of pts**
Low speed/high lift	0.1 – 0.5	30 – 150	$-10°$ .. $40°$	$\pm 30°$	10–12 000
Transonic	0.3 – 1.2	100 – 350	$-10°$ .. $20°$	$\pm 20°$	15–40 000
Supersonic	1.2 – 3.0	350 – 1000	$-5°$ .. $15°$	$\pm 8°$	5–10 000

† α is angle of attack, defined as angle between airfoil and relative wind speed.
‡ β is slip angle or sideslip, defined as angle between the leading edge and normal to relative wind speed.

Table 1.1: Wind tunnel classification and typical requirements for wind tunnel tests.

pressure reading techniques suffer from limited data points across the surface and readings are sometimes impossible in areas of high interest such as the trailing edges of wings, very thin parts of turbine blades or sharp corners. On the rotating parts the measurements are extremely difficult due to tubing or wiring.

To summarise, the drawbacks of standard aerodynamical pressure measurements are:

- pressure information is only obtained from a discrete number of points
- labour intensive manufacture of models
- some areas cannot be measured
- techniques are unsuitable for rotating parts and thin pieces

1.1.2 PSP techniques

To overcome these problems, a new non-contact optical testing method has been developed [1]. The surface is coated with an oxygen sensitive dye, which changes its luminescent properties as a function of oxygen molar concentration and in this case a function of pressure. Typically luminescence quenching of the dye is involved. Initially the intensity of luminescence was used to monitor pressure changes. However luminescence lifetime measurement is, in principle, equivalent and shows the same dependence on oxygen concentration. Moreover, it offers other advantages not available with the intensity-based techniques.

The surface of the paint is illuminated, usually by a flash lamp with spectral filters or LED arrays, and imaged by a CCD camera. Alternatively the excitation is provided by a

scanning laser beam and the luminescence is collected by appropriate optics and a single photodiode. These techniques constitute Pressure Sensitive Paint (PSP) technology.

This new PSP technology by its nature has many advantages compared to standard techniques:

+ information is available on a quasi-continuous grid,
+ data can be obtained from every surface that is optically accessible,
+ using synchronous measurements, rotating parts can be imaged and pressure recorded remotely [2, 3],
+ paint is relatively cheap and easily applied [4].

On the other hand, PSP techniques have also some problems and challenges for users:

- temperature correction of the oxygen pressure profile is required,
- high initial investment,
- large data files and problems with their manipulation.

In particular, the temperature sensitivity is an issue that must be addressed. The temperature changes in wind tunnels are significant. First, the whole tunnel becomes hot from air friction and therefore the temperature continually increases, and secondly, local areas on the model can become hot or cool due to aerodynamic heating or cooling respectively. Effective methods for handling temperature sensitivity are reviewed in Section 1.7 and one of them – a dual luminophore approach – is utilised in our work.

A useful demonstration of the need for accurate, quasi-continuous pressure profiles is presented in Figure 1.1. From this figure it is clear, that the computational fluid dynamics calculations are not fully reliable and therefore, wind tunnel tests are still a valuable part of the process of aircraft design and testing. PSP has the potential to decrease the duration of wind tunnel tests and to produce valuable data for further development and therefore, create an economic advantage for users.

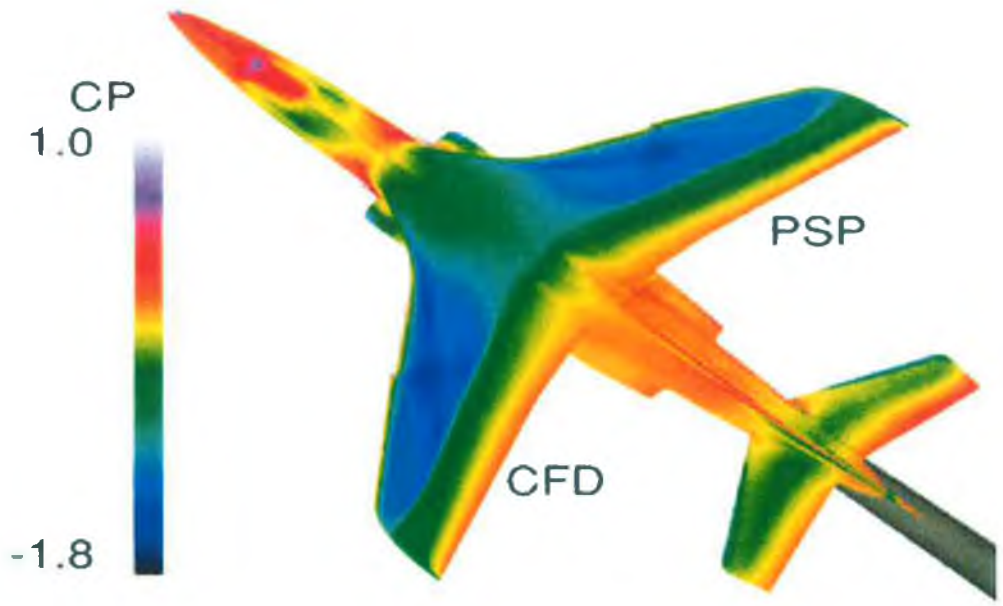

Figure 1.1: Comparison of CFD (Computational Fluid Dynamics) calculations and PSP data. The difference is visible just behind the cockpit and on the fuselage behind the wings. Image from [5].

1.1.3 History of PSP

The quenching of luminescence by oxygen was first reported by German scientists Kautsky & Hirsch in 1935 [6]. Almost half century later in 1980, the surface flow visualisation technique based on oxygen quenching of fluorescence was first demonstrated [7]. In the early 1980s, the idea of using this technique for pressure measurements on aerodynamic models had been developed, and a qualitative experiment was performed at the University of Washington (UW) [8]. In the summer of 1989, what appeared to be the first quantitative demonstration of the PSP technique took place at the National Aeronautics and Space Administration (NASA), Ames Research Center, using the coating developed at UW.

Totally unknown to the western world and protected by secrecy, Russian scientists had been researching the same topic since the late 1970s at the Central Aero-Hydrodynamic Institute (TsAGI) in the former Soviet Union. Inspired by work from the 1960s on the oxygen quenching properties of luminophores, Pervushin and Nevsky developed the first pressure-sensitive coating in 1981 and obtained the first pressure measurements in 1982 [9]. By the mid-1980s, another TsAGI group started work in this field, and developed a new

polymer based PSP, using "lifetime" and later "intensity-based" methods. The Russian research became known to the West through an advertisement for an "Optical Pressure and Temperature Measurement System" that appeared in the February 12, 1990, issue of Aviation Week & Space Technology [1, 10].

Over the next decade, PSP research has spread to aerospace institutions in many parts of the world. The main players are NASA, Boeing (and formerly McDonnell Douglas, acquired later by Boeing) and Purdue University – all in the United States. In Europe the main institutions involved are British Aerospace (BAe) and British Defense Evaluation and Research Agency (DERA) in the UK, Deutsche Forschungsanstalt für Luft- und Raumfahrt e.V. (DLR) in Germany, Office National d'Etudes et de Recherches Aerospatiales (ONERA) in France. Other important players are the National Aerospace Laboratory (NAL) in Japan and TsAGI in Russia.

In recent years, research on some PSP aspects also began at Dublin City University (DCU), Ireland, with wind tunnel tests are carried in cooperation with University of Limerick.

Luminescence quenching affects both the intensity and lifetime of typical luminophores. Both approaches may be adopted in PSP applications. Current PSP techniques employ mainly an intensity-based approach which is susceptible to drift and aging of both light source and detector as well as to paint inhomogeneities. The model is illuminated by a lamp or a scanning laser beam and two images are taken. A so-called "wind-off" image is taken under no airflow prior to the "wind-on" image in the wind tunnel. The wind-off image is used as a reference for intensity fluctuations due to paint thickness variations and uneven illumination. After aligning both images and ratioing intensities, the pressure is calculated (using equations discussed later in this chapter). In contrast, the luminescence lifetime approach used here eliminates many of the problems associated with intensity imaging. The lifetime is an intrinsic property of the luminophore, which, unlike intensity, is virtually independent of external perturbations. With this approach, the requirement for a wind-off image is eliminated [11].

However, luminescence properties are also dependent on temperature, which can differ significantly across a model in a wind tunnel, as well as fluctuating during prolonged tests. Many different techniques have been developed to correct for this temperature dependence. Early work used an additional infrared camera to provide a temperature correction for the pressure profile [12]. Other authors have used a separate temperature

sensitive paint containing a thermographic phosphor, for example a uv-excited rare-earth ion [13, 14]. These strategies have necessitated the use of separate paints [15], separate light sources and in some cases two cameras [16].

Besides methods based on oxygen quenching, the research on direct pressure measurements using pressure dependent chemical equilibrium of excited-state complexes [17, 18] was recently reported. The change in absolute pressure shifts the point of chemical equilibrium causing change in the proportion or reagents and causing a observable color change. Such paint was then tested in water, an environment nearly without oxygen [19]. Recent advances in fluorescence lifetime imaging in biochemical applications bring new concepts, which could possibly be utilised in PSP. This is discussed in Chapter 7.

1.2 Luminescence and luminescence quenching

1.2.1 Introduction to luminescence processes

Luminescence is defined as light emission that cannot be attributed simply to temperature of the emitting body. It involves radiative transitions between different energy levels in the material. As the electronic energy levels are unique for each material, so also are the luminescence properties characteristic of each material.

First the molecule/material must be excited by delivering a form of the energy. Depending on the origin of energy causing excitation, we refer to photoluminescence (energy in form of a photon), cathodoluminescence (accelerated electrons), radioluminescence (x-rays, α-particles), bioluminescence (chemical reaction in live organism), sonoluminescence (sound), electroluminescence (electric current). In the case of pressure-sensitive paint, photoluminescence is the only type of luminescence used and therefore we will focus on this.

A photon absorbed by a molecule raises the molecule from the ground state to one of the excited states, as seen in Figure 1.2. Energy tends to decay non-radiatively by internal conversion and intersystem crossing (converting excess energy to heat) down to the lowest excited singlet (S) or triplet (T) state. In a typical molecule the ground state is a singlet (all electrons are paired and spin is zero, $S = 0$, therefore $2S + 1 = 1$). A radiative transition occurs between the lowest singlet state S_1 and the ground state S_0. The emitted light is called fluorescence and the typical lifetime is often less than 10^{-9} s.

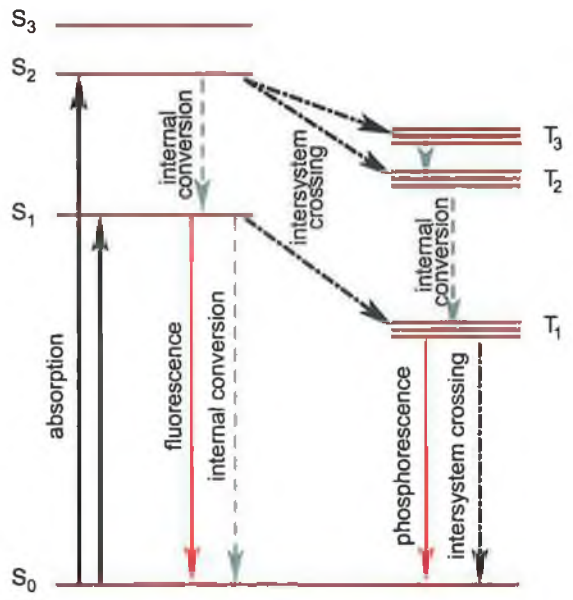

Figure 1.2: Jabłoński diagram of luminescence processes. S_0 is singlet ground state, S_1, S_2, and S_3 are singlet excited states, T_1, T_2, and T_3 are excited triplet states. Internal conversion and intersystem crossing are non-radiative processes, fluorescence and phosphorescence are radiative processes (yielding light).

A transition between the lowest triplet state T_1 (spin is equal to 1, $S = 1$, therefore $2S + 1 = 3$) and the ground state S_0 is quantum-mechanically forbidden but due to an interaction with the environment there is still a finite probability for the transition to occur. Emission from the triplet to the singlet state is termed phosphorescence. The transition time is considerably longer (milliseconds to seconds) than for a singlet-singlet transition. However, it is not an absolute rule and often fluorescence can be longer lived than phosphorescence (e.g. delayed fluorescence) or both processes are connected and cannot be distinguished. Consequently the terms fluorescence and phosphorescence are frequently misused. In this work we use the general term luminescence when referring to any of fluorescent or phosphorescent processes.

As a part of the excitation energy is 'lost' between excitation and emission, the emitted light is shifted spectrally towards longer wavelengths and lower energies. Energy is usually dissipated into vibrational (phonon) modes in the molecule. The difference between the excitation and emitted energy is termed the Stokes shift. A large Stokes shift is favourable for easy separation of excitation light during detection of luminescence and also the effects

of resonance energy transfer (see section 1.2.3) and reabsorption are suppressed.

A luminescent process can be characterised by its intensity (for each wavelength), but also each transition is characterised by a rate constant, κ, which expresses the probability per unit time that an electron in a particular excited state will de-excite to the ground state. The reciprocal value of the rate constant is called the lifetime ($\tau = 1/\kappa$) and represents the average length of time that the electron spends in the excited state. For each transition, it is usual to distinguish the radiative and multiple non-radiative decays in the form of decay rates, κ_{R}, and multiple decay rates, κ_{NR}, and lifetimes, τ_{R}, and multiple lifetimes, τ_{NR}. As both processes compete with each other, the observed luminescence lifetime, τ, is determined by

$$\kappa = \kappa_{\mathrm{R}} + \sum \kappa_{\mathrm{NR}}\,, \tag{1.1}$$

$$\frac{1}{\tau} = \frac{1}{\tau_{\mathrm{R}}} + \sum \frac{1}{\tau_{\mathrm{NR}}}\,, \tag{1.2}$$

where indexes R and NR refer to radiative and non-radiative processes, respectively and the sums run through all non-radiative processes. If additional processes are involved (e.g. quenching) another term is added to the sum in Equation 1.2 to express changes in the observed lifetime.

The quantum efficiency η of luminescence is determined by

$$\eta = \frac{\kappa_{\mathrm{R}}}{\kappa_{\mathrm{R}} + \sum \kappa_{\mathrm{NR}}}\,. \tag{1.3}$$

As other non-radiative channels are added or some of the current channels are promoted, the quantum efficiency decreases.

1.2.2 Lifetime

Luminescence lifetime, sometimes referred to as decay time, is an important property of luminescent systems.

When a system that exhibits a single lifetime decay is excited by continuous light, it produces a continuous response in emitted luminescence. When the light is switched off, a decay in observed luminescence whose time profile is proportional to $\sim \mathrm{e}^{-t/\tau}$, where τ is the "observed lifetime", is observed. This lifetime is the time taken for the intensity to drop to 1/e of its original intensity.

An interesting property of lifetime is that the time constant τ (lifetime) can also be observed in the rising signal after the light source is switched on. The luminescence again

follows an exponential rise in the form of $\sim (1 - e^{-t/\tau})$. Both effects are illustrated in Figure 1.3.

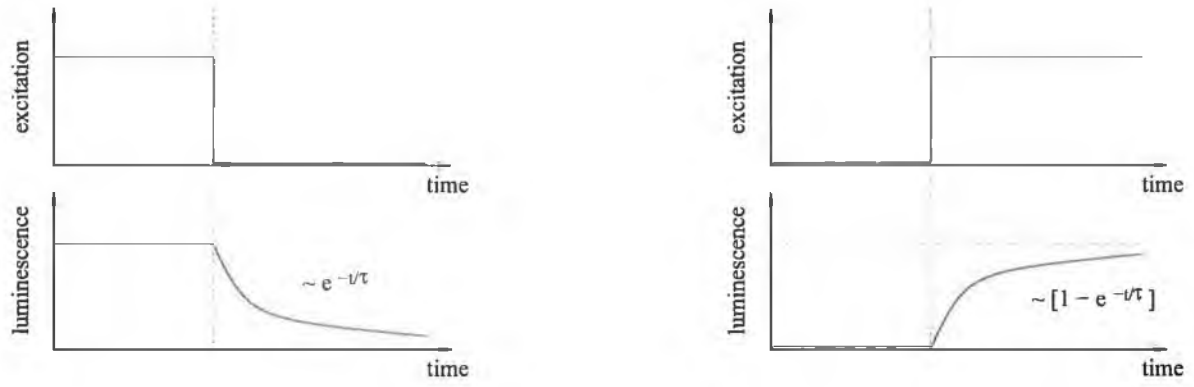

Figure 1.3: Definition of lifetime – exponential decay (left) and exponential rise (right).

1.2.3 Luminescence quenching

Luminescence quenching refers to any process that decreases the luminescence intensity. Some types of quenching influence only luminescence intensity (e.g. static quenching), but other quenching effects (e.g. collisional quenching) quench lifetime(s) as well.

As some types of luminescence quenching are caused by molecular interactions, quenching can be used to detect changes in the local molecule environment caused by some external factor (e.g. change of pH, concentration of analyte, temperature). In this project, quenching is used to detect changes in oxygen pressure at a surface. In general, quenching occurs without any permanent change to the molecule, the process is reversible, and by measuring the quenching, the changes in external parameters can be determined.

Dynamic quenching

Dynamic quenching is an important type of quenching for gas sensing applications. Here a collisional encounter between the quencher and the excited state is involved and the excited state is de-excited (Figure 1.4). The lifetime and intensity of the emission are decreased by dynamic quenching. So-called Stern-Volmer kinetics apply to the simplest

dynamic quenching processes according to the well-known Stern-Volmer equation* first published in a paper in 1919 [20]

$$\frac{I_0}{I} = 1 + K_{\mathrm{SV}}[Q]\,, \tag{1.4}$$

where I_0 and I are respectively the fluorescence intensities in the absence and presence of quencher and $[Q]$ is the concentration of the quenching species. For PSP, the concentration $[Q]$ of quenching species in the paint is equal to the product of the solubility of the gas and partial pressure of gas outside the paint (Henry's law) [21]. The proportionality constant K_{SV} is known as the Stern-Volmer coefficient and

$$K_{\mathrm{SV}} = \tau_0 k_{\mathrm{q}}\,, \tag{1.5}$$

where k_{q} is the bimolecular quenching constant. It can be shown that the ratio I_0/I can be replaced by τ_0/τ, yielding the lifetime version of the Stern-Volmer equation [22]

$$\frac{\tau_0}{\tau} = 1 + K_{\mathrm{SV}}[Q]\,. \tag{1.6}$$

The dependence of K_{SV} on the unquenched lifetime τ_0 has implications for sensitivity as discussed in Section 2.2.2.

Static quenching

Static quenching is another process where an interaction between the luminophore and a quencher is involved. Static quenching involves the formation of a ground state complex that is not luminescent. Pure static quenching reduces the intensity of luminescence but does not necessarily decrease the lifetime of emission as static quenching effectively reduces the number of luminescently active molecules.

Concentration quenching

Concentration quenching is a process where a molecule is quenched by an adjacent molecule of the same type. Therefore, it is more likely to occur at higher concentration of

*The ratio of I_0/I can be looked at as the decrease of quantum efficiency of luminescence as $I_0/I = \eta_0/\eta$ at otherwise unchanged conditions. Knowing, that $\tau_0 = 1/(\kappa_{\mathrm{R}} + \kappa_{\mathrm{NR}})$, then the non-radiative quenching rate constant is linearly proportional to the concentration of quencher through the quenching constant: $\kappa_{\mathrm{q}} = 1/\tau_{\mathrm{q}} = k_{\mathrm{q}}[Q]$. Using Equation 1.3, one can show that $I_0/I = \eta_0/\eta = [\kappa_{\mathrm{R}}/(\kappa_{\mathrm{R}} + \kappa_{\mathrm{NR}})]/[\kappa_{\mathrm{R}}/(\kappa_{\mathrm{R}} + \kappa_{\mathrm{NR}} + k_{\mathrm{q}}[Q])] = (\kappa_{\mathrm{R}} + \kappa_{\mathrm{NR}} + k_{\mathrm{q}}[Q])/(\kappa_{\mathrm{R}} + \kappa_{\mathrm{NR}}) = 1 + k_{\mathrm{q}}[Q]/(\kappa_{\mathrm{R}} + \kappa_{\mathrm{NR}}) = 1 + \tau_0 k_{\mathrm{q}}[Q]$.

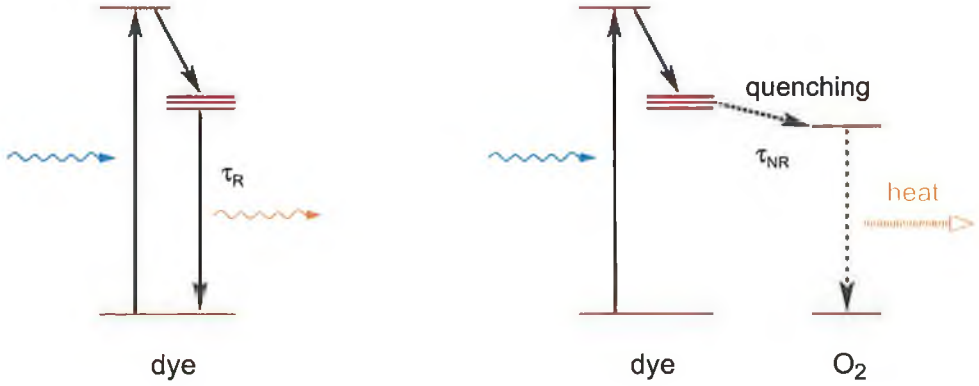

Figure 1.4: Modified Jabłoński diagram of dynamic oxygen quenching of luminescence. On the left, the absorbed photon is re-emitted with a Stokes shift (lower energy) with typical radiative rate $1/\tau_R$. On the right, the energy of the absorbed photon is captured by the oxygen molecule without release of light. The rate of this process is traditionally described in terms of lifetime τ_{NR}.

luminophore (self-quenching). The mechanism can be visualised as radiationless transfer of energy between molecules (particularly where the Stokes shift is small) or through formation of aggregates (common for large molecules such as porphyrins) or via a Stern-Volmer mechanism in solution. Concentration quenching can cause problems for particular applications due to the fact that increasing the concentration of the luminophore does not necessary imply an increase in luminescence signal level.

Colour quenching

Colour quenching is a mechanism where the photons that are emitted are reabsorbed by a strongly coloured component of the sample. Colour quenching does not shorten excited state lifetimes. Colour quenching can be minimised by reducing the sample pathlength for a given concentration of fluorescent dye.

Resonance energy transfer

Colour quenching is often accompanied by another quenching process based on resonance energy transfer (RET). This is a radiationless process where an excited luminophore (donor) transfers excitation energy to a neighbour (acceptor) that has an absorption spectrum that overlaps with the donor's emission spectrum. RET is based on dipole–

dipole interaction and therefore is only efficient for molecules in very close proximity (typically less than a few nm). For this reason it is only seen in concentrated solutions in the absence of specific interactions. RET-based concentration quenching can be reduced by dilution. The commonly used name for RET is fluorescence (or Förster) resonance energy transfer (FRET).

1.2.4 Multiple-component decays

The time-resolved intensity of luminescence in the case of a single lifetime τ can be described as a single exponential decay $I(t) = I(0)\,\mathrm{e}^{-t/\tau}$, where $I(0)$ is emission intensity at time $t = 0$, when the excitation light is turned completely off. Such a decay, observed for example with a pulsed light source (laser) and photomultiplier tube (PMT), should give a straight line graph for a semi-logarithmic plot of intensity versus time.

Many luminescent species do not exhibit single exponential decays. For multi-component decays, the time-resolved luminescence can be written as $I(t) = \sum_{i=1}^{n} I_i\,\mathrm{e}^{-t/\tau_i}$, where τ_i and I_i are individual lifetimes and intensities. Frequently, a continuous distribution of lifetimes is observed when time-resolved luminescence intensity is $I(t) = \int_{\tau=0}^{\infty} F(\tau)\mathrm{d}\tau$, where $F(\tau)$ is the distribution of lifetimes. The analysis of such complex decays is a challenging task [23].

In general, there can be several reasons for multiple decay times. Different lifetimes are attributed to different energy levels in luminescent molecules and materials with a complicated energy-level structure can experience multi-exponential decay. Furthermore, luminescence properties of molecules are often strongly dependent on the local environment and, for example in an amorphous sensor matrix (binder), each molecule experiences a different environment and therefore has a different lifetime. This is manifested as a multiple exponential decay. Differently located luminescent probes are also typically subject to different degrees of quenching and a transition from single to multiple lifetime can be observed with varying concentration of quencher.

1.3 Ruthenium complexes and oxygen sensitivity

The right choice of luminescent compound is crucial for successful deployment of a luminescence sensor. Initially, for oxygen sensing, organic dyes such as pyrene derivatives [24]

or porphyrins [25] were used. However, they suffer from disadvantages such as short-wavelength excitation, small Stokes shift and short unquenched lifetimes. These issues add complexity to the measurements.

In recent years transition metal complexes have been widely used for oxygen sensing [26]. These complexes exhibit strong optical absorption, larger Stokes shift and have relatively long lifetime (100 ns to 10 μs). In particular, ruthenium complexes exhibit high oxygen sensitivity due to their long unquenched lifetime, while their absorption bands in the blue spectral region allow the use of widely available LEDs as excitation sources.

A typical example of a ruthenium complex is $[Ru(bpy)_3]^{2+}$ where bpy is 2,2'-bipyridine. It was originally developed for use in solar-energy conversion in the hope that charge transfer between strongly oxidant Ru^{III} and bpy^- could be used to split water into oxygen and hydrogen.

An excellent complex for oxygen sensing is Ru^{II}-tris-(4,7-diphenyl-1,10-phenanthroline) abbreviated also as $[Ru(dpp)_3]^{2+}$. It has an unquenched lifetime in nitrogenated ethanol of $\sim 5\,\mu$s and is easily incorporated into a wide range of binder matrices.

In Section 2.2, the properties of this complex are discussed in greater detail.

1.4 PSP imaging – theory and equations

1.4.1 Modified Stern-Volmer equation

The standard Stern-Volmer relation, Equation 1.4, assumes that the reference measurement is made without the presence of a quencher, e.g. at vacuum or nitrogen atmosphere. In the wind tunnel this is not usually possible, so a modified version of the Stern-Volmer equation is used. The reference measurement is usually made under ambient atmospheric conditions. Therefore from the standard Stern-Volmer equation ($I_0/I = \tau_0/\tau = 1 + K_{SV}[Q]$) a modified version, not requiring I_0, is derived by dividing two Stern-Volmer equations, one written for the measured condition and the second for the reference conditions. It yields $I_{ref}/I = \tau_{ref}/\tau = (1 + K_{SV}[Q])/(1 + K_{SV}[Q_{ref}])$ and as the denominator $(1 + K_{SV}[Q_{ref}])$ is constant, the equation can be written in the form

$$\frac{I_{ref}}{I} = A + B\frac{p}{p_{ref}} = \frac{\tau_{ref}}{\tau}, \tag{1.7}$$

where subscript 'ref' refers to some known pressure, typically atmospheric pressure. Constants $A = (1 + K_{SV}[Q_{ref}])^{-1}$ and $B = K_{SV}/(1 + K_{SV}[Q_{ref}])$ can be determined from

the Stern-Volmer constant K_{SV} and reference quencher concentration $[Q_{ref}]$ at reference conditions, but this is equivalent to determining A and B during calibration.

The constants A and B are temperature dependent, so during full calibration of the paint the temperature functions $A(T)$ and $B(T)$ are recorded.

1.4.2 Non-dimensional coefficients

Many wind tunnel tests use a scale model. To relate data acquired from a scale model to the full-scale vehicle without including the model size and specific wind tunnel pressure conditions, non-dimensional coefficients are used. Ideally, these coefficients depend only on the size and shape of the model and the angle at which the air flow hits the model. For wind tunnel tests the non-dimensional pressure coefficient C_p [27] is calculated as

$$C_p = \frac{p - p_\infty}{\frac{1}{2}\rho v_\infty^2}, \tag{1.8}$$

where p is the pressure at a particular point, p_∞ is the pressure far from the model (free stream pressure), ρ is the density of air (usually quoted as $\rho = 1.225\,\mathrm{kg/m^3}$) and v_∞ is the speed of air far from the model. The pressure coefficient C_p is de facto relative pressure in units of the dynamic pressure ($\frac{1}{2}\rho v^2$) in the tunnel.

1.5 Two-dimensional oxygen profiling

Conventional oxygen sensors are based on electrochemical principles [28]. These sensors are capable typically of single point measurements. It means that the read value is a single number representing the averaged value of the measured quantity (e.g. oxygen concentration) over the effective sensing area. In some cases spatial resolution is required. It was shown by Reimers *et al.* [29], that miniaturisation of the sensor head using miniature electrodes and mechanical scanning can produce one-dimensional profiles of oxygen distribution in sediments.

Optical methods of detection allow, in principle, less complex methods for spatial distribution mapping, by using scanning methods or camera systems.

Scanning methods

A typical scanning configuration uses a static excitation laser and a static detection system. Using a computer-controlled mirror, the laser beam is deflected and scans across

the sample surface. The laser is pulsed and time-resolved luminescence follows the same optical path as the laser beam (opposite direction) into the detection system, where a photomultiplier tube or photodiode detects the light intensity. Using a fast analog-to-digital converter the time-resolved luminescence signal is acquired and pressure at the point evaluated. Thus the spatial profile can be recorded, depending on the number of required points, in a timescale of a few minutes [30].

In an alternative configuration, often employed when a microscope is used, the whole sample is excited and the detector scans across the sample. Another variation includes systems that use a scanning laser beam and static collection optics [31]. Scanning systems are used exclusively for lifetime imaging.

Camera systems

Two dimensional oxygen profiles can also be acquired using a camera. Using a camera is, in principle, equivalent to the use of thousands to millions of photodetectors in parallel. This accelerates the whole process of profile acquisition. In reality, the increase in speed is not so dramatic as the sensitivity of each pixel is not equivalent to the sensitivity of a single light detector. There are several methods for pressure profile extraction. The first, the intensity approach, uses scientific grade CCDs to record luminescence intensity images using exposure times of seconds. Lifetime-based systems use gated cameras to produce a set of images at exposure times in the range of microseconds, which, after processing, is converted into an image of the pressure profile over the model.

To our knowledge, only one scanning system is commercially available [30]. Camera-based systems are widespread, currently using mainly the intensity approach. For industrial applications the camera systems are favoured due to the increased data acquisition speed as every decrease of measurement time saves 1000s $/hour in wind tunnel costs.

1.6 Intensity and lifetime measurement approaches

The relation of the intensity and lifetime to the oxygen partial pressure was referred to briefly earlier in the chapter. The intensity of the luminescence is not only a function of oxygen pressure, but also of many other factors, including intensity of excitation light at the particular point, $I_{\text{exc.}}$, sensitivity of the detection system, including the collecting optics and overall configuration, S_{det}, thickness of the paint, h, concentration of active

luminescence molecules, $c_{\text{lum}}(t)$, which can change in time, and temperature, T:

$$I = I(p_{O_2}, I_{\text{exc}}, S_{\text{det}}, c_{\text{lum}}(t), T)\,.$$

On the other hand, the true lifetime is typically independent of the excitation intensity, sensitivity of the detection system and concentration changes of luminophore

$$\tau = \tau(p_{O_2}, T)\,.$$

Therefore, intensity-based methods must compensate for all these parameters or keep them constant between calibration and actual measurement. In contrast the lifetime measurement needs to be compensated for just temperature and therefore should, in principle, be simpler.

For this reason, lifetime measurements are becoming more popular in luminescence detection [32, 33], particularly when relatively low cost phase detection techniques are available to measure lifetime in the range of microseconds.

1.7 Temperature corrections

In general, luminescence properties of materials are temperature dependent. In many experiments the temperature can be controlled and therefore, temperature dependence of luminescence is not an issue. However, for PSP the temperature changes are an intrinsic feature of the experiment. In high speed wind tunnels the effect of aerodynamic heating and/or cooling at different surfaces becomes significant, causing a temperature difference between various pieces of the model. Even in slow speed wind tunnels the temperature is difficult to control as the tunnel is not an isothermal device and it heats up continuously by air friction.

Therefore, rather than control the temperature it is more desirable to measure the temperature and then use this information for correcting the luminescence information related to pressure. In some cases, separate information about the temperature distribution can be useful. The paint designed specially for temperature measurements is named temperature sensitive paint (TSP).

1.7.1 Sources of temperature variation

Typically, the temperature sensitivity of pressure related luminescence is caused by

- temperature sensitivity of the luminescent complex and
- temperature sensitivity of the solubility and diffusion coefficients of oxygen in the binder material, causing a change in local concentration of oxygen seen by the sensing luminophore.

The total temperature sensitivity of the paint is due to a combination of these factors and must be treated as a whole.

1.7.2 Methods for temperature correction

A range of methods is employed to compensate for temperature effects in PSP.

One approach for creating a temperature-independent paint is to select a luminophore and binder with opposite temperature characteristics, where temperature effects cancel out [34] in a certain range of temperatures. Some work in the laboratory of the author was devoted to development of a temperature independent ruthenium complex. Another approach for intensity-based measurements is the use of a temperature sensitive buffer layer, which changes reflectivity with temperature [35]. With increasing temperature, the increase in reflectivity compensates for the decreasing luminescence. Both these approaches involve removing the temperature sensitivity of the paint.

Alternatively, thermo-couples can be positioned over the surface and the temperature in between them interpolated. The use of an extra infra-red (IR) camera to record the surface temperature was also reported by Engler [36], Liu [37] and Le Sant [38]. Registering temperature and pressure images to overlay corresponding areas is a particular problem as temperature and pressure images are acquired from two different places.

A common approach is to use pressure and temperature sensitive paint (PSP/TSP systems). The use of dual luminophore paint (binary paint), where emission of the luminescence occurs at two different wavelengths allowing for two spectrally separated intensity measurements, was reported by Khalil *et al.* [39]. In this work we report the use of a dual-luminophore paint with separation in lifetime rather than in wavelength.

1.8 Temperature sensors

The majority of temperature-correction luminophores used in PSP measurements have been ions of rare-earth elements, e.g. europium (Eu^{3+}) [40], which in the form of Y_2O_3:Eu^{3+}

show very sharp emission lines (linewidth of a few nanometres) and require UV excitation. Y_2O_2S:Sm is another temperature phosphor reported for high temperature applications (300–1400 K) [41].

Other phosphors can also be used such as common phosphors used in the light industry. These phosphors have the advantage of very high brightness.

The luminophore chosen for the work reported here is manganese-doped magnesium-fluorogermanate (MFG) phosphor which is used as a colour corrector in high pressure mercury vapour lamps and has also been used in commercial fibre optic temperature sensing applications [42]. Its lifetime is around $\tau \sim 3.5$ ms at room temperature with change of -0.008 ms/°C. Detailed discussion of its electronic levels is carried in Section 2.3.1.

1.9 Sol-gel materials

Optical oxygen sensors require a porous, transparent matrix or binder for immobilisation of the oxygen-sensitive luminophore. One of the very promising approaches has been to use the sol-gel process for encapsulation of optically active compounds into a silica glass matrix. Its preparation is simple and the material itself is compatible with various coating techniques (dip, spin, knife, spray coating). The resultant coating is tough, inert, has high chemical and photochemical stability and has low optical absorption in the visible and near infrared region of spectra. Generally, the sol-gel matrix has advantages over the commonly used polymer matrix, such as better optical quality, ability to tailor for different applications, and flexibility regarding coating techniques.

The sol-gel process is used increasingly in the fabrication of chemical and biochemical sensors, e.g. ammonia [43], nitrogen monoxide [44], carbon dioxide [45, 46], hydrogen sulphide [47], pH [48, 49] and oxygen sensors [50]. The use of sol-gel for PSP applications is relatively new and to our knowledge the use of sol-gel material is reported for the first time here.

Generally, the microporous sol-gel matrix entraps molecules of the sensing material. The size of the pores, which is determined by the exact preparation method, is selected to be smaller than the size of the sensing molecules but large enough for diffusion of the analyte through the matrix towards the sensing molecule, hence minimising dye leaching.

The sol-gel process uses silicon alkoxide precursors, which undergo hydrolysis and polycondensation reactions followed by temperature treatment, which controls the densi-

fication process. The microporous glass acts as a support matrix for sensing molecules, which are added to the initial sol. The sensing molecules can be susceptible to degradation at high temperatures and therefore the low temperature processing is a useful feature of the process.

Detailed discussion of sol-gel materials and techniques is in Section 2.1.

1.10 Objectives of this thesis

The principal objective of the research program reported in this thesis was to develop a dual-luminophore paint capable of simultaneous pressure and temperature measurements. The second, parallel, aim was to assemble a suitable data acquisition system and to evaluate the methods for data acquisition to achieve reasonable precision and noise in pressure values.

Several constraints were placed on the system design, including

- no moving parts in the system,
- preferably using a single light source,
- using a single camera to avoid problems with the image registration of temperature and pressure profiles,
- not using wind-off images to avoid registration of wind-on and wind-off images,
- luminophores selected should have different lifetimes to enable easy separation of lifetimes.

The paint formulation, based on sol-gel materials, should be easy to apply and remove and reasonably durable during the wind tunnel tests.

Finally the performance of the paint and the data acquisition system will be tested in a medium speed wind tunnel experiment.

1.11 References

[1] A. Vollan and L. Alati, "A new optical pressure measurement system (OPMS)," *ICIASF Record, 14th International Congress on Instrumentation in Aerospace Simulation Facilities*, pp. 10–16, 1991.

[2] S. Alaruri, "An endoscopic imaging system for turbine engine pressure sensitive paint measurements," *Opt. Laser Eng.*, vol. 36, pp. 277–287, 2001.

[3] J. H. Bell, E. T. Schairer, L. A. Hand, and R. D. Mehta, "Surface pressure measurements using luminescent coatings," *Annu. Rev. Fluid Mech.*, vol. 33, no. 1, pp. 155–206, 2001.

[4] B. G. McLachlan and J. H. Bell, "Pressure-sensitive paint in aerodynamic testing," *Exp. Therm. Fluid Sci.*, vol. 10, no. 4, pp. 470–485, 1995.

[5] D. Ahlstrom, "New paint spots flaws in designs of aircraft," *The Irish Times*, 12th June 2000.

[6] H. Kautsky and H. Hirsch, "Detection of minutest amounts of oxygen by extinction of phosphorescence," *Z. Anorg. Allg. Chem.*, vol. 222, p. 126, 1935.

[7] J. I. Peterson and R. V. Fitzgerald, "New technique of surface flow visualization based on oxygen quenching of fluorescence," *Rev. Sci. Instrum*, vol. 51, no. 5, pp. 670–671, 1980.

[8] J. Kavandi, J. Callis, M. Gouterman, G. Khalil, D. Wright, E. Green, D. Burns, and B. McLachlan, "Luminescent barometry in wind tunnels," *Rev. Sci. Instrum.*, vol. 61, no. 11, pp. 3340–3347, 1990.

[9] M. M. Ardasheva, L. B. Nevskii, and G. E. Pervushin *J. Appl. Mech. Tech. Phys.*, vol. 26, pp. 469–474, 1985.

[10] R. H. Engler, K. Hartmann, and B. Schulze, "Aerodynamic assessment of an optical pressure measurement system (OPMS) by comparison with conventional pressure measurements in a high speed wind tunnel," *ICIASF Record, 14th International Congress on Instrumentation in Aerospace Simulation Facilities*, pp. 17–24, 1991.

[11] M. Gouterman, "Oxygen quenching of luminescence of pressure sensitive paint for wind tunnel research," *J. Chem. Educ.*, vol. 74, no. 6, pp. 697–702, 1997.

[12] E. Gartenberg and A. S. J. Roberts, "Twenty-five years of aerodynamic research with infrared imaging," *Proceedings of SPIE - The International Society for Optical Engineering*, vol. 1467, pp. 338 – 356, 1991.

[13] S. Alaruri, T. Bonsett, A. Brewington, E. McPheeters, and M. Wilson, "Mapping the surface temperature of ceramic and superalloy turbine engine components using laser-induced fluorescence of thermographic phosphor," *Opt. Lasers Eng.*, vol. 31, no. 5, pp. 345–351, 1999.

[14] L. M. Coyle and M. Gouterman, "Correcting lifetime measurements for temperature," *Sensors and Actuators B: Chemical*, vol. 61, no. 1-3, pp. 92–99, 1999.

[15] L. Creswell and M. Cripps, "Independent pressure and temperature measurements from double layer paint using fluorescent lifetime and radiometric imaging," in 8^{th} *Annual Pressure Sensitive Paint Workshop*, (NASA Langley), pp. 1–7, 2000.

[16] G. M. Buck, "Surface temperature/heat transfer measurement using a quantitative phosphor thermography system," *AIAA Journal*, vol. 91-0064, pp. 1–12, 1991.

[17] L. A. Kelly, "Fluorescent temperature sensor based on perylene/exciplex interconversion," in 9^{th} *Annual PSP Workshop*, (Washington DC, USA), p. unpublished, 7 – 11 April 2002.

[18] N. Chandrasekharan and L. A. Kelly, "A dual fluorescence temperature sensor based on perylene/exciplex interconversion," *J. Am. Chem. Soc.*, vol. 123, no. 40, pp. 9898–9899, 2001.

[19] M. Hamner, A. Fontaine, and P. Atsavapranee, "Development of a new pressure sensitive luminescent coating," in 41^{th} *Aerospace Sciences Meeting and Exhibit*, vol. AIAA-2003-0091, (Reno, Nevada), 2003.

[20] O. Stern and M. Volmer, "Über die Abklingungszeit der Fluoreszenz," *Phys. Z.*, vol. 20, pp. 183–188, 1919.

[21] J. W. Holmes, "Optical pressure measurement (PSP)," Oct. 1997. Modern Optical Flow Measurement Advanced School, Udine, Italy.

[22] J. R. Lakowicz, *Principles of Fluorescence Spectroscopy.* New York: Kluwer Academic/Plenum Publishers, second ed., 1999.

[23] A. A. Istratov and O. F. Vyvenko, "Exponential analysis in physical phenomena," *Rev. Sci. Instrum.*, vol. 70, no. 2, pp. 1233–1257, 1999.

[24] R. H. Engler, M.-C. Merienne, C. Klein, and Y. Le Sant, "Application of PSP in low speed flows," *Aerosp. Sci Technol.*, vol. 6, no. 5, pp. 313–322, 2002.

[25] Y. Amao, K. Asai, T. Miyashita, and I. Okura, "Novel optical oxygen sensing material: Platinum porphyrin-fluoropolymer film," *Polymers for Advanced Technologies*, vol. 11, no. 8-12, pp. 2663–2668, 2000. `http://dx.doi.org/10.1002/1099-1581(200008/12)11:8/12<705::AID-PAT23>3.0.CO;2-L`.

[26] K. S. Schanze, B. F. Carroll, S. Korotkevitch, and M. F. Morris, "Temperature dependence of pressure sensitive paints," *AIAA Journal*, vol. 35, no. 2, pp. 306–310, 1997.

[27] J. N. Demas, B. A. DeGraff, and P. B. Coleman, "Oxygen sensors based on luminescence quenching," *Anal. Chem.*, vol. 71, no. 23, pp. 793A–800A, 1999.

[28] A. J. Bard, ed., *Electrochemical Methods: Fundamentals and Applications.* John Wiley & Sons, first ed., 1980.

[29] C. E. Reimers, K. M. Fischer, R. Merewether, K. L. Smith Jr., and R. A. Jahnke, "Oxygen microprofiles measured in situ in deep ocean sediments," *Nature*, vol. 320, pp. 741–744, 1986.

[30] A. Davies, "SUrface PRessure Measurement using Optics (SUPREMO)," tech. rep., Advanced Technology Centres (Sowerby), BAE Systems, 2000.

[31] L. M. Coyle, D. Chapman, G. Khalil, E. Schibli, and M. Gouterman, "Non-monotonic temperature dependence in molecular referenced pressure-sensitive paint (MR-PSP)," *J. Lumin.*, vol. 82, no. 1, pp. 33–39, 1999.

[32] C. McDonagh, C. Kolle, A. K. McEvoy, D. L. Dowling, A. A. Cafolla, S. J. Cullen, and B. D. MacCraith, "Phase fluorometric dissolved oxygen sensor," *Sensors and Actuators B: Chemical*, vol. 74, no. 1-3, pp. 124–130, 2001.

[33] E. Rabinovich, M. J. O'Brien, S. R. J. Brueck, and G. P. Lopez, "Phase-sensitive multichannel detection system for chemical and biosensor arrays and fluorescence lifetime-based imaging," *Rev. Sci. Instrum.*, vol. 71, no. 2, pp. 522–529, 2000.

[34] A. Mills and F. Williams, "Chemical influences on the luminescence of ruthenium diimine complexes and its response to oxygen," *Thin Sol. Films*, vol. 306, no. 1, pp. 163–170, 1997.

[35] J. Ingram, D. Oglesby, N. Watkins, J. Jordan, and B. Leighty, "Solving pressure sensitive paint challenges using chemistry," in 9^{th} *Annual PSP Workshop*, (Washington DC, USA), 7 – 11 April 2002.

[36] R. H. Engler, "Description and assessment of a new optical pressure measurement system (OPMS) demonstrated in the high speed wind tunnel of DLR in Gottingen," 1992. DLR paper FB-92-24, ISBN 0939-2963.

[37] T. Liu, B. T. Campbell, S. P. Burns, and J. P. Sullivan, "Temperature and pressure sensitive luminescent paints in aerodynamics," *Appl. Mech. Rev.*, vol. 50, no. 4, pp. 227–246, 1997.

[38] Y. Le Sant, M. Marchand, P. Millan, and J. Fontaine, "An overview of infrared thermography techniques used in large wind tunnels," *Aerospace Science and Technology*, vol. 6, no. 5, pp. 355 – 366, 2002. `http://dx.doi.org/10.1016/S1270-9638(02)01172-0`.

[39] G. E. Khalil, C. Costin, J. Crafton, G. Jones, S. Grenoble, M. Gouterman, J. B. Callis, and L. R. Dalton, "Dual-luminophor pressure-sensitive paint: I. ratio of reference to sensor giving a small temperature dependency," *Sens. Actuators B: Chem.*, vol. 97, no. 1, pp. 13–21, 2004.

[40] B. Zelelow, G. E. Khalil, G. Phelan, B. Carlson, M. Gouterman, J. B. Callis, and L. R. Dalton, "Dual luminophore pressure sensitive paint: II. Lifetime based measurement of pressure and temperature," *Sens. and Act. B: Chemical*, vol. 96, no. 1-2, pp. 304–314, 2003.

[41] J. P. Feist and A. L. Heyes, "The characterization of Y_2O_2S:Sm powder as a thermographic phosphor for high temperature applications," *Meas. Sci. Technol.*, vol. 11, pp. 942–947, 2000.

[42] K. A. Wickersheim and M. H. Sun, "Fluorooptic thermometry," *Med. Elect.*, vol. 103, pp. 84–91, 1987.

[43] C. Malins, T. M. Butler, and B. D. MacCraith, "Influence of the surface polarity of dye-doped sol-gel glass films on optical ammonia sensor response," *Thin Sol. Films*, vol. 368, no. 1, pp. 105–110, 2000.

[44] D. J. Blyth, J. W. Aylott, D. J. Richardson, and D. A. Russell, "Sol-gel encapsulation of metalloproteins for the development of optical biosensors for nitrogen monoxide and carbon monoxide," *Analyst*, vol. 120, p. 2725, 1995.

[45] C. von Bültzingslöwen, A. K. McEvoy, C. McDonagh, B. D. MacCraith, I. Klimant, C. Krause, and O. S. Wolfbeis, "Sol-gel based optical carbon dioxide sensor employing dual luminophore referencing for application in food," *Analyst*, vol. 127, no. 11, pp. 1478–1483, 2002.

[46] C. von Bültzingslöwen, A. K. McEvoy, C. McDonagh, and B. D. MacCraith, "Lifetime-based optical sensor for high-level pCO_2 detection employing fluorescence resonance energy transfer," *Anal. Chim. Acta*, vol. 480, no. 2, pp. 275–283, 2003.

[47] M. Krihak and M. R. Shahriari, "Active sol-gel materials for fibre optic chemical sensors," in *Proc. Soc. Photo-Opt. Instrum. Eng.*, vol. 2293, pp. 88–98, 1994.

[48] C. Malins, H. G. Glever, T. E. Keyes, J. G. Vos, W. J. Dressick, and B. D. MacCraith, "Sol-gel immobilised ruthenium(II) polypyridyl complexes as chemical transducers for optical pH sensing," *Sens. Act. B: Chemical*, vol. 67, no. 1-2, pp. 89–95, 2000.

[49] C. S. Burke, L. Polerecky, and B. D. MacCraith, "Design and fabrication of enhancedpolymer waveguide platforms for absorption-based optical chemical sensors," *Meas. Sci. Technol.*, vol. 15, no. 6, pp. 1140–1145, 2004.

[50] C. McDonagh, B. D. MacCraith, and A. K. McEvoy, "Tailoring of sol-gel films for optical sensing of oxygen in gas and aqueous phase.," *Anal. Chem.*, vol. 70, no. 1, pp. 45–50, 1998.

Chapter 2

Materials and Methods

The two main components of pressure-sensitive paint are the oxygen-sensitive (and temperature-sensitive) luminophores and the binder or immobilisation matrix. The matrix of choice for this work is based on the sol-gel process, which can produce porous (oxygen-permeable) films. A brief account of the process will be given in this chapter, as well as a description of the oxygen-sensing complex ($[Ru^{II}$-tris-(4,7-diphenyl-1,10-phenanthroline)$]^{2+}$) and temperature-sensitive phosphor manganese-doped magnesium-fluorogermanate (MFG). The instrumentation and characterisation techniques used in the course of the project will also be described.

2.1 Introduction to sol-gel materials

The sol-gel process involves the preparation of ceramic materials or glasses by hydrolysis and condensation of the appropriate metal alkoxide, followed by a temperature programme [1, 2]. Sol-gel glasses can be made at lower temperatures ($< 100\,°C$) than those required for traditional glass melts ($> 1100\,°C$) [1]. This allows for organic molecules (e.g. chemical sensing molecules), which will not survive high temperatures, to be incorporated into the sol-gel glass in the early stages of its formation.

2.1.1 Sol-gel processing

The stages of the sol-gel process are shown in Figure 2.1. A sol is produced from a liquid mixture of precursor, solvent and catalyst. An example of a *precursor* is $Si(OC_2H_5)_4$ (tetra-ethoxy-silane, known as TEOS) where the central silicon atom is surrounded by

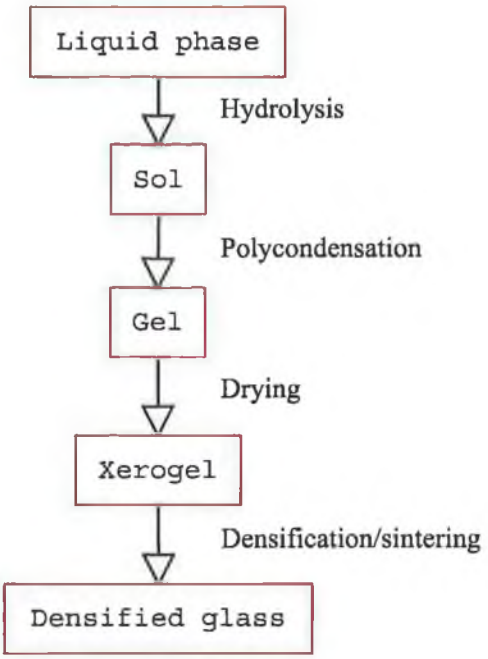

Figure 2.1: Outline of sol-gel process for glass fabrication.

ligands, which are in this case ethoxy groups. The *sol* is a colloidal suspension of solid particles in a liquid with particle size $< 1\,\mu$m, which results from the hydrolysis and polycondensation of the organic components. The sol stage of the process is the stage at which thin films are fabricated.

Progressive polycondensation increases the size of particles above $1\,\mu$m while forming the *gel*. The gel can be subject to temperature treatment which controls the drying and densification process and partially defines the structure of the final film (e.g. porosity).

The basic hydrolysis and condensation processes are described below. Parameters influencing kinetic reaction, methods for film formation and encapsulation of other materials into the sol-gel are also discussed.

2.1.2 Hydrolysis and condensation

A gel is created by hydrolysis and polycondensation of organometallic compounds (e.g. alkoxides), which are dissolved in solvent (e.g. alcohol) in the presence of a limited amount of water, using a mineral acid or base catalyst. *Hydrolysis* is the reaction which replaces alkoxide groups (OR) with hydroxyl groups (OH) by the nucleophilic attack on silicon

atoms by oxygen [1], forming the hydrolysed molecule and alcohol. R represents an alkyl group (C_xH_{2x+1}):

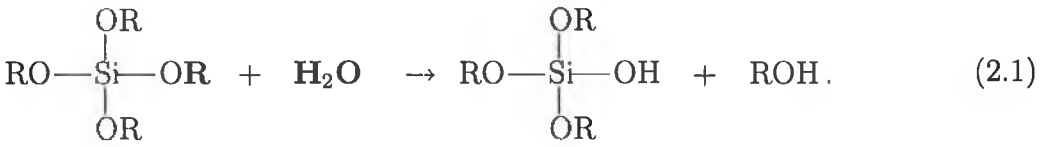

(2.1)

The process continues when two partially hydrolysed molecules of precursor link together in a nucleophilic condensation reaction producing siloxane bonds ($\equiv Si-O-Si\equiv$) and water as a by-product:

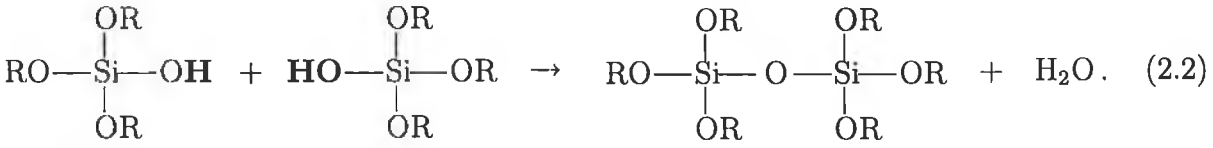

(2.2)

When one hydrolysed and one non-hydrolysed function group react the by-product formed is alcohol:

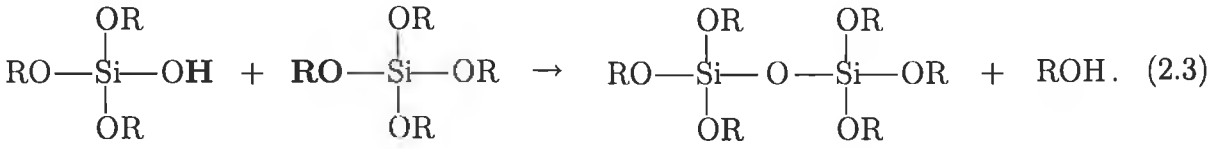

(2.3)

The process of hydrolysis and condensation proceeds to build polymeric networks of siloxane bonds. The functionality of a monomer (number of bonds which a monomer can form) defines the type of the network which can be formed. For a tetrafunctional monomer (shown in the example above) a branched 3-dimensional network can be formed. The gel is formed when such a network is created with pores of submicrometer dimensions and the sol can support stress elastically. The time needed for this process to finish is called the gelation time, t_g.

2.1.3 Aging and drying

Aging is the term used to describe the process that occurs after the components have been mixed together to form a sol and prior to the film deposition stage. The sol can be stored either at ambient or elevated temperatures and hydrolysis and condensation continue. This increases the connectivity of the sol-gel which increases its viscosity, which is necessary for film deposition.

Drying is the removal of excess liquid from the porous network leading to the formation of the dried gel or xerogel. The *xerogel* is a highly porous structure and this porosity plays a key role in the particular optical sensing application, in this case PSP.

2.1.4 Factors affecting structure

There are a number of variables that affect the hydrolysis and condensation rates and hence, the microstructure of the gel. These include temperature, type and concentration of catalyst (acid or base), type of solvent, type of alkoxide precursor and ratio of water to precursor, concentration of reactants, addition sequence, time of mixing and pressure. All of these factors play an integral part in the formation of the microstructure of the sol-gel material by varying the hydrolysis and condensation reactions rates. Of these parameters, the influence of water-to-precursor ratio and pH value will be discussed here.

Influence of water to precursor ratio (R value)

The R value is the molar ratio of water to metal (silicon) alkoxide precursor and it plays a significant role in the structural evolution of the sol-gel materials. Both the size of the sol-gel particles and the amount of cross-linking is dependent on the R value and pH.

Because water is produced as a by-product of the condensation reaction, an R value of 2 is theoretically sufficient for complete hydrolysis and condensation to yield anhydrous silica as shown by the net reaction [1]

$$n\,\mathrm{Si(OR)_4} + 2n\,\mathrm{H_2O} \rightarrow n\,\mathrm{SiO_2} + 4n\,\mathrm{ROH}\,. \tag{2.4}$$

However, this value has been shown to be insufficient for complete hydrolysis and condensation to occur. This is due to reverse reactions and a number of competing processes. Hence an R value greater than 2 is commonly used to complete hydrolysis before completing condensation and drying. Increasing the R value of the sol serves to promote hydrolysis, which in turn leads to a decrease in gelation time. However as the R value is further increased, the sol becomes more dilute, which increases the gel time due to the decrease in relative silica content. This relation is evident from Figure 2.2. The position of the minimum in the curve is dependent on the experimental conditions, in particular the pH of the reaction.

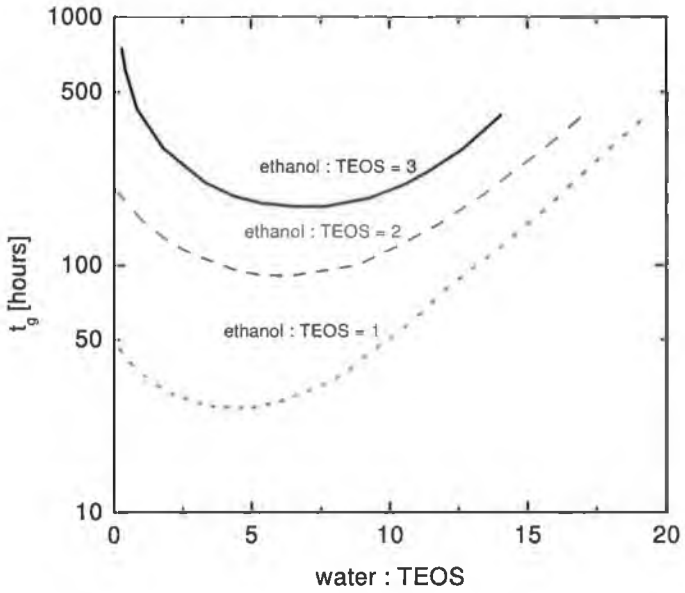

Figure 2.2: Variation of sol gelation time, t_g, with R value and ethanol to TEOS ratio [3].

Influence of sol pH

Numerous literature citations mention the sensitivity of the sol-gel chemistry and differences in gel structure to the preparation conditions [4]. The pH of the solution has a dramatic effect on the glass structure, creating monolithic structures under acidic conditions versus spherical particles under extreme basic conditions.

Silica has its isoelectric point at a pH value of approximately 2. This point represents the situation where the electron mobility and surface charge of the silica are zero. Therefore, a sol of $\mathrm{pH} < 2$ is said to be acid-catalyzed, while sols with pH higher than 2 are base-catalyzed. The characteristics of acid catalysis are fast hydrolysis and relatively long gel times, resulting in a fine network structure of linear chains with pore size $< 2\,\mathrm{nm}$. Base catalysis yields slow hydrolysis and increased condensation rates resulting in highly branched structure [1]. The gel time is maximal for pH value $1.5-2$ and minimal (the fastest reaction) for pH around 4 [5]. In this project, the optimum condition for the sol-gel-based PSP paint were found to correspond to $\mathrm{R} = 4$ and $\mathrm{pH} = 1$.

2.1.5 Organically modified silicates (ORMOSILs)

The surface of a standard alkoxide-based sol-gel film, for example using TEOS, is predominantly covered with hydroxyl groups (OH). As a consequence, the surface is hydrophilic (wettable) and supports the adsorption of a layer of water molecules, which coats the inside of pores. For some applications the hydrophilicity is undesirable and hydrophobicity is required. In sol-gel applications the commonly used technique to prepare hydrophobic materials is chemical modification of sol-gel precursors. Such modified precursors lead to materials known as ORMOSILs (ORganically MOdified SILicates). In this case the modified precursors have one or more alkoxy groups (OR) replaced with alkyl group (R'). The alkyl group is not hydrolysed and takes the place of the hydroxyl ions forming Si-R' group on the surface. These are non-polar and give rise to a hydrophobic surface.

A hydrophobic surface is necessary for the PSP application as the relevant mechanism of oxygen sensing involves the gas diffusing into the pores of the sol-gel paint, accessing the oxygen sensitive ruthenium complex which has been immobilised in the paint (see next Section 2.1.6) and subsequently giving rise to an oxygen dependent change in optical properties of the paint. The presence of adsorbed water molecules block the pores and impedes oxygen diffusion. Hence, a hydrophobic surface is desirable for effective oxygen sensing.

Another advantage of using ORMOSILs is decreased leaching of entrapped dye compounds from sol-gel films [6, 7]. In addition, films approximately 10 times thicker than those formed with standard TEOS-based recipe can be prepared with little or no cracking [8].

A typical example of an organically modified silicon alkoxide precursor is methyltriethoxysilane (MTEOS, $CH_3(C_2H_5O)_3Si$), in which a methyl group replaces one of the ethoxy groups. This precursor is used to form the PSP paint employed in this work.

2.1.6 Encapsulation of luminophores within the sol-gel matrix

Encapsulation of molecules

Sol-gel materials have advantages over polymers as host matrices for sensor molecules, for example: better optical quality and the ability to tailor the matrix for specific applications. Sol-gel matrices can be used to entrap sensor molecules (large organic molecules), while, due to the porous nature of the material, allowing analyte molecules (low molecular

weight) to diffuse into the matrix. These characteristics of sol-gel films have been exploited in a large variety of sol-gel-based optical sensors for different analytes including oxygen [9], carbon dioxide [10, 11], ammonia [12], pH [13, 14], and water vapour [15].

Sensing molecules can also be entrapped by direct covalent bonding with the sol-gel matrix. This eliminates the possibility of dye leaching but occasionally covalent bonding can alter the luminescence properties of fluorescent species, for example, reducing sensitivity.

Post-doping can also be used, however, in this case the reagent is immobilised by very weak forces of chemi– or physi– sorption, which makes such materials problematic in conditions when leaching can be a problem. For this project, encapsulation in a sol-gel matrix is employed and provides a robust support for the desired sensing mechanism to occur.

Encapsulation of powder particles

In some cases the sensing compound is not available in soluble form. This is the case for the magnesium-fluorogermanate-based temperature sensor (Section 2.3.1). The material is in the form of grains of a crystalline phosphore. The grain size is larger than the pore size of the sol-gel and this can influence the process of condensation in the vicinity of grain. The surface tension between the sol-gel and powder can cause the precipitation of the powder from the film giving rise to an inhomogeneity between the film and sol-gel. Strategies for overcome this problem depend on coating method and are described in Section 2.1.7.

Response time

In the paint, the sol-gel (binder) serves as a transport medium for oxygen to be delivered and quench molecules of the dye and therefore must be permeable to oxygen and have a suitably high diffusion coefficient, D, of oxygen. This is true for porous sol-gels. Engler [16] noted that the relaxation time of the paint associated with a step change in pressure is

$$t_{\text{relaxation}} = \frac{4h^2}{\pi^2 D}, \tag{2.5}$$

where h is the thickness of the paint. For a typical MTEOS-based film the response time is in the range of tens of milliseconds [17]. Furthermore, the response time cannot be less

then the lifetime of the used luminophore.

Some authors have reported direct attachment of the sensing dye to the surface without using any binder. Direct attachment is realised on anodised aluminium (AA), when the dye is adsorbed to the microporous structures at the surface [18]. As limited diffusion is involved, the response time is fast. However, the application is limited to metal surfaces such as aluminium, which limits the use of the method in PSP.

2.1.7 Coating methods

Four techniques used for thin film coating are described in the following paragraphs — dip–, knife–, spin– and spray–coating.

Dip-coating

Dip-coating is the simplest method of deposition of the sol onto a substrate. The substrate is immersed into the sol and then withdrawn at a constant speed upwards. The dip-coating process can be divided into five stages [1]: immersion, start-up, deposition, drainage and

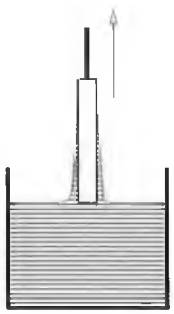

Figure 2.3: Schematic of dip-coating.

evaporation. The theoretical description of film formation is nontrivial and the result is determined by a selected viscosity model of the sol. For Newtonian fluids the relation between film thickness, t, and dip speed, U, can by calculated by the Landau-Levich equation [19] as

$$t = 0.94 \frac{(\eta U)^{2/3}}{\sigma^{1/6}(\varrho g)^{1/2}}, \tag{2.6}$$

where ϱ is solution density, g is acceleration due to gravity, η is the dynamic viscosity and σ is the surface tension. Clearly, if all the other factors are constant, the film thickness is

proportional to the withdrawal speed $U^{2/3}$. Therefore thickness increases with dip speed.

Typically dip-coating can be used to coat films on planar substrates.

Knife-coating

Knife coating, also known as spread coating or blade coating, is a technique where the sol is deposited onto the substrate and excess sol is then swept away by the blade. The thickness of the deposited film is defined by the distance between blade and the substrate, speed of motion, contact angle of blade and viscosity of the sol [20]. The method itself could be adapted for continual coating and therefore is popular in industry when high throughput is required. Reproducibility of deposited films using this method is relatively

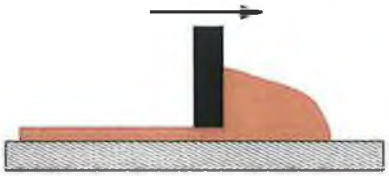

Figure 2.4: Schematic of knife-coating.

poor comparing to dip and spin-coating. Also knife-coating is suitable only for planar surfaces, which limits its application in PSP.

Spin coating

Spin coating is a method employing centrifugal force to dispense the material homogeneously onto the substrate and create uniform films. Figure 2.5 illustrates the spin-coating process. The substrate is held in a horizontal position (typically on a vacuum chuck) and the liquid material is dispensed close to the axis of rotation. The chuck is then programmed to rotate at a predefined acceleration (ramping), until the final speed is reached. The rotation of the substrate causes the material to spread over the surface of the substrate due to centrifugal force. Excess material is drained at the edges of the substrate.

The film thickness is the result of the balance between centrifugal and viscous drag forces. Adding the condition of mass conservation it can be shown that the film thickness is completely independent of any radial dependence [21], provided that the viscosity is not shear-dependent and does not vary over the substrate.

As the film becomes thinner, the ratio of surface to volume grows and the evaporation becomes the driving force behind thinning. The final film thickness depends on the angular velocity of rotation, number and duration of ramps, density and viscosity of material [22]. As the evaporation and gelation, induced by increased concentration of sol, influence viscosity, the prediction of film thickness using the theoretical model can be inaccurate for sol-gels with short gelation times.

Figure 2.5: Schematic of spin-coating.

The technique offers several advantages over dip-coating including the ability to deposit films on a single side of a substrate without masking. It is compatible with a broader range of viscosities and has improved film uniformity [23]. Spin coating is not compatible with coating of non-planar surfaces used in PSP but was used extensively for the production of samples for characterisation.

Spray coating

Spray coating is a method especially suitable for coating of irregularly shaped objects. It uses compressed gas for forming an aerosol from the sol which is then sprayed onto a sample. Figure 2.6 shows the setup for spray-coating. Pressurised gas (e.g. nitrogen or air) enters from the left, draws sol from the container and mixes with it, forming an aerosol, which is driven from the nozzle by the gas flow onto the sample. The droplets in the aerosol are subject to rapid evaporation as the surface-to-volume ratio is high. The droplet size is inversely proportional to the gas pressure and proportional to the nozzle size [24].

The wetting properties and roughness of the surface are important for continuous coating [25].

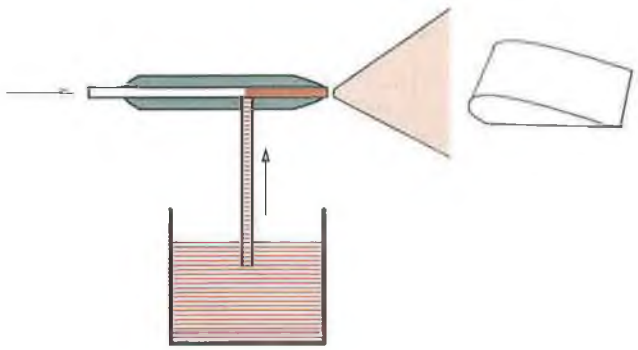

Figure 2.6: Schematic of spray-coating apparatus.

The thickness of the film is determined by the duration of spraying and in general, produce a homogeneous film without precipitation of powder particles. Moreover, the wasted sol is minimised compared to other methods.

2.1.8 Comparison of coating techniques

All of the above methods have been used during the course of this project. Dip and spin-coating produce very reproducible results. Spin coating is capable of producing samples with homogeneous thickness across large areas. The dip-coated films are usually wedge shaped with a thicker film at the bottom of the sample.

Dip and spin-coating methods are not optimal for coating sol with dispersed powder suspension as the forces forming the thin film can segregate the powder particles giving rise to an inhomogeneous film. From this point of view, spray-coating is more effective.

For characterisation of PSP the coated samples are usually planar, and therefore compatible with all the above methods. But if real models for aerodynamic test are to be coated, dip-coating becomes impractical due to the large amount of sol required (typically comparable to the volume of the coated object) and spin– or knife– coating are totally unusable. Spray coating is again the most attractive as only a few millilitres of sol are required for coating large objects.

Although optical quality and homogeneity of films produced by spray-coating is relatively poor compared to other techniques (partially due to manual spraying), for the PSP technique described here, the uniformity of film thickness is, in principle, not essential. The PSP system must compensate for other sources of non-uniformity over the surface

of the object, for example, the variation of intensity of illumination and temperature variation.

In summary, in this work, a combination of dip and spray-coating was used for sample preparation. Occasionally, spin-coating was used when high uniformity over a large sample area was desired.

2.2 Transition metal complexes for oxygen sensing

As stated previously, transition metal complexes are excellent candidates for luminescence-based oxygen sensing applications due to their large Stokes shift, long unquenched lifetime and high quenching sensitivity.

2.2.1 Electronic states of transition metal complexes

Transition metal complexes are characterised by partially filled d-orbitals [26]. The d-orbitals are associated with the metal, for example ruthenium has six d electrons. The presence of the ligands splits the five degenerate d-orbitals into triply degenerate lower (t_2) and doubly degenerate higher (e) orbitals as illustrated in Figure 2.7 on the left. The splitting, Δ, arises from the different spatial orientations of the orbitals in relation to the ligands and is determined by the crystal-field strength, which is determined by the geometry, ligand and type of metal atom [27].

The organic ligands have π and σ orbitals, but only the π orbitals are spectroscopically important in UV and visible spectroscopy. The bonding π levels are filled, antibonding π^* are vacant.

The spectroscopic states are derived from a combination of orbital configurations shown in Figure 2.7 on the right. In the ground state, all electron spins are paired. The total spin is zero, which makes the ground state singlet state. There are tree types of excited states – (1) metal centered d–d states, (2) ligand localised π–π^* states and (3) metal-to-ligand charge transfer transitions (MLCT).

The transition between the d-orbitals on the metal atom ($t_2 \rightarrow e$) is formally forbidden and therefore d–d transitions are weak, characterised by low radiative rate and weak emission. The π–π^* transitions are localised on the organic ligands and typically, are very similar to the corresponding transitions of free ligands. Principally, the new excited

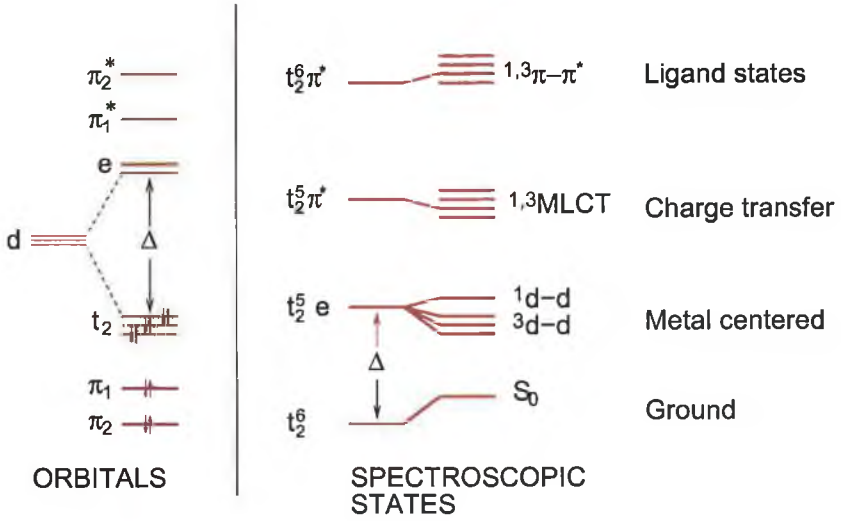

Figure 2.7: Simplified orbital and electronic states of metal-ligand complexes. Each arrow represents an electron with its associated spin. The *d* orbitals are associated with the metal and are split by energy Δ due to the crystal field strength. Splitting is strong enough so the t_2 orbitals are filled.

state is a MLCT transition when both metal and organic ligands are involved. For ruthenium complexes, the metal-to-ligand charge transfer transition arises from promoting an electron from a metal orbital to a ligand orbital ($t_2^5\pi^{*1}$ configuration). The MLCT transitions tend to be strongly allowed compared to *d*–*d* transitions, therefore, they have short radiative lifetimes and are more easily accessible for optical pumping due to spin-orbit coupling [26, 27].

As the light emission always occurs from the lowest excited state, for luminescence to occur, the crystal field must be strong enough to raise the *d*–*d* state above the MLCT state (Figure 2.7 represents only weak separation). If such a condition is not fulfilled the complex is non-luminescent due to low situated non-luminescent *d*–*d* states (e.g. in iron organic complexes).

The separation of the MLCT states and *d*–*d* states determines the sensitivity of the decay times (and quantum efficiency) to temperature. If these states are close together, then thermal excitation of *d*–*d* states increases with increasing temperature and is followed by rapid radiationless decay.

2.2.2 Ruthenium complexes and oxygen quenching

The complex used for this work, for its large Stokes shift, excellent photostability and long unquenched lifetime, is Ru(II) tris-(4,7-diphenyl-1,10-phenanthroline)*, whose structure is shown schematically in Figure 2.8.

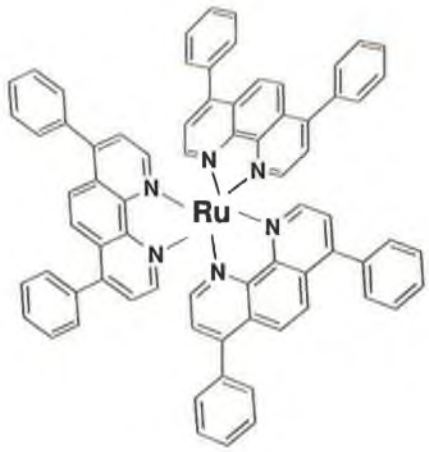

Figure 2.8: Model of molecule of ruthenium complex – $[Ru(dpp)_3]^{2+}$.

A Jabłoński diagram for $[Ru(dpp)_3]^{2+}$ is shown in Figure 2.9 [26]. After absorption,

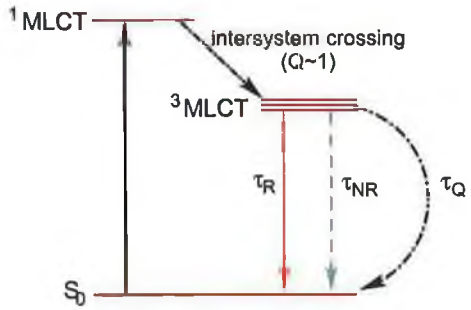

Figure 2.9: A simplified Jabloński diagram for a metal-ligand complex of $[Ru(dpp)_3]^{2+}$, including dynamic quenching channel.

the complex undergoes fast and efficient intersystem crossing to the triplet MLCT state, with a relatively long lifetime (star represents the excited complex):

$$D + h\nu \rightarrow D^* . \tag{2.7}$$

*often this complex is shorten in form of $[Ru(Ph_2phen)_3]^{2+}$ or $[Ru(dpp)_3]^{2+}$.

From this triplet state either emission with radiative lifetime τ_R occurs

$$D^* \rightarrow D + h\nu \tag{2.8}$$

or the non-radiative decay with non-radiative lifetime τ_{NR}

$$D^* \rightarrow D + \Delta \tag{2.9}$$

or quenching by the environment is observed with quenching lifetime τ_Q

$$D^* + Q \rightarrow D + Q^* . \tag{2.10}$$

A long lived triplet state is ideal for oxygen sensing, because, unlike other molecules, the ground state of molecular oxygen is a triplet state and energy transfer between molecules is allowed when the energy donor and the energy acceptor have the same spin multiplicity (in this case triplet).

A relatively long lifetime of the excited state allows for an oxygen molecule to interact with the excited state and quench it. This gives excellent sensitivity of $[Ru(dpp)_3]^{2+}$ to oxygen. However, the long lived excited state is also sensitive to the environment and for reliable sensing must be shielded from other oxidants. This is achieved by embedding the sensing molecule in the gas permeable and solvent impermeable membrane. Candidate materials for membranes are polymers or sol-gel materials as discussed in section 2.1.6.

Generally, the Stern-Volmer plot (Equation 1.4) for quenching of ruthenium complexes embedded in amorphous solid matrices is nonlinear. This nonlinearity is a consequence of the sensing molecules being located in two or more sites characterised by different quenching constants K_q (Equation 1.5). This matrix inhomogeneity gives rise to downward curved plots. The nonlinear Stern-Volmer plot can be explained by a three parameter Stern-Volmer equation [28]. This non-linear behaviour with oxygen concentration for an amorphous solid host is in contrast with the observation in solution, where theoretically predicted linear dependence in Stern-Volmer plots is rigorously observed.

The $[Ru(dpp)_3]^{2+}$ complex exhibits excellent sensitivity to oxygen. The emission intensity decreases by about a factor of 4 on going from nitrogen to an atmosphere of pure oxygen, for typical sol-gel paints.

2.2.3 Spectral properties of $[Ru(dpp)_3]^{2+}$

Optical excitation and emission spectra of $[Ru(dpp)_3]Cl_2$ complex are shown in Figure 2.10. Both were obtained with Spex FluoroMax 2 spectrofluorometer (Jobin Yvon

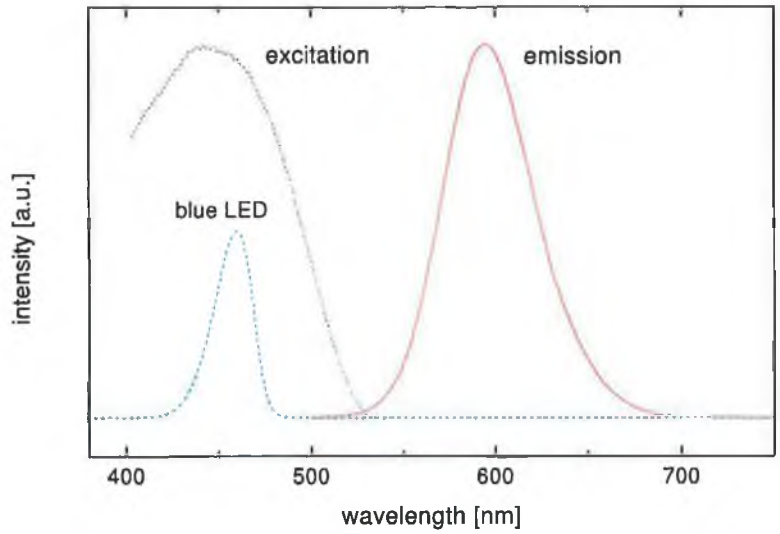

Figure 2.10: Emission and excitation spectra of $[Ru(dpp)_3]Cl_2$ complex. Excitation spectra acquired with detection at 600 nm, emission spectra with excitation at 450 nm.

Inc., Edison, NJ, USA) in ethanol solution. The emission exhibits a maximum at around 600 nm in the red, while excitation is most efficient around 450 nm in the blue region. For comparison, a blue LED (Nichia NSPB500) emission spectrum is superimposed, showing the good overlap with the excitation spectra.

2.2.4 Other types of optical oxygen sensors

In addition to the ruthenium transition metal complexes, other types of fluorophores are used for pressure-sensitive paints, for example porphyrins. A porphyrin is a heterocyclic macro-cycle made from four pyrrole subunits linked on opposite sides through four methine bridges and can be used for oxygen sensing when coordinated with Pt^{II}/Pd^{II} atoms [29]. The oxygen sensitivity of porphyrins is extremely high so at ambient conditions the luminescence is usually completely quenched which makes it unfavourable in PSP systems. The extreme sensitivity can be reduced by a low oxygen permeable binder.

2.3 Temperature sensitive phosphors

2.3.1 Manganese activated magnesium-fluorogermanate (MFG)

Magnesium-fluorogermanate (MFG) is a thermographic phosphor which is commonly used for colour correction of high pressure mercury-vapour lamps [30] and has also been used in commercial fibre optic temperature sensing applications [31, 32]. Excitation of the activator, Mn^{4+}, gives rise to a temperature-dependent, phosphorescent decay ($\tau \sim 3.5\,\mathrm{ms}$).

Depending on the composition on the matrix (content of magnesia) it can take different content of quadrivalent manganese into the lattice. It was shown that the composition $3.5MgO\,0.5MgF_2GeO_2$ gives a lattice capable of incorporating the largest amount of quadrivalent manganese Mn^{4+}. The concentration of 0.8% by weight of manganese is adopted in commercially available phosphors as it gives highest fluorescence emission, maximum temperature stability and highest inversion point (around 250 °C) [30].

The photoluminescence of MFG is caused by the quadrivalent Mn^{4+} which serves as activator. The quadrivalent state of manganese is in $3d^3$ configuration and paramagnetic resonance measurements indicate a surrounding of oxygen ions in octahedral symmetry [33].

It is well known that ions, incorporated in a crystal lattice, are subjected to internal electric fields (crystal fields) which cause splitting and mixing of the electron energy levels of the isolated ions and the exact splitting depends on the strength of the crystal field and the geometry of the neighbouring ions. Approximate calculations of such splitting for $3d^3$ electron configurations in octahedral crystal fields was done by Tanabe *et al.* [34] and the result is in Figure 2.11. The diagram shows the difference in electronic energy ΔE relative to the ${}^4A_2$ ground state as a function of the parameter Dq of the crystal field strength.

On the left hand side of the diagram are states of the free Mn^{4+} ion. Each of these splits up into various components. The ${}^4F$ ground state of the free ion splits into three components labelled ${}^4F_2$, ${}^4F_1$ and ${}^4A_2$. According to Kemeny and Haake [35], the optical absorption occurs from the ground state ${}^4A_2$ to threefold degenerate ${}^4F_2$ and ${}^4F_1$, as the energies observed in the absorption spectra (Figure 2.13) cannot be explained for absorption into different states. Moreover, the transitions into doublet states are far less probable because of the necessary spin flip.

Thus, the centre absorbs at $Dq \approx 240\,\mathrm{cm}^{-1}$ into the states ${}^4F_2$ ($24\,000\,\mathrm{cm}^{-1} \approx 417\,\mathrm{nm}$)

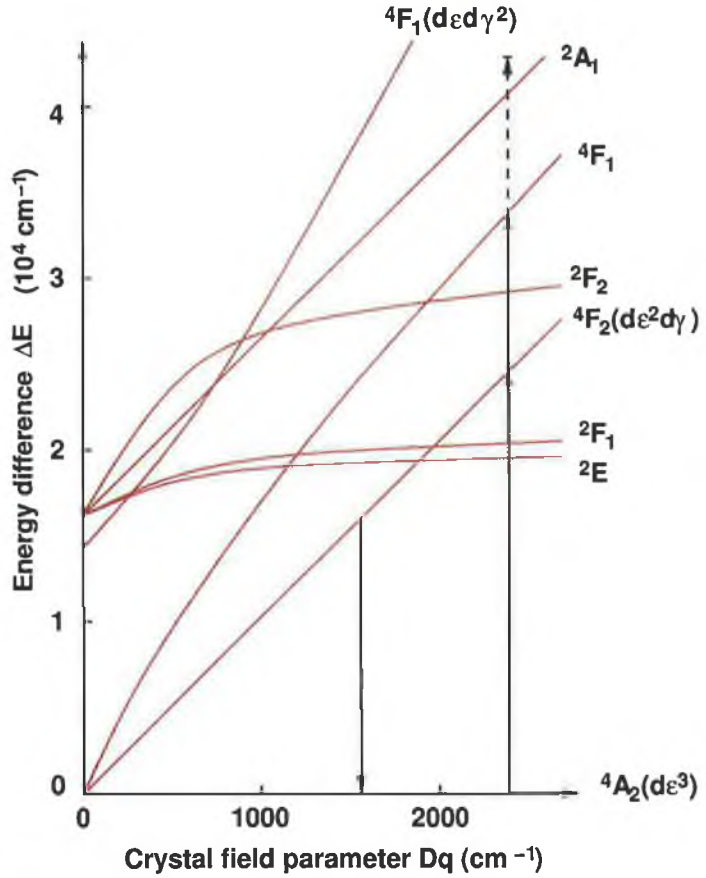

Figure 2.11: Electronic energy difference relative to the $^4A_2$ ground state as a function of the crystal field parameter Dq for the Mn^{4+} ion in octahedral symmetry [35].

and $^4F_1$ ($35\,000\,\mathrm{cm}^{-1} \approx 285\,\mathrm{nm}$).

The de-excitation, return to the ground state $^4A_2$, follows strong lattice relaxation, i.e., a lowering of Dq. Regardless of whether absorption takes place into the lower or higher state ($^4F_2$, $^4F_1$), the emission spectrum always exhibits the same shape, with a wavelength around 645 nm. Thus, only one excited state is involved in the emission. Considering the energy difference, the most likely is the $^4F_2$ state. Electrons excited to the higher states fall non-radiatively into the $^4F_2$ state from which radiation occurs.

The mechanism of this transition cannot be represented in this Dq diagram (Figure 2.11) since there is no value of Dq at which energies of these two excited states are equal (except $Dq = 0$). Energy crossover, therefore, must involve another degree of freedom not shown in the Figure 2.11.

The emission spectrum (Figure 2.12 and Figure 2.13) also shows two close peaks at

around 630 nm and 660 nm, whose relative intensity is temperature dependent [30], but their separation is too small to be both from $^4F_2$ and $^4F_1$. It is assumed therefore, that the threefold degenerate $^4F_2$ state is split and splitting is caused by the Jahn-Teller effect [36]. If the center were in perfect octahedral symmetry, only one group of peaks would appear in the emission spectra, which is contradictory to the experiment. Because of the tetragonal or trigonal distortion, another configuration coordinate, Q_2, must be introduced in addition to Q_1 (corresponding to Dq in Figure 2.11, characterising the crystal field). The threefold degenerate state $^4F_2$ is split into a twofold degenerate and non-degenerate level. The two levels are named $^4F_2'$ and $^4F_2''$. Figure 2.12 explains the structure of the spectrum. The group of peaks around 630 nm is represented by the transitions a, b and c from $^4F_2''$ to $^4A_2$. More transitions are possible (and observed) from $^4F_2'$ to $^4A_2$.

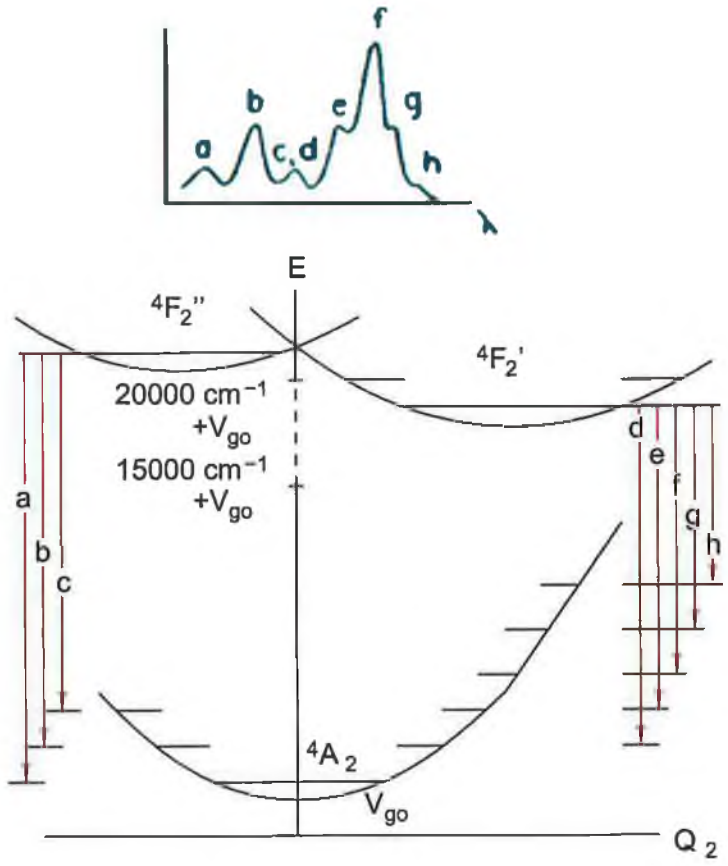

Figure 2.12: Total energy diagram of $^4A_2$, $^4F_2'$ and $^4F_2''$ as a function of Q_2 (corresponding do x-axis). Individual emission peaks are correlated to specific transitions [35].

The occupancy of both excited states ${}^4F_2''$ and ${}^4F_2'$ is in thermal equilibrium. Thus, it is clear that increasing the temperature causes the intensity of the emission in the group around 630 nm to increase at the expense of the emission intensity of the group around 660 nm. Applying kinetic equations to this model one can calculate the temperature dependence of the observable lifetime as

$$\tau^{-1} = \gamma + \frac{\gamma_q \, \mathrm{e}^{-V_q/kT}}{1 + 2\,\mathrm{e}^{-\Delta V/kT}}, \tag{2.11}$$

where γ is the probability of radiative transitions ${}^4F_2', {}^4F_2'' \rightarrow {}^4A_2$ ($\gamma \approx 287\,\mathrm{s}^{-1}$), γ_q is the probability of non-radiative transitions (temperature quenching) and $\gamma_q \approx 10^{12}\,\mathrm{s}^{-1}$, V_q is the quenching energy ($V_q \approx 1.36\,\mathrm{eV}$) and ΔV is the energy difference between states ${}^4F_2'$ and ${}^4F_2''$ ($\Delta V \approx 32.9\,\mathrm{meV}$), k is Boltzmann constant and T is temperature. The slight deviation of experimentally observed lifetime to the Equation 2.11 at low temperature is probably explained by the increasing asymmetry of the instantaneous positions of the Mn-ion with respect to the surrounding oxygen ions. The observed decay is reported to be purely exponential [35].

The reported increase in total emission with temperature, when not excited in resonance with the excitation peaks, can be easily understood. Before the temperature quenching can interfere, the absorption occurs from higher phonon levels of the ground state and therefore, the atomic absorption coefficient, α, increases with temperature. Thus, total emission increases. The increase in absorption coefficient α is confirmed in transmission measurements. For resonant excitation the absorption is only slightly dependent, as the absorption takes place mostly from the lowest level of the ground state.

Finally, the excitation and the emission spectra of MFG:Mn (donated by Meldform Metals Ltd., England) is presented together with emission of blue and UV LED (460 nm and 376 nm) in Figure 2.13. The maxima in excitation spectra lie near 420 nm and around 300 nm. The group of emission peaks, discussed earlier, appear between 620 and 670 nm, with maxima at around 655 nm and 630 nm.

The difference in intensity of emitted light while excited by blue and UV LED is negligible. For safety reasons, the harmless light source (blue LED) would be more preferred for PSP measurements performed in open environments, such as wind tunnels.

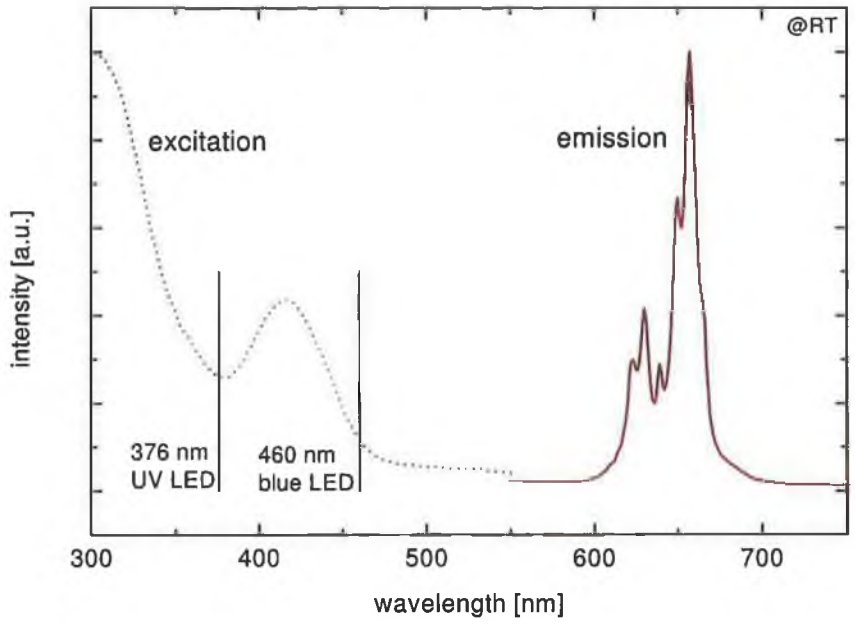

Figure 2.13: Emission and excitation spectra of manganese doped magnesium-fluorogermanate (MFG) complex at room temperature. Excitation spectra acquired with detection at λ_{em} = 657 nm, emission spectra with excitation at λ_{ex} = 420 nm.

2.3.2 Europium doped yttrium oxide

Europium doped yttrium oxide (Y_2O_3:Eu) is an efficient red-emission phosphor and has been used in fluorescent lights, as well as being widely used in cathode ray tubes (CRT), plasma displays and field emission displays (FED) [37]. The Y_2O_3 matrix shows excellent chemical stability and therefore is often used as base matrix to be doped with various ions. Y_2O_3:Eu is traditionally prepared by a high-temperature solid-state reaction at 1400–1500 °C for several hours. Recently a new method of preparation by a sol-gel method was demonstrated [38].

The distinct luminescence spectra of this material correspond to Eu^{3+} ion and its $4f$ electrons as no transition between the activator and a solid state band is present [37].

The excitation and emission spectra of Y_2O_3:Eu (6.5% of Eu), donated by Sylvania Osram, are shown in Figure 2.14. It shows relatively narrow emission and excitation lines. The narrow excitation line means that Y_2O_3:Eu requires an excitation source tuned to this line, which limits the number of potential light sources.

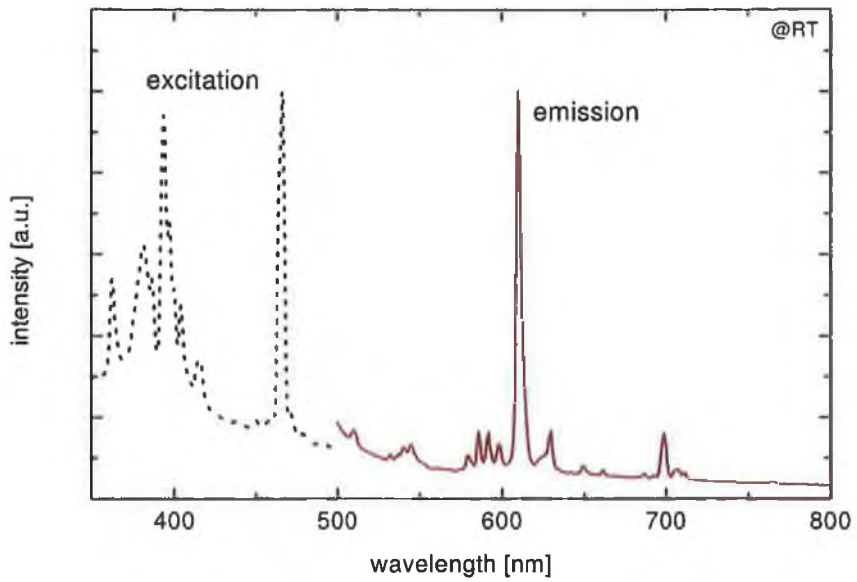

Figure 2.14: Emission and excitation spectra of Y_2O_3:Eu at room temperature. Excitation spectra acquired with detection at $\lambda_{em} = 610\,nm$, emission spectra with excitation at $\lambda_{ex} = 420\,nm$.

2.4 Instrumentation and characterisation techniques

As mentioned previously, the experimental arrangement for PSP consists of three parts: (i) the light source, (ii) the paint and (iii) the detector system. The paint has already been described in Section 2.1, while sources and the detection system will be discussed in the following paragraph. In this section the instrumentation for varying gas pressure will be described as well as the temperature control system used. At the end of the section, various ancillary techniques used in the project will be described.

2.4.1 Light sources for PSP

Continuous light sources

For intensity based PSP systems, very stable and intense light sources are required. The source needs to be matched to the spectral properties of the paint. High intensity of the source allows for shorter exposure times and measurements over large surfaces. Xenon and mercury lamps [39] or tungsten halogen lamps [40] equipped with appropriate spectral filters have been widely used. An integral part of the light source is a stabilised power

supply. Some pulsed light sources described below can be used for continuous illumination as well. Lasers are also used in PSP applications, for example 337 nm emission from a nitrogen line [41].

Pulsed light sources

For lifetime-based measurements, pulsed or modulated sources are required.

Q-switched Nd:YAG lasers have been widely used. Usually, the second (532 nm) or third (355 nm) harmonics are used for excitation [42]. Use of xenon flash lamps has also been reported [39]. With the recent advances in production of semiconductor light sources for the next generation of DVD players, the blue and ultraviolet light emitting diodes have became readily available. These wavelengths are suitable for excitation of some of PSP/TSP luminophores and are also easily modulatable.

2.4.2 Blue LED bank

In this work, an externally triggered multi-LED bank PRS100B (Photonic Research Systems, UK) was employed. The LED bank consists of an array of 10 × 10 blue LEDs (Nichia, Japan) and a blue short pass filter is used to filter the long wavelength tail of radiation. It is controlled by a TTL input where HI corresponds to the LEDs switched on, and LO corresponds to the LEDs switched off. The emission peak is at 460 nm. It can be modulated up to frequencies in the MHz region. For some experiments we used a UV-LED bank (PRS100UV) with emission at 376 nm.

2.4.3 Detection system

The detection systems consists of collection optics, optical filters and the light detector. The selection of the filters is important and ideally, the excitation and detection filters should be spectrally crossed to block excitation light from the detector. For time-resolved measurements, the filters are not necessary if the luminescence light collection occurs in periods when the excitation light is off and could lead to "filter-free luminescence detection" [43].

Two different cameras systems were used in the course of this project: an image-intensified gated CCD camera (DiCAM Pro, PCO, Germany) and interline frame transfer CCD camera system (Imagex 2000, Photonic Research Systems, UK).

DiCAM Pro camera

The DiCAM Pro (PCO, Germany) is a 12 bit image-intensified gated CCD camera. A schematic diagram of the camera is shown in Figure 2.15. Light incident on the camera microchannel plate (MCP) (Hamamatsu V7670U-70) is intensified and later detected by the CCD chip, which is cooled by a Peltier cooler down to $-11\,°C$. The MCP, through its gated gain, is used as a fast shutter. The CCD chip contains 1280×1024 pixels (SVGA

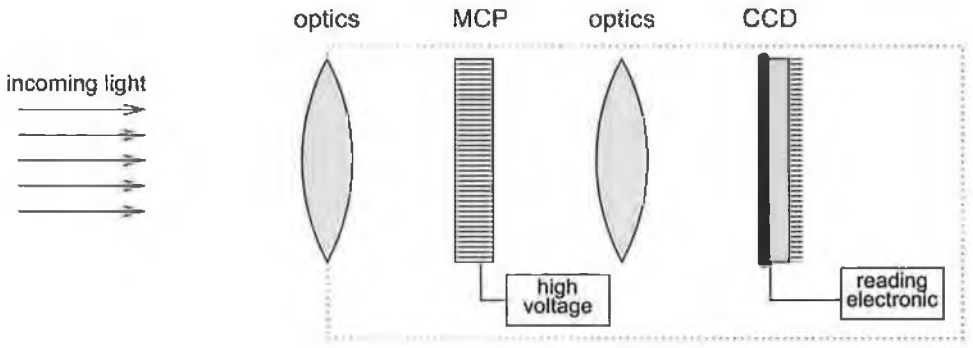

Figure 2.15: Function diagram of gated CCD camera DiCAM Pro. Light entering camera is focused to the MCP, amplified and focused onto CCD chip.

resolution), each pixel of size $6.7\,\mu m \times 6.7\,\mu m$ and full well capacity $25\,000\,e^-$. The analog to digital conversion factor is $5\,e^-$/count and the scan rate is 12.5 MHz with readout noise 7–8 e^-. Internal binning in the camera is possible between 1...8 pixels and 1...32 pixels horizontally and vertically, respectively.

The camera is capable of exposure times down to 3 ns [44] and the exposure can be TTL triggered externally. The delay time between the triggering pulse and the exposure is variable in steps down to 20 ns. All the camera parameters are computer controlled [45].

Imagex 2000 system

The second camera used was an Imagex 2000 system (Photonic Research Systems, UK).It is a phase-sensitive system for luminescence lifetime measurements with quoted resolution $< 1\,\mu s$. The system comprises a modulated interline transfer CCD camera, interface and modulated light source PRS100B (or other). The resolution of the CCD chip is 752×582 pixels at 14 bits per pixel with correlated double sampling and attached cooling to 40 °C under room temperature with peak sensitivity at 550 nm and 50% sensitivity at 430–

730 nm. The interface allows for modulation of light sources in discrete steps up to 500 kHz. The read out time is 0.8 s for medium resolution and 3 s for high resolution [46].

2.4.4 Trigger circuit

A special triggering circuit was designed to allow for computer control of the excitation frequency and to correct phase shift between signals for triggering of the excitation source and the camera. The circuit allows discrete frequencies from 1 MHz down to millihertz to be set. Available frequencies are given in table B.1 and a detailed description of the circuit is in Appendix B.

2.5 Other techniques and tools

Spectroscopy

Most of the spectra shown were obtained using a Spex FluoroMax 2 spectrofluorometer (Jobin-Yvon Inc., USA).

Optical filters

In order to avoid damaging the camera's image intensifier by exposing it to spurious light, a long-pass Schott glass OG550 filter was fitted to the objective. For the phase measurements the polyester optical filters of red (Lee #135) and blue (Lee #168) colour were utilised (LEE Filters, UK [47]).

Mass flow controllers

To emulate pressure changes, various concentrations of oxygen in nitrogen were employed, both from compressed gas bottles (BOC Gases, Ireland). The concentration was controlled by two mass flow controllers C7300 (Unit Instruments, Ireland) of maximum flow rate 2 l/min.

The whole gas-mixing system was managed by a personal computer running a LabVIEW 6*i* program (Figure 2.16). It allowed automatic remote control of concentration (0–100%) and total flow (0–2 l/min). The program provided log file with date, time, concentration, flow and temperature (read through the thermocouple).

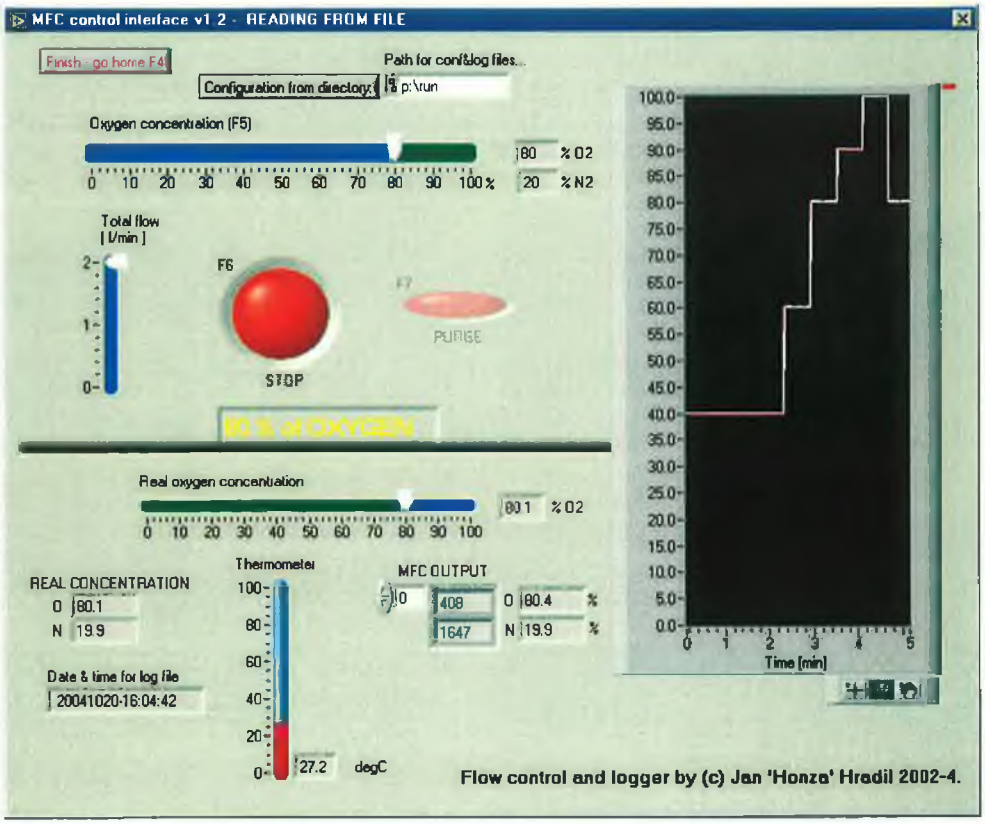

Figure 2.16: Screen of remotely controlled LabView program for concentration control.

Direct lifetime measurements with PMT

Direct lifetime measurements with a photomultiplier tube were taken using a pulse generator PG501 (Tektronix), single Nichia-blue LED or PRS100B blue LED bank, photomultiplier tube 1P28 (Hamamatsu, Japan) with high voltage power supply PM 28B (E.M.I. Electronics Ltd., UK) and HP 54600A oscilloscope (100 MHz) with data read-out through RS-232 into a personal computer.

Flow cell

Samples were characterised in an air-tight flow cell of volume approx 22 cm^3 fitted with two glass windows at adjacent walls of the cell. The cell is shown in Figure 2.17. The sample itself was held in a holder at approximately 45° to the windows. For large samples (e.g. full 4" wafer) a large flow cell was constructed with a perspex window forming the front wall of the flow cell. The total volume of the large flow cell shown in Figure 2.18 is

Figure 2.17: Flow cell (5 × 3 × 1.5 cm) with gas heater attached on the left side for sample characterisations (concentration and temperature runs).

approximately 1600 cm^3.

Air heater

When the calibration required elevated temperature, the passing gas mixture was heated prior to entering the flow cell by an air heater RS 200-2480 (Radionics, Ireland) of maximum power of 200 W at 240 V.

Phase measurements

For the phase measurements with the fibre-optic high-spatial-resolution probe, signal processing was carried out using the 7225 DSP Lock-in amplifier (AMTEK, Inc., Signal Recovery, USA) [48].

Coating

The spray-coated samples were sprayed with an airbrush obtained from a Sprite Major Airbrush Kit (Devilbiss Aerograph, UK), with nitrogen as the driving gas. The dip-coated samples were coated using an in-house computer-controlled dip-coater at typical speeds of 3 mm/min. Spin-coated samples were prepared with a spin-coater, model P6712 (Specialty Coating Systems, USA).

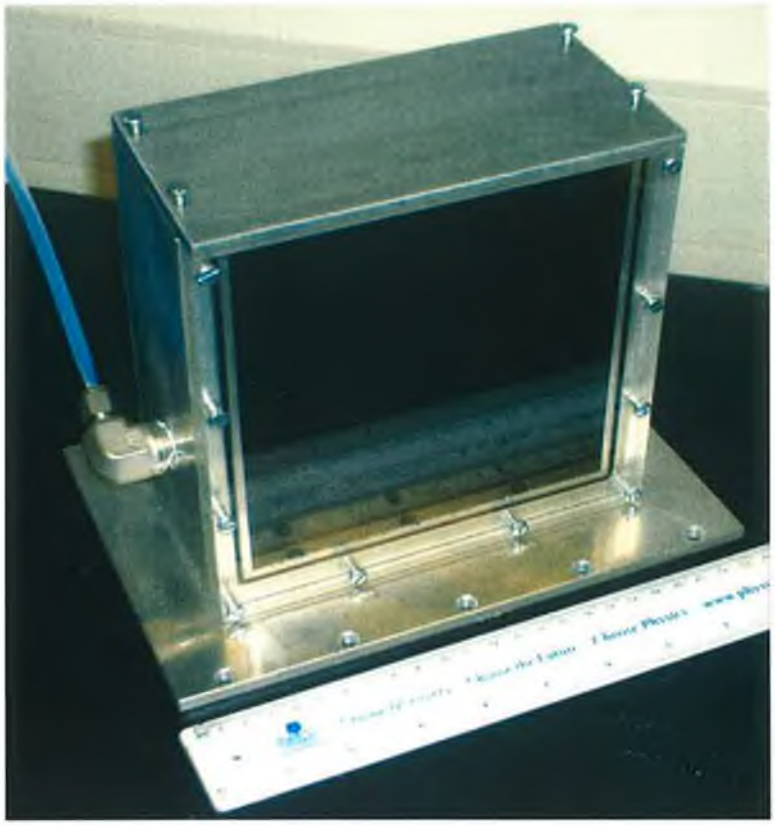

Figure 2.18: Large flow cell (15 × 14.5 × 7.5 cm) for sample characterisations.

2.6 References

[1] C. J. Brinker and G. W. Scherer, *Sol-gel science: The physics and chemistry of sol-gel processing.* Boston: Academic Press, 1990.

[2] L. L. Hench and J. K. West, "The sol-gel process," *Chem. Rev.*, vol. 90, pp. 33–72, 1991.

[3] L. C. Klein, "Sol-gel processing of silicates," *Ann. Rev. Mater. Sci.*, vol. 15, pp. 227–248, 1985.

[4] D. Cropek, P. Kemme, J. Day, and J. Barrios, "Sol-gel stabilization of heavy metal waste," Tech. Rep. ERDC/CERL TR-00-6, US Army Corps of Engineers Engineer Research and Development Center, 2000.

`http://owww.cecer.army.mil/TechReports/cropek_solgel_stabilization/cropek_solgel_stabilization.post.pdf`.

[5] C. J. Brinker, K. Keefer, D. Schaefer, and C. Ashley, "Sol-gel transition in simple silicates," *J. Non-Cryst. Solids*, vol. 48, p. 47, 1982.

[6] R. Makote and M. M. Collinson, "Organically modified silicate films for stable pH sensors," *Anal. Chim. Acta*, vol. 394, no. 2-3, pp. 195–200, 1999.

[7] F. Ismail, C. Malins, and N. J. Goddard, "Alkali treatment of dye-doped sol-gel glass films for rapid optical pH sensing," *Analyst*, vol. 127, no. 2, pp. 253–257, 2002.

[8] G. R. Atkins, R. M. Krolikowska, and A. Samoc, "Optical properties of an ormosil system comprising methyl- and phenyl-substituted silica," *J. Non-Cryst. Solids*, vol. 265, no. 3, pp. 210–220, 2000.

[9] C. McDonagh, B. D. MacCraith, and A. K. McEvoy, "Tailoring of sol-gel films for optical sensing of oxygen in gas and aqueous phase.," *Anal. Chem.*, vol. 70, no. 1, pp. 45–50, 1998.

[10] C. von Bültzingslöwen, A. K. McEvoy, C. McDonagh, and B. D. MacCraith, "Lifetime-based optical sensor for high-level pCO_2 detection employing fluorescence resonance energy transfer," *Anal. Chim. Acta*, vol. 480, no. 2, pp. 275–283, 2003.

[11] C. von Bültzingslöwen, A. K. McEvoy, C. McDonagh, B. D. MacCraith, I. Klimant, C. Krause, and O. S. Wolfbeis, "Sol-gel based optical carbon dioxide sensor employing dual luminophore referencing for application in food," *Analyst*, vol. 127, no. 11, pp. 1478–1483, 2002.

[12] C. Malins, T. M. Butler, and B. D. MacCraith, "Influence of the surface polarity of dye-doped sol-gel glass films on optical ammonia sensor response," *Thin Sol. Films*, vol. 368, no. 1, pp. 105–110, 2000.

[13] C. Malins, H. G. Glever, T. E. Keyes, J. G. Vos, W. J. Dressick, and B. D. MacCraith, "Sol-gel immobilised ruthenium(II) polypyridyl complexes as chemical transducers for optical pH sensing," *Sens. Act. B: Chemical*, vol. 67, no. 1-2, pp. 89–95, 2000.

[14] C. S. Burke, L. Polerecky, and B. D. MacCraith, "Design and fabrication of enhancedpolymer waveguide platforms for absorption-based optical chemical sensors," *Meas. Sci. Technol.*, vol. 15, no. 6, pp. 1140–1145, 2004.

[15] S. Saavedra, P. Skrdla, N. Armstrong, S. Mendes, and N. Peyghambarian, "Sol-gel based planar waveguide sensor for water vapour," *Anal. Chem*, vol. 71, no. 7, pp. 1332–1337, 1999.

[16] R. H. Engler, C. Klein, and O. Trinks, "Pressure sensitive paint systems for pressure distribution measurements in wind tunnels and turbomachines," *Meas. Sci. Technol.*, vol. 11, pp. 1077–1085, July 2000.

[17] P. Bowe, "Characterisation of porosity and sensor response times of sol-gel-derived thin films for oxygen sensor applications," Master Thesis, School of Physical Sciences, Dublin City University, Dublin, Ireland, Jan. 2003.

[18] H. Sakue and J. P. Sullivan, "Time response of anodized aluminum pressure-sensitive paint," *AIAA Journal*, vol. 39, pp. 1944–9, 2001.

[19] I. Strawbridge and P. F. James, "The factors affecting the thickness of sol-gel derived silica coatings prepared by dipping," *J. Non-Cryst. Sol.*, vol. 86, no. 3, pp. 381–393, 1986.

[20] J. K. Kim and B. R. Min, "Theoretical study of the knife coating process. The effect of the contact angle of the knife on the knife coating," *Plastics, Rubber and Composites Processing and Applications*, vol. 20, no. 2, pp. 101–106, 1993.

[21] A. G. Emslie, F. T. Bonner, and L. G. Peck, "Flow of a viscous liquid on a rotating disk," *J. Appl. Phys.*, vol. 29, no. 5, pp. 858–862, 1978.

[22] D. Meyerhofer, "Characteristics of resist films produced by spinning," *J. Appl. Phys*, vol. 49, no. 7, pp. 3993–3997, 1978.

[23] J. B. Wachtman and R. A. H. (Editors), *Ceramic Films and Coatings.* William Andrew Publishing/Noyes, first ed., 1993.

[24] G. E. McCreery and C. M. Stoots, "Drop formation mechanisms and size distributions for spray plate nozzles," *Int. J. Multiphase Flow*, vol. 22, no. 3, pp. 431–452, 1996.

[25] O. Goerke, E. Feike, T. Heine, A. Trampert, and H. Schubert, "Ceramic coatings processed by spraying of siloxane precursors (polymer-spraying)," *J. Europ. Ceram. Soc.*, vol. 24, no. 7, pp. 2141–2147, 2004.

[26] J. R. Lakowicz, *Principles of Fluorescence Spectroscopy.* New York: Kluwer Academic/Plenum Publishers, second ed., 1999.

[27] J. N. Demas and B. A. DeGraff, "Applications of luminescent transition platinum group metal complexes to sensor technology and molecular probes," *Coord. Chem. Rev.*, vol. 211, no. 1, pp. 317–351, 2001.

[28] J. N. Demas and B. A. DeGraff, "Luminescence-based sensors: microheterogeneous and temperature effects," *Sens. and Act. B: Chem.*, vol. 11, no. 1-3, pp. 35–41, 1993.

[29] M. Gouterman, "Oxygen quenching of luminescence of pressure sensitive paint for wind tunnel research," *J. Chem. Educ.*, vol. 74, no. 6, pp. 697–702, 1997.

[30] K. K. Gopinathan, R. Lakshminarayanan, N. Rajaram, M. I. A. Siddiqd, and C. C. Suryanarayana, "Magnesium fluogermanate red phosphor: temperature dependence of the emission spectra," *Indian J. Phys.*, vol. 51B, pp. 423–440, 1977.

[31] K. A. Wickersheim and M. H. Sun, "Fluorooptic thermometry," *Med. Elect.*, vol. 103, pp. 84–91, 1987.

[32] K. A. Wickersheim and M. H. Sun, "Fibreoptic thermometry and its applications," *J. Microw. Power*, pp. 85–94, 1987.

[33] F. A. Kröger and J. V. Boomgaard *J. Electrochem. Soc.*, vol. 97, p. 377, 1950.

[34] Y. Tanabe and S. Sugano, "On the absorption spectra of complex ions 2," *J. Phys. Soc. of Japan*, vol. 9, no. 5, pp. 766–779, 1954.

[35] G. Kemeny and C. H. Haake, "Activator center in magnesium fluorogermanate phosphors," *J. Chem. Phys.*, vol. 33, pp. 783–789, 1960.

[36] Jahn and Teller, "Stability of polyatomic molecules in degenerate electronic states," *Proc. Roy. Soc.*, vol. A161, p. 220, 1937.

[37] O. M. Ntwaeaborwa, K. T. Hillie, and H. C. Swart, "Degradation of Y_2O_3:Eu phosphor powders," *physica status solidi (c)*, vol. 1, pp. 2366–2371, 2004.

[38] J. Zhang, Z. Tang, Z. Zhang, W. Fu, J. Wang, and Y. Lin, "Synthesis of nanometer Y_2O_3:Eu phosphor and its luminescence property," *Mat. Sci. Eng. A*, vol. 334, no. 1-2, pp. 246–249, 2002.

[39] R. H. Engler, M.-C. Merienne, C. Klein, and Y. Le Sant, "Application of PSP in low speed flows," *Aerosp. Sci Technol.*, vol. 6, no. 5, pp. 313–322, 2002.

[40] J. W. Holmes, "Analysis of radiometric, lifetime and fluorescent lifetime imaging," in *Proceedings of CEAS Wind Tunnels and Wind Tunnel Test Techniques conference, Cambridge*, Aug. 1997.

[41] L. M. Coyle and M. Gouterman, "Correcting lifetime measurements for temperature," *Sensors and Actuators B: Chemical*, vol. 61, no. 1-3, pp. 92–99, 1999.

[42] X. Lu, I. Manners, and M. A. Winnik, "Polymer/silica composite films as luminescent oxygen sensors," *Am. Chem. Soc.*, vol. 34, no. 6, pp. 1917–1927, 2001.

[43] P. Langer, R. Muller, S. Drost, and T. Werner, "A new method for filter-free fluorescence measurements," *Sensors and Actuators B: Chemical*, vol. 82, no. 1, pp. 1–6, 2002.

[44] Hamamatsu corporation, "Image intensifiers - data sheet," 2004. `http://www.hpk.co.jp/Eng/products/ETD/pdf/II_TII0001E03.pdf`.

[45] PCO, *DiCAM Pro - User manual.* PCO AG, Germany, 2000.

[46] Photonic Research Systems, *Imagex 2000 - User manual.* Photonic Research Systems Ltd., 1999.

[47] `http://www.leefilters.com/`.

[48] `http://www.signalrecovery.com/7225.htm`.

Chapter 3

PSP imaging: experimental configuration and image processing

In this chapter a number of different PSP system configurations are described and the lifetime-based system chosen for this project is justified. The data acquisition and image processing system used is described.

3.1 Intensity versus lifetime-based PSP

For PSP or TSP (Temperature Sensitive Paint) measurements the effect of quenching on luminescence must be recorded. Two different approaches to record changes in luminescence signal are used — intensity and lifetime.

3.1.1 Intensity approach

Currently, most PSP measurements are carried out by monitoring the intensity of the emission from the surface to be profiled as a function of the pressure. Under continuous illumination, a CCD camera records the pressure profile by carrying out "wind-off" and "wind-on" measurement as discussed below. This is also called the radiometric approach.

The intensity of emitted luminescent light is affected by many factors that are not related to pressure or temperature changes. These factors include the intensity of illumination, the sensitivity of the detection system (including mechanical stability of experimental setup), thickness and temperature of the paint layer and the concentration of

luminescent dye in the paint (sensing layer).

The concentration of dye in the paint can change due to a process called leaching, when the active luminescence molecules are washed off from the sensing layer. The effective concentration can also change as a result of photon-induced chemical damage (photobleaching), which renders a proportion of the molecules non-luminescent. These factors affect the long-term stability of intensity-based sensors. Therefore, each individual sensor must be effectively calibrated against reference conditions to correct for all the above effects.

One solution is the production of two intensity images, traditionally called "wind-off" and "wind-on", which are referenced against each other. Under continuous illumination, the "wind-off" image is taken in the wind tunnel when the wind is switched off and the model surface is under ambient pressure and temperature and the reference intensity, I_{ref}, is recorded. Then the tunnel is turned on and the "wind-on" intensity image, I, is acquired. Assuming that no change in illumination, efficiency of collection optics or photobleaching occurred, the change in intensity can be attributed to oxygen quenching caused by a change in air pressure, and the pressure can be determined using Stern-Volmer calibration (Equation 1.7).

Such intensity-based PSP systems suffer from two main disadvantages:

- misalignment between wind-on and wind-off images and
- inability to simply incorporate and detect luminescence from a second luminescent material e.g. for temperature corrections.

The misalignment of the wind-on and wind-off images is caused by the wind causing deformation of the model or supports. To correct for this, the model surface is covered with a set of registration marks and images are first manipulated in order for the marks to overlap [1]. Then the calculation of the ratio I_{ref}/I can be carried out pixel by pixel. The marks reduce the surface area available for PSP measurements. Furthermore, because of the movement of the model, the illumination conditions can change between wind-off and wind-on images, as the distances from the light source and detection system changes and shadow patterns shift.

In general, the need for wind-on and wind-off images brings problems which are difficult to solve.

For temperature correction, it is desirable to incorporate more than one luminophore into the paint to be able to detect changes in more than one parameter (e.g. pressure and temperature). This simple intensity approach is not able to distinguish between signals from more than one luminophore. There are two options: (i) separation of the signals spectrally using optical filters (if the luminescence spectra do not overlap) or (ii) separation of them in the time domain. The first approach was reported by Zelelow *et al.* [2] where the setup required filter changers in front of the camera. The second approach involves measuring lifetime and is described in the next paragraph.

3.1.2 Lifetime approach

Assuming that one can determine the lifetime of the luminophore or some quantity proportional to the lifetime, then the "wind-off" image is not needed. As the lifetime is an intrinsic property of the luminescent molecule (or phosphor), regardless of illumination conditions, efficiency of detection system, concentration of dye* and paint thickness, the lifetime version of the Stern-Volmer equation (Equation 1.7) can be rewritten, simply by dividing it by the reference lifetime τ_{ref}, in the form of

$$\tau^{-1} = \frac{A}{\tau_{\mathrm{ref}}} + \frac{B}{\tau_{\mathrm{ref}}\, p_{\mathrm{ref}}} p\,. \tag{3.1}$$

The parameters on the right hand side are all constant, except the pressure, p, showing that one universal calibration is sufficient for all sensors without the need for referencing lifetime to any known condition. In the case of PSP, this means that there is no need for wind-off images. The determination of lifetime, τ, in wind-on conditions is sufficient for pressure determination (knowing the universal calibration for the particular paint).

Furthermore, if more than one luminophore with a different lifetime is employed, all lifetimes can be measured and more than one parameter (e.g. pressure, temperature) can be determined. As this separation happens in the time domain, it requires just a change in camera gating (software change), as opposed to the mechanical change for spectral separation (filter change).

Methods for lifetime determination can be divided into two categories — pulsed luminescence lifetime measurement and modulated luminescence lifetime measurement. In short, the pulsed methods use a single pulse to excite the sample and then the decay

*At high concentration of dye the lifetime can be reduced by effect of concentration quenching.

of the luminescence intensity is measured. In modulated methods, the sample is excited with a periodically changing signal, where the period of the signal is comparable with the measured lifetime, and usually a phase shift is determined (more details are presented in Section 5.5).

The dominant approach currently used in pressure sensitive paint applications is the intensity approach requiring wind-off images, but recently increase in number of studies is being devoted to lifetime based measurements. Intensity based measurements seem to have better accuracy in a real application, but the lifetime methods are rapidly improving, driven by the advantages described above. These issues are addressed again in Chapter 7.

3.2 Luminescence lifetime detection

Lifetime from the surface can be read point by point using scanning techniques, where the lifetime is extracted by many methods known from lifetime spectroscopy [3]. The full temporal resolution of luminescence can be easily obtained and lifetime calculated.

Using a camera is, in principle, equivalent to the use of thousands to millions of photodetectors in parallel. This accelerates the whole process of profile acquisition, but does not allow the recording of temporal information for each pixel in such detail as single point or scanning techniques.

3.2.1 CCD cameras

PSP applications tend to use charge coupled device (CCD) cameras to acquire the images of the pressure distribution. The CCD is a light-sensitive device, usually made of silicon. It consists of an array of light-sensitive pixels where each individually convert incoming photons to electrons and accumulate the resulting charge. The pixel is the smallest region on the chip that can be resolved. The size of pixel limits the resolution of the chip.

The image acquisition from the CCD consists of three main phases — (i) cleaning phase, when all the charge in each pixel is removed, (ii) exposure phase, when the accumulation of charge happens; the exposure time, also called integration time, controls the amount of the charge accumulated and finally (iii) read-out phase, when the charge is sequentially read-out from each pixel. According to the method used for read-out, the CCD chips are divided to three main categories:

- **full frame device** -- this device has no shuttering features and the read-out of the image happens while continuously exposing pixels. Such devices require an external shutter.

- **frame transfer device** — the chip is split into two areas, where one half is light-sensitive and the charge from it is quickly transported to the second light-insensitive half and then read-out.

- **interline transfer device** — every second column of pixels is masked and light insensitive. Charge can be transfered very quickly (during one clock tick) from the light sensitive pixels to the shielded columns.

The read-out process transfers the charge from each pixel gradually to the side of the chip, where it is converted to the voltage reading and the voltage signal is amplified and digitised.

Intensity-based imaging techniques tend to use CCD chips with high dynamic range (at least 12 bit) and low noise, which is achieved by removing thermal noise by cooling the chip.

3.2.2 Camera systems for lifetime imaging

As discussed above, the lifetime approach should be better than the intensity-based approach. Now the implications of the lifetime based approach in conjunction with using a camera system for the image acquisition will be discussed.

The single point measurement and measurement with a camera have a few fundamental differences. First, the pressure profile is acquired in parallel, with the data from each point of the model corresponding to the same moment in time, not in sequence, as in the scanning case. This also decreases the total acquisition time.

Secondly, the camera typically is not capable of recording the same temporal information as a single point measurement. The full recording of temporal information would require typical data acquisition speeds of 10^6 Gb/s*, which is unrealistic taking into account serial reading of data from the CCD chips and the noise which would be introduced

*For SVGA resolution CCD camera, 12 bit resolution and time window of 10 μs with 100 data points, $800 \cdot 600 \cdot 12\text{b} \cdot 100/10^{-5}\,\text{s} = 5.6 \cdot 10^5$ Gb/s, assuming continuous read-out, which is not taking into account the exposition (integration) time needed.

at such high read-out speeds. Using CMOS cameras in place of CCDs could improve the situation, but, the required data flow (even temporary) is beyond the scope of current technology and the problem must be tackled in a different way.

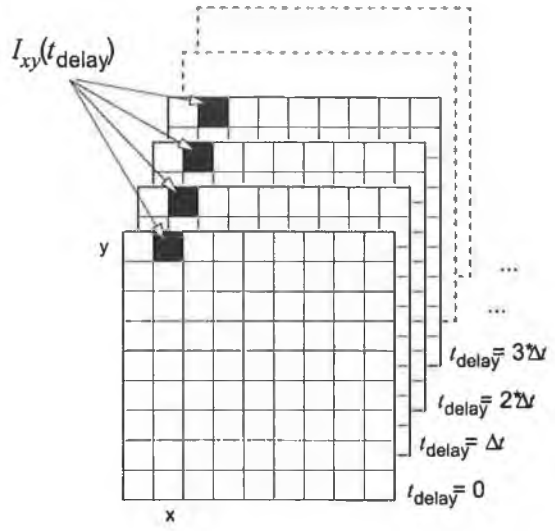

Figure 3.1: Recording multiple images with different exposition conditions (here time delays) and making calculations on per-pixel basis on values I_{xy}.

Fortunately, the use of periodic excitation, together with a gating technique, can be a solution to the problem. The gating allows for recording of the light between selected times during the excitation period. After the exposure, the information is read-out and in the following excitation period the gate with different settings is triggered and the process continues. By selecting appropriate gates, a set of images, each containing intensity information of light levels at particular times and exposure times is obtained, as shown in Figure 3.1. The set of images is processed on a pixel-by-pixel basis, according to the gating strategy used for recording, and for each pixel the lifetime, or number related to lifetime or pressure information is obtained. It results in the final lifetime/concentration/... image, which is then further interpreted.

The advantage of using periodic excitation is the possibility of the integration of the light over consecutive periods into one image using several identical gatings. The CCD is continuously exposed and the gating system lets through light just during selected times. This is very useful when the exposure times are short and the light intensity accumulated over one pulse/period is small.

3.2.3 Principle of gated camera systems

To achieve adequate gating, two strategies can be used. The first involves a system on an interline transfer CCD chip, when the charge is transported from adjacent pixels to select charge corresponding to the light incoming during the gate-periods. When enough charge is stored, the whole image is read-out. This principle is used in the Imagex 2000 system from Photonic Research Systems, UK [4].

Another strategy uses a shutter placed in front of the CCD chip. The shutter selects the light corresponding to the gating periods and the CCD chip naturally provides the integration over the periods. The challenge is to implement a shutter with a minimum gating time in the range of tenths of nanoseconds to microseconds. For this timescale the mechanical shutters are too slow.

The method of choice is to use an image intensifier with high on/off ratio ($>10^4$:1). While the image intensifier is off, virtually no light passes through; when it is on, the incident light is amplified, which corresponds to opening the shutter. This method is used in the DiCAM Pro camera [5]. In some image intensifiers the gain can be modulated in time, which would enable phase detection in the system. In our system, a microchannel plate is used as an image intensifier.

Microchannel plate (MCP)

A microchannel plate (MCP) is, in principle, a secondary electron multiplier. Initially it was developed for intensifying low intensity images and for detectors of x-rays in medical imaging and particle physics. In PSP systems MCPs are used as shutters in on/off mode. An MCP consists of a photocathode in front, where incoming photons are converted to electrons (Figure 3.2). Each electron enters one of the millions of channels in an array. When the electron hits the wall of a channel, secondary electrons are produced and accelerated by the high voltage applied across both ends of the MCP and their numbers are multiplied in a similar way as in the photomultiplying tube (PMT).

At the output, the electrons reach a phosphor which converts them to photons. If a high voltage is not applied, the electrons are not multiplied and do not reach the phosphor and no light at the output is generated.

Image intensifiers are switchable at the nanosecond time scale [6]. The image intensifiers have a number of properties, which are not always desirable and they are worth

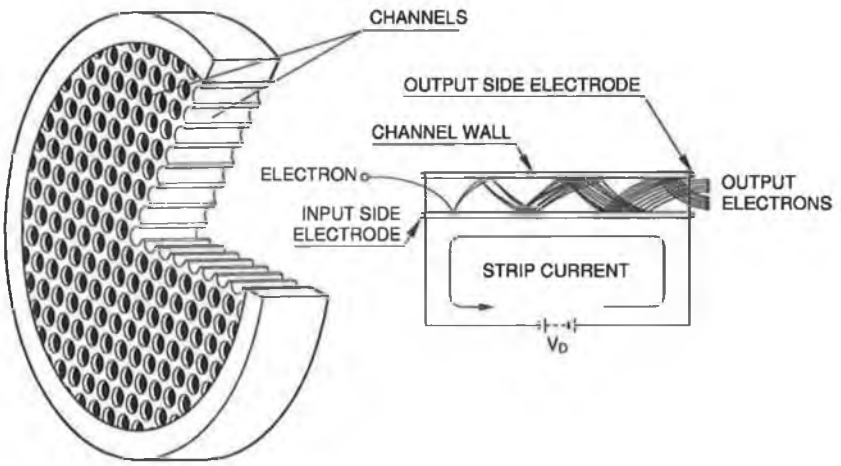

Figure 3.2: Principle of operation of Microchannel Plate (MCP). The photocathode and light emitting phosphor are not displayed.

briefly mentioning:

- Loss of image resolution. The image resolution is defined by the number of channels and grain size of used phosphor.
- Increase of noise. This is an intrinsic property of PMT amplification.
- Slow decay time of the phosphor. It can complicate fast consecutive measurements.

3.3 Selection criteria for PSP systems

The PSP/TSP system is an application of optical sensing driven by industrial demand and therefore, some practical limitations exist. For example, significant modifications of the wind tunnel are not possible and therefore only a limited control of temperature is possible. In addition, background light can remain and generally, the industrial-like environment is hostile for the operation of precision equipment.

Therefore, the PSP system should be robust and not contain any mechanically sensitive parts. It should also be able to compensate for variations in temperature as mentioned in Section 1.7.

For these reasons, it was decided to use a single camera system with a single light source and to develop a dual-luminophore, temperature and pressure-sensitive paint. Utilising the lifetime approach enables separation of temperature and pressure information in the

time domain, avoiding the use of spectral filtering. The system consists of a TTL modulated light source (LED array PRS100B), trigger circuit and gated camera DiCAM Pro or Imagex 2000 system, all described in detail in Section 2.4.

3.3.1 Luminophore selection

The ruthenium complex, $[Ru(dpp)_3]^{2+}$, has been widely used in oxygen sensor applications. As well as being highly emissive, the complex has strong absorption in the blue-green region of the spectrum which, is compatible with high-brightness blue LEDs. The high degree of overlap between the complex absorption band and the output of the LED is shown in Figure 3.3. The relatively long lifetime ($\sim 5\,\mu s$) ensures high oxygen sensitivity. The complex is optically stable and is easily incorporated into a variety of binder matrices.

As discussed previously, magnesium fluorogermanate ($3.5MgO\,0.5MgF_2\,GeO_2 : Mn$) or MFG, is a thermographic phosphor which is used in commercial fibre optic temperature sensing applications [7]. Excitation of the activator, Mn^{4+}, gives rise to a temperature-dependent, phosphorescent decay ($\tau \sim 3\,ms$). The absorption spectrum has a peak at 420 nm, which, as shown in Figure 3.3, overlaps considerably with the blue LED output. Emission peaks at 655 nm and 630 nm are spectrally close to the 610 nm emission of the ruthenium complex.

As discussed in Section 2.1, the sol-gel material was chosen as the optimum oxygen permeable binder. $[Ru(dpp)_3]^{2+}$ and MFG were entrapped by embedding them into a sol.

Clearly, the overlapping absorption bands, summarised again in Figure 3.3, of the luminophores facilitates the use of a single excitation source. The temporally separated lifetimes, $\sim 5\,\mu s$ for the ruthenium complex and $\sim 3\,ms$ for MFG, allow the use of a single gated camera for the acquisition of both luminescent decays.

3.3.2 Selected camera system

Two systems capable of lifetime measurements were evaluated. These were the gated DiCAM Pro camera and Imagex 2000 system, both are described in detail in Section 2.4.3. As the DiCAM Pro is more versatile, it was used for the initial experiments presented in the following chapter. Data obtained with Imagex 2000 system are presented in Chapter 6.

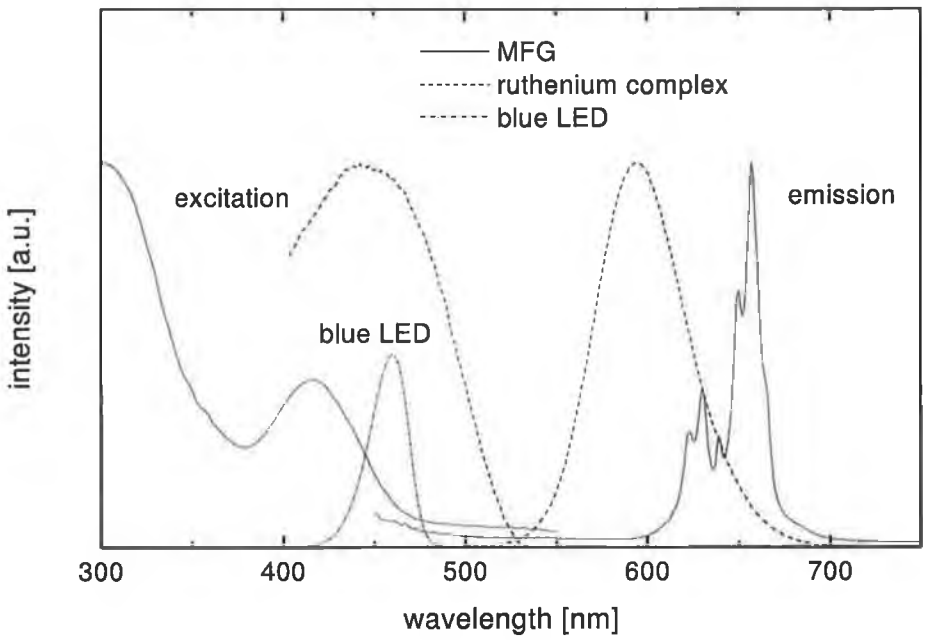

Figure 3.3: Excitation and emission spectrum of $[Ru(dpp)_3]^{2+}$, MFG and emission of 460 nm LED.

3.4 Conclusion

In this chapter, the advantages of using lifetime methods for PSP systems over intensity-based approaches were detailed, including the detection of multiple parameters using the same paint and acquisition system. The principle of gated camera systems, suitable for acquisition of two-dimensional lifetimes was explained leading to the selection of the optimum lifetime system, capable of acquiring full information about the temporal profile of luminescence. These conclusions form the basis for the experiment presented in the next chapter.

3.5 References

[1] J. H. Bell and B. G. McLachlan, "Image registration for luminescent paint sensors," *AIAA Journal*, vol. 93-0178, Jan 1993.

[2] B. Zelelow, G. E. Khalil, G. Phelan, B. Carlson, M. Gouterman, J. B. Callis, and L. R. Dalton, "Dual luminophore pressure sensitive paint: II. Lifetime based measurement

of pressure and temperature," *Sens. and Act. B: Chemical*, vol. 96, no. 1-2, pp. 304–314, 2003.

[3] J. R. Lakowicz, *Principles of Fluorescence Spectroscopy*. New York: Kluwer Academic/Plenum Publishers, second ed., 1999.

[4] Photonic Research Systems, *Imagex 2000 - User manual*. Photonic Research Systems Ltd., 1999.

[5] PCO, *DiCAM Pro - User manual*. PCO AG, Germany, 2000.

[6] Hamamatsu corporation, "Image intensifiers - data sheet," 2004. `http://www.hpk.co.jp/Eng/products/ETD/pdf/II_TII0001E03.pdf`.

[7] K. A. Wickersheim and M. H. Sun, "Fibreoptic thermometry and its applications," *J. Microw. Power*, pp. 85–94, 1987.

Chapter 4

Temperature-corrected PSP measurements using a single camera and dual lifetime approach

4.1 Proof of principle

The PSP/TSP system developed in this work utilises two luminophores and its advantages were discussed in previous chapters. In this chapter the experimental results obtained using the selected PSP system are presented.

4.1.1 Dual luminophore paint formulation

The ruthenium complex tris-(4,7-diphenyl-1,10-phenanthroline) ($[Ru(dpp)_3]^{2+}$) was synthesised and purified as described elsewhere [1], and manganese-activated magnesium-fluorogermanate $3.5MgO\,0.5MgF_2\,GeO_2 : Mn$ (or MFG) was purchased from Meldform Metals Ltd. The sol-gel precursor methyltriethoxysilane (MTEOS) and hydrochloric acid were purchased from Aldrich, USA.

The dual-luminophore sol-gel paint was prepared by the hydrolysis and condensation of methyl-triethoxysilane (MTEOS) in an ethanol solution. A water to silane molar ratio R of 4:1 was used. In order to produce highly dispersed particles of MFG within the sol-gel film, it was necessary to reduce the particle size of this phosphor from the as-received average diameter of approximately $10\,\mu m$ to approximately $0.15\,\mu m$. This was achieved

using an attrition mill.

To a mixture of 4.15 g of ethanol containing 16 mg of dissolved $Ru(dpp)_3Cl_2$, 1.04 g of 0.10 M hydrochloric acid was added and mixture was stirred for 30 minutes. Then 2.56 g of MTEOS was added dropwise and the mixture was stirred for another 90 minutes in a sealed beaker to allow the hydrolysis and condensation reactions to proceed. The 0.35 g of MFG was then added and the mixture sonicated for 30 minutes. This was followed by a further stirring for 90 minutes. The final concentrations of $[Ru(dpp)_3]^{2+}$ and MFG in the sol-gel were 0.2 and 5 mass percent, respectively. The relative concentrations of the luminophores were chosen to optimise the signal-to-noise ratio, while avoiding agglomeration effects, which would affect the measured lifetimes.

Various coating techniques were evaluated. Spray coating was found to be the most effective coating method due to the fact that it can produce a sufficiently thick coating layer in one cycle, while retaining the MFG powder in suspension in the paint layer. The test pieces (2 cm × 2 cm pieces of silicon wafers) were spray-coated and the films cured overnight at 70 °C to accelerate the drying process.

In the work presented here, the paint prepared following this recipe is referred to as *standard PSP&TSP paint.*

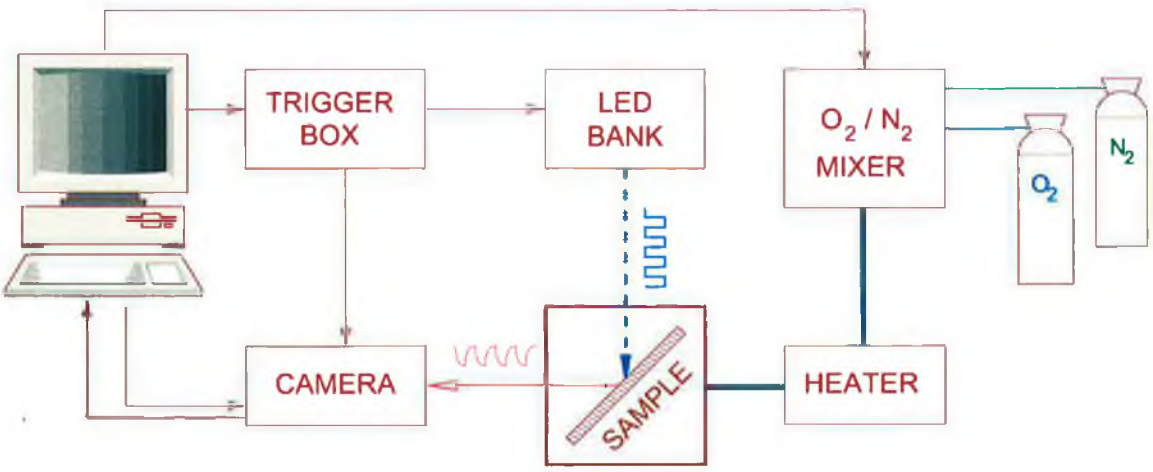

Figure 4.1: Setup for calibrating of PSP and TSP paint.

4.1.2 Measurement protocol

The sample was inserted into a flow cell and illuminated using a 460 nm blue LED bank, driven by the frequency generator at 40 Hz in a purpose-built calibration system, a block diagram of which is shown in Figure 4.1. On the right hand side, the computer-controlled mixing system for oxygen and nitrogen and heater delivers the gas mixture into the flow cell. The computer-controlled trigger box (Appendix B) is linked to the LED bank and the camera and the acquired images are stored in the computer.

The calibration process is controlled from a separate computer running the Linux operating system and bash scripts. This controls both the PC (MS Windows 98) attached to the camera (DiCAM Pro) and that controlling the gas mixing. Attempts to realise all in one computer lead to high instability of the system.

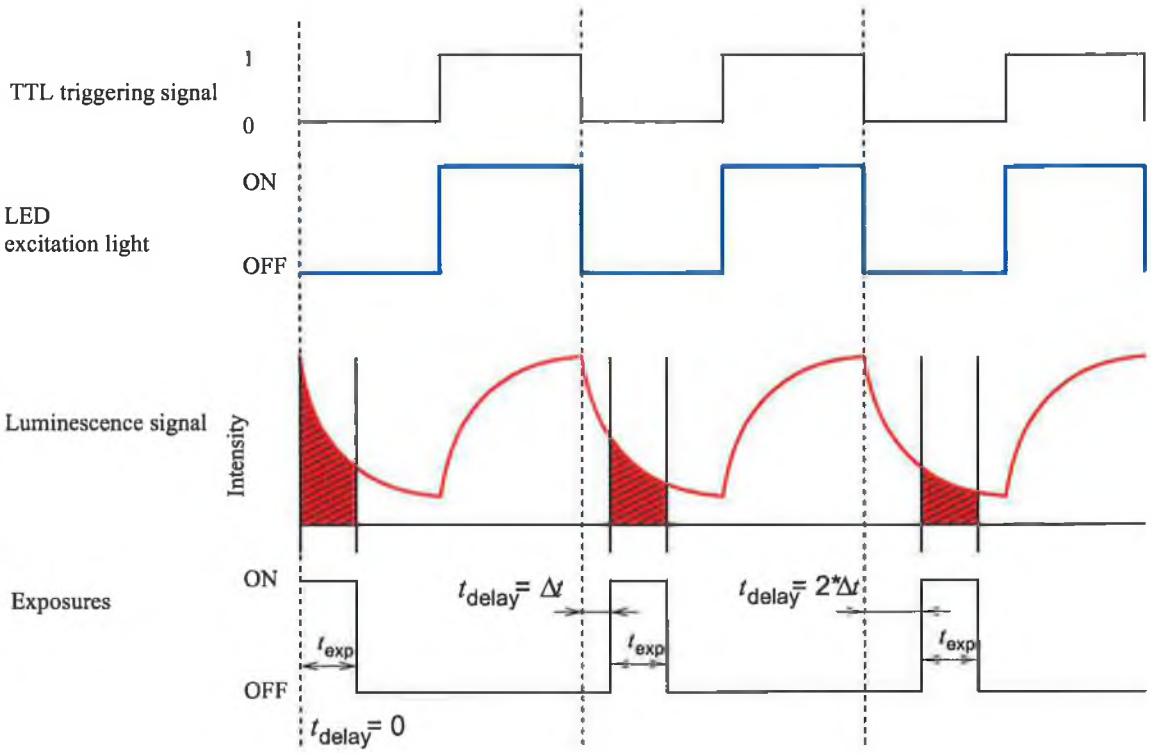

Figure 4.2: Timing diagram of luminescence measurements showing incrementing delay time.

The timing protocol for the camera and modulated LED bank is shown in Figure 4.2. To simplify the diagram only one luminophore and only one set of exposures is shown. During the "on" cycle of the LED, the combined luminescence intensity of both lu-

minophores increases to a maximum. When the LED is switched off, the DiCAM Pro camera is triggered with a controlled delay in order to eliminate light from the LED. To capture the time decay of the emission of the ruthenium complex, a camera exposure time of $t_{\text{exp}} = 2\,\mu\text{s}$ is selected and the delay time, t_{delay}, after the trigger is incremented in $\Delta t = 1\,\mu\text{s}$ steps. In this manner, data is collected that enable determination of the decay time of the ruthenium complex. The sequence for the MFG (temperature sensor) decay involves a longer exposure time of $t_{\text{exp}} = 0.5\,\text{ms}$, with the delay incremented in 1 ms steps. For each measurement sequence, the image is integrated, usually over 256 triggering cycles, and several images are averaged. As MFG has a lifetime approximately 3 orders of magnitude larger than that of $[\text{Ru(dpp)}_3]^{2+}$, it is assumed that the luminescence from MFG will contribute an almost constant background signal during the $[\text{Ru(dpp)}_3]^{2+}$ measurement sequence, while the luminescence from $[\text{Ru(dpp)}_3]^{2+}$ will have decayed to zero during the MFG sequence. Typical dual lifetime data are shown in Figure 4.3. The time axis (x-axis) is scaled differently on the left and the right side (μs vs. 1000's μs). The data in this figure were acquired at ambient pressure in nitrogen, and temporal profiles of luminescence for three different temperatures are shown.

The resulting temporal profile is shown in Figure 4.3. The temporal intensity profile, $I(t)$, is exponential and the decay times, τ, are calculated by a least squares fit to a single exponential decay, with variable baseline in the form

$$I(t) = A\,\mathrm{e}^{-t/\tau} + C\,, \tag{4.1}$$

where A and C are the fit parameters. In this particular case, the lifetimes at ambient conditions (room temperature and 20% concentration of oxygen in nitrogen) are summarised in table 4.1.

temperature [°C]	$\tau_{\text{ruth.}}$	τ_{MFG}
24	2.31 μs	3.49 ms
53	1.92 μs	3.33 ms
65	1.63 μs	3.22 ms

Table 4.1: Temperature variations of the lifetime of ruthenium complex in standard PSP&TSP paint at ambient oxygen concentration (20% oxygen in nitrogen at atmospheric pressure).

The variable baseline is selected to accommodate the changing background level of luminescence from the long-lived luminophore (MFG), even if this causes higher uncertainty

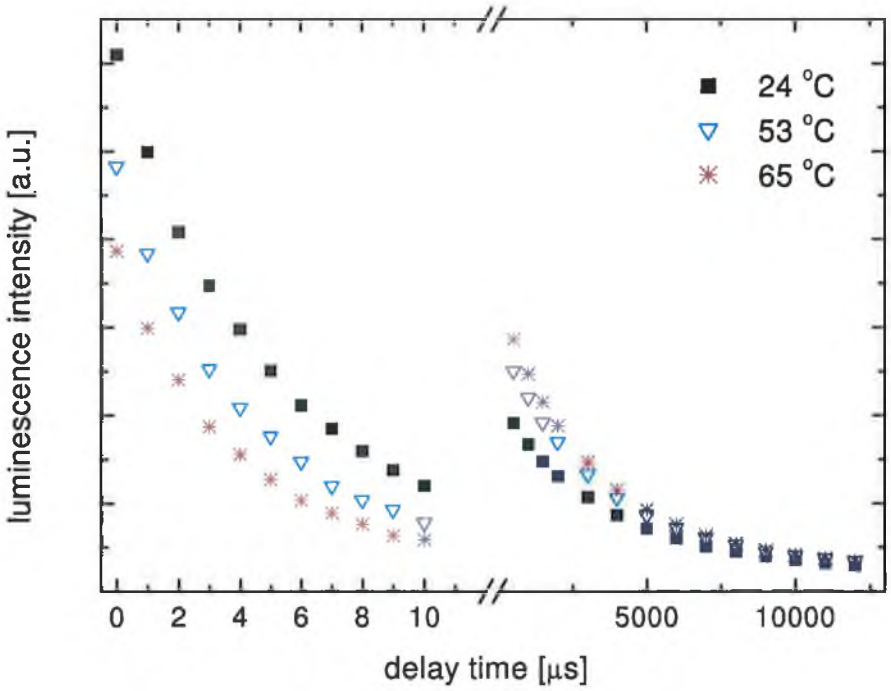

Figure 4.3: Principle of dual-lifetime approach. Two exponential decay curves of MFG and $[Ru(dpp)_3]^{2+}$ at 0% oxygen concentration in 100% nitrogen (at atmospheric pressure) at 24 °C (squares), 53 °C (triangles) and 65 °C (stars). The timescale (x-axis) is different for small and large values of time. The left and right hand sides of the x-axis have different y-scales. Errorbars of luminescence intensity is smaller than the size of the points.

of the fit.

It is clear from Figure 4.3 and table 4.1 that the lifetimes of the two luminophores are sufficiently different to enable the single camera measurement. The variation of the ruthenium complex lifetime with temperature at constant oxygen concentration, shown in table 4.1, illustrates the need for temperature correction of the pressure profile.

4.2 Temperature corrections

In order to establish the feasibility of dual-lifetime measurements, calibration measurements were made, using the same measurement protocol as described in Section 4.1.2. Full temperature and concentration calibration was carried out.

4.2.1 Temperature calibration

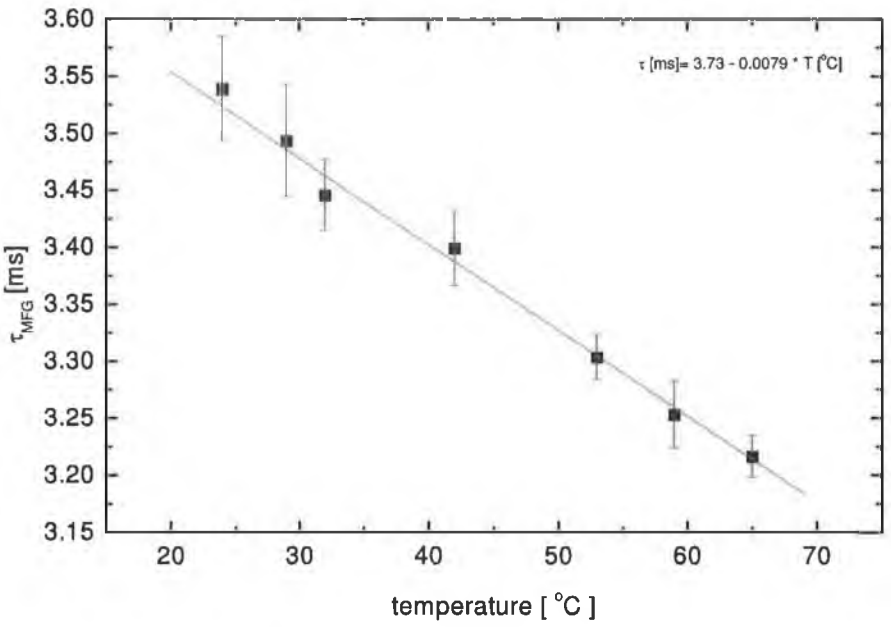

Figure 4.4: Temperature calibration curve of MFG lifetime, including standard deviation error bars.

The temperature dependence of the MFG lifetime was measured over the range from 20 °C to 65 °C. The measurement was made on a singly-doped MFG paint (i.e. containing no ruthenium complex), as well as with a co-doped standard PSP&TSP paint. The data were identical in both cases, indicating that there is no interaction between the luminophores. Figure 4.4 shows the linear MFG temperature dependence with a gradient of −0.2% decay time per °C of decay time at room temperature. The linear fit gives the following parameters: $\tau_{\mathrm{MFG}} = 3.73 - 0.0079\,T$, with lifetime, τ_{MFG}, is in milliseconds and temperature, T, in °C. The MFG lifetime is not sensitive to oxygen, within the experimental error, thus enabling this phosphor to be used to correct the pressure data for temperature dependence. Reduction of errorbars in Figure 4.4 is discussed in Section 4.2.3.

4.2.2 Temperature corrected PSP calibration data

Pressure calibration data were generated by measuring $[\mathrm{Ru(dpp)_3}]^{2+}$ lifetimes, following the same protocol described in Section 4.1.2, over the range 0–100% oxygen partial pressure at ambient pressure and over the temperature range from 20 °C to 65 °C. The data

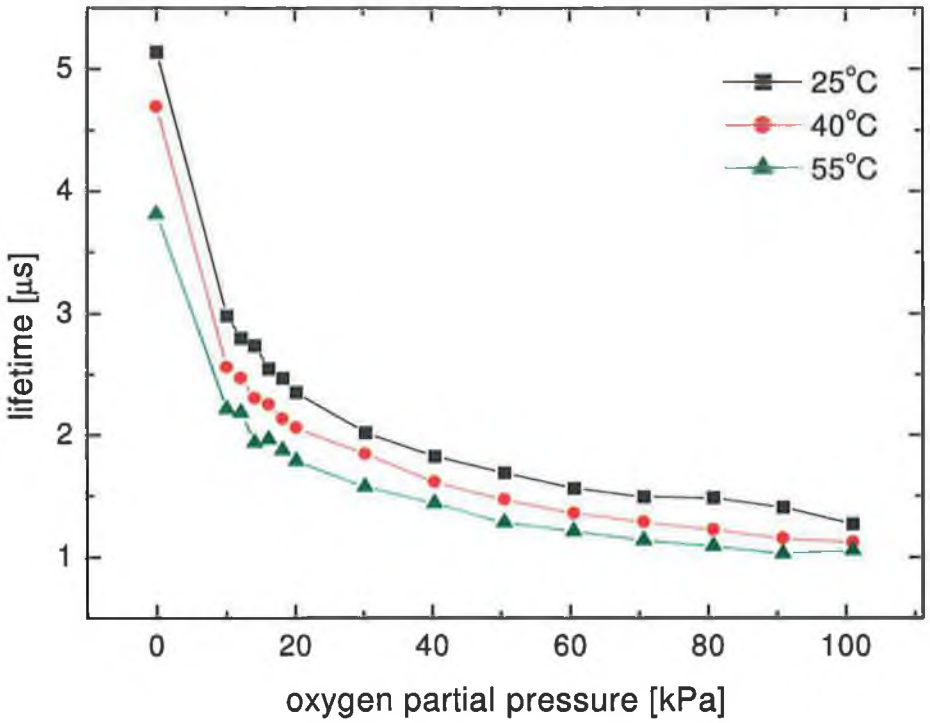

Figure 4.5: Calibration curve for ruthenium lifetime vs. pressure for different temperatures.

in Figure 4.5 represent a 8×8 pixels region of the surface, with 4×4 pixels binning in the CCD at three representative temperatures. The data were fitted to generate numerically a quasi-continuous set of lifetime data over a continuous range of temperature and oxygen pressure. A typical PSP measurement using this single camera system involves acquiring a two-dimensional $[Ru(dpp)_3]^{2+}$ lifetime image (pressure profile) and an MFG lifetime image (temperature profile) of the test surface. Using the calibration data, the MFG temperature calibration curve of Figure 4.4 and the temperature profile, the pressure profile of the test surface can be temperature-corrected. While the protocol for producing temperature-corrected PSP images using this single-camera system has been established, currently there are limitations as a result of insufficient signal-to-noise ratio (SNR). The error in temperature, based on the standard deviation in MFG lifetime (SD = $32\,\mu$s), is currently $\pm 4\,^{\circ}$C. Our objective is to achieve an error better than $\pm 1\,^{\circ}$C. In this regard, strategies for improving SNR are discussed in the next paragraph and in greater detail in Chapter 5.

4.2.3 Signal to noise limitation and improvement strategies

Strategies to improve system SNR include (i) increasing the number of photons incident on the camera, (ii) cooling the camera, (iii) increasing signal averaging and (iv) choosing an appropriate detection strategy (measurement protocol). With regard to (i), it is considered that the luminophore concentrations and paint thickness have been optimised in this system. Furthermore, the LED illumination and collection optics have been adjusted to maximise the detected signal. Concerning (ii), the CCD chip in the camera is cooled to $-11\,°C$. A number of combinations of exposure times, integration times and binning strategies will be discussed and evaluated in Chapter 5, in order to reduce the lifetime errors. Binning during image post-processing is an alternative strategy to overcome the limitation of the capacity of the CCD chip wells and 12-bit camera resolution. This has to be balanced with respect to reduction in spatial resolution. However, limited binning can significantly reduce the noise levels, while maintaining adequate image resolution.

4.2.4 Alternative temperature-sensitive phosphors

The MFG phosphor used in the PSP&TSP paint showed acceptable temperature sensitivity of the luminescence lifetime. However, the achieved precision was not completely satisfactory and therefore, other temperature-sensitive phosphors were characterised in the search for a brighter phosphor. Two available phosphors were characterised: (i) the tin modified manganese-doped magnesium-fluorogermanate, which we refer to as MFG:Sn and (ii) the europium doped yttrium oxide (Y_2O_3:Eu). Both phosphors were donated by Osram Sylvania, USA. The excitation and emission spectra of MFG:Sn are almost indistinguishable from the spectra of MFG.

Temperature dependences of lifetime were recorded using the pulsed single blue LED and photomultiplier described in Section 2.5 from sample of phosphor immobilised in standard MTEOS sol-gel on a silicon coupon. The results are displayed in Figure 4.6.

The MFG:Sn phosphor shows similar temperature dependence of lifetime as MFG and exhibits relatively high brightness, which increases with increasing temperature.

The lifetime dependence of Y_2O_3:Eu shows the opposite trend — increasing lifetime with increasing temperature. The emitted intensity of luminescence is much weaker and this contributes to the high error in the lifetime data. The blue LED, with its wide spectrum, is not matched with the sharp lines in the excitation spectra of Y_2O_3:Eu.

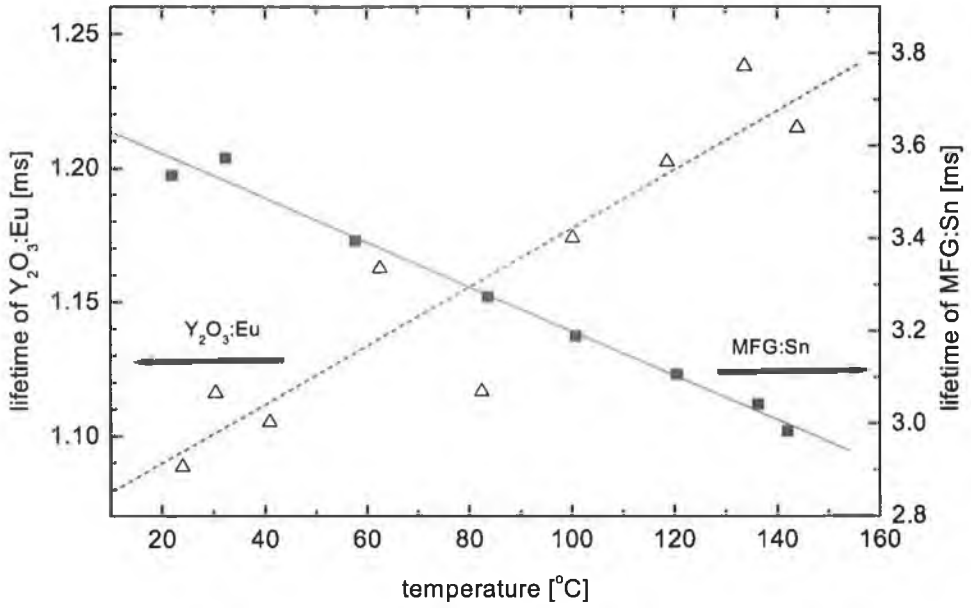

Figure 4.6: Temperature dependence of the lifetime of two temperature-sensitive phosphors: Y_2O_3:Eu (triangles) and MFG:Sn (squares).

The temperature sensitivity of the lifetime of both phosphors is similar, in the region of 0.1–0.2%/ °C (with opposite signs) to the sensitivity of MFG, but the overall Y_2O_3:Eu performance is worse due to the low emission level. We can conclude that the use of MFG as a temperature-sensitive phosphor in the paint was a good choice.

4.3 Conclusion

In this chapter an innovative technique for temperature-correction in PSP applications has been demonstrated. A key feature of this technique is the use of a single camera and a single excitation source. A new sol-gel based paint formulation has been developed which incorporates both a pressure-sensitive and a temperature-sensitive luminophore. The low-cost, porous, sol-gel paint can be easily applied over a large area. The two luminophores were chosen so that the two luminescent processes can be distinguished temporally without the need for a second camera or excitation source. A single light source and single camera luminescence decay time acquisition method has been developed.

While preliminary calibration data have been generated over the range of temperatures and pressures that would typically occur in wind tunnel testing, noise limitations in the

system prohibit pressure profiling and temperature correction to the level of accuracy required. These issues will be addressed in the next chapter. A brief study of alternative temperature-sensitive phosphors was also presented.

The work contained in this chapter was published in Measurement Science and Technology [2].

4.4 References

[1] R. J. Watts and G. A. Crosby, "Spectroscopic characterization of complexes of ruthenium (ii) and iridium (iii) with 4,4'-diphenyl-2,2'-bipyridine and 4,7-diphenyl-1,10-phenanthroline," *J. Am. Chem. Soc.*, vol. 93, p. 3184, 1971.

[2] J. Hradil, C. Davis, K. Mongey, C. McDonagh, and B. D. MacCraith, "Temperature-corrected pressure-sensitive paint measurements using a single camera and a dual-lifetime approach," *Meas. Sci. Technol.*, vol. 13, no. 10, pp. 1552–1557, 2002. `http://stacks.iop.org/0957-0233/13/1552`.

Chapter 5

PSP error analysis

Chapter 4, lifetime-based PSP measurements using the protocol described in Section 4.1.2 were reported. The measurements suffered from a relatively high error in lifetime, resulting in a correspondingly high error in air pressure. Clearly, this affected the quality of the PSP measurement.

In this chapter, several methods for error reduction in lifetime are discussed and the results of several experiments in error minimisation will be presented. Alternative methods for lifetime measurement (compared to that used in Chapter 4) are discussed and results are presented. It must be emphasised that the measurements discussed in this chapter represent "single point" lifetime measurements and lifetime errors obtained using the various protocols and methods refer to a single point on the specimen. The next chapter will address the problem of the spatial variation in lifetime of the sample.

5.1 Sources of errors in lifetime PSP systems

It is useful firstly to revisit the data acquisition process and comment on the sources of errors in each step.

5.1.1 Excitation

The first stage of a luminescence measurement is the excitation of the luminophore with a source of radiation. At this stage, the temporal and spatial distribution of the excitation light intensity on the surface of the model is created. The stability of the light source is important. In the case of lifetime measurement, the pulse-to-pulse repeatability

is crucial in the case where the lifetime is determined during a number of subsequent pulses. However, the non-correlated random variations in pulse-to-pulse intensity can be partially eliminated by averaging over multiple pulses, which is often necessary for light accumulation (Section 5.3.2).

5.1.2 Emission

The second stage of the data collection is the emission of luminescence from the paint. Here, any movement of the model may affect the measurement. Photobleaching, which is important in radiometric methods, is less of a problem unless it happens within the timescale of the single lifetime measurement. In the industrial wind tunnel, the sensitivity of the paint can be influenced also by the contamination of the paint by an oil (e.g. that used for fan lubrication).

5.1.3 Projection

The third stage is the projection of the emitted radiation onto the detector (camera) through the optical system. Image distortion and other abberations must be taken into account when the pressure data are overlaid with the CFD model data. Ideally, the mapping function should not depend on the light distribution (removed lens flare, no self-illumination). The resolution can be decreased by the resolution of the image intensifier.

5.1.4 Spatial sampling, gating and digitisation

The next phase of the process is spatial sampling of the image projected onto the CCD matrix. The continuous light intensity is mapped onto the discrete distribution matrix of the light sensitive elements (pixels). The signal in each pixel is then sequentially read out and digitised, pixel by pixel. It is at this stage that the quality of the CCD chip comes into play and all the negative effects (e.g. smear and nonlinearity) can appear. These can be due either to non-optimal design, or running the CCD in a non-optimum regime (saturation/over-exposing). The gating technology determines the temporal resolution and the leakage of the light emitted outside of the gates into the images. The gating errors can be spatially dependent, correlated with the response function of the image intensifier.

5.1.5 Digital image processing

The digitised data are stored and then processed using mathematical manipulation leading to the measured values of pressure and temperature if needed. The error introduced in this step depends on the selected numerical algorithms.

5.2 Methods for error reduction: general

In general most effort should be directed towards the maximisation of the luminescence signal in order to improve the signal to noise ratio (SNR) and, therefore, minimise the random error in the results.

During excitation, a powerful light source or multiple light sources should be used to reach high illumination and the arrangement of the light sources should create near constant illumination (low contrast) on the surface, permitting the use of the full dynamic range of the detector for all pixels and avoiding decreased SNR at under-illuminated areas. To achieve a high signal, a projection system with high f-number lenses is recommended.

To maximise the impact of the error reducing strategies, the majority of these general recommendations for the measurements reported in Chapter 4 were implemented. The light source (10×10 array of ultrabright LEDs) produced nearly homogeneous ($\pm 10\%$) illumination in area of 100×100 mm, which is more than adequate for the samples used. The camera objective of maximal f-number, $f/2.8$, was positioned 35 cm from the samples to simulate the conditions during wind tunnel measurements and the necessity of accessing the airfoil through the side window of the wind tunnel.

The whole measurement should take a minimum amount of time in order to reduce the influence of the drift of external parameters (e.g. movement, temperature). A short test time eliminates the possibility of paint degradation (photobleaching, abrasion) while acquiring the temporal profile of luminescence.

As the measurements using current protocols take minutes or tens of minutes, the concentration of oxygen and temperature are carefully stabilised to avoid unnecessary drift.

The sampling, gating and digitisation process is mainly software-controlled and can therfore, be easily adjusted. Many possible adjustments are covered in the following Section 5.3. The selected camera should have a broad dynamic range, good linearity, low read-out noise and low dark current.

5.3 Methods for error reduction: acquisition protocol modification

5.3.1 CCD signal to noise ratio

The signal to noise ratio (SNR) is the ratio of the signal level, S, and the noise, N, which consists of contributions from all noise sources, N_i. For uncorrelated noise sources, their amplitudes can be summed, yielding

$$\mathrm{SNR} = \frac{S}{N} = \frac{S}{\sqrt{N_1^2 + N_2^2 + \cdots}}, \tag{5.1}$$

where $N_1, N_2, \cdots$ are noise contributions from the individual noise sources.

The three main sources of noise in CCD chips are photon noise, read noise and dark noise.

Photon noise

The photon noise is due to the statistical nature of light. The number of incoming photons exhibits a Poissonian statistical distribution, where the relation between the signal (number of photons) and noise fluctuations N_{photon}, has a square root relation

$$N_{\mathrm{photon}} = \sqrt{\sigma^2} = \sqrt{S} = \sqrt{\text{number of photons}}, \tag{5.2}$$

$$\mathrm{SNR} = \frac{S}{N_{\mathrm{photon}}} = \frac{S}{\sqrt{S}} = \sqrt{S}\ . \tag{5.3}$$

Therefore increasing the number of photons collected improves the SNR. The number of collected photons is limited by the maximum number of electrons which can be held by each individual pixel (full well capacity). An increase in exposure time results in linear increase in the number of collected photons, but also increases the dark current, which decreases the available dynamic range.

Read noise

The read noise comes from the transfer of charge on the chip and from the digitisation process. It is determined mainly by the frequency of the read out clock (i.e. by the number of pixels per seconds that are read out).

Dark current

The dark noise (current) is due to thermally generated photons on the CCD chip. With increasing exposure time, the dark current also increases. If the dark current is greater then the equivalent current from the signal photons, the increased exposure time for reducing photon noise is counterproductive. Dark current follows also the Poissonian statistic and, therefore, introduces random noise into the signal. Typically, the CCD chip is cooled as reducing its temperature by 25 degrees reduces the dark current by a factor of more than 100.

5.3.2 Integration and averaging

In general, for lifetime measurements, the exposure time is usually comparable to the lifetime. Therefore, it is relatively short (microseconds or less) and the amount of the light accumulated during one exposure is very small. Consequently, additional steps to acquire more light are often necessary.

The method used in this work to determine lifetime is presented in Figure 5.1, which shows a gated camera with an image intensifier in front of the CCD chip. A typical setup involves periodic illumination as shown in Figure 5.1 by the blue trace (first curve). Assuming that the temporal profile of the luminescence is the same after each pulse, we can introduce integrating and averaging steps.

Firstly, having set the desired delay between the excitation pulse and the gate and other parameters (e.g. gain, binning etc. denoted as S_1), the CCD chip accumulates (integrates) all the light during several consecutive pulses (denoted as *integration on CCD* in Figure 5.1). The number of pulses averaged is usually called the number of *loops*. During this time, the CCD chip remains passive and, at the end of this period, the frame is read out from the CCD chip into the memory. This integration increases the signal level and can sometimes be sufficient. It is important to avoid overexposure of the image by employing too many loops.

Secondly, if the signal to noise ratio is low, it can be further increased by averaging several images with the same gating settings (S_1). This is shown in Figure 5.1 as *external averaging* and is typically employed outside the camera. This averaged picture is then saved to the disk and/or further processed. The next image acquisition is started with different settings (S_2), followed by the same integration and averaging.

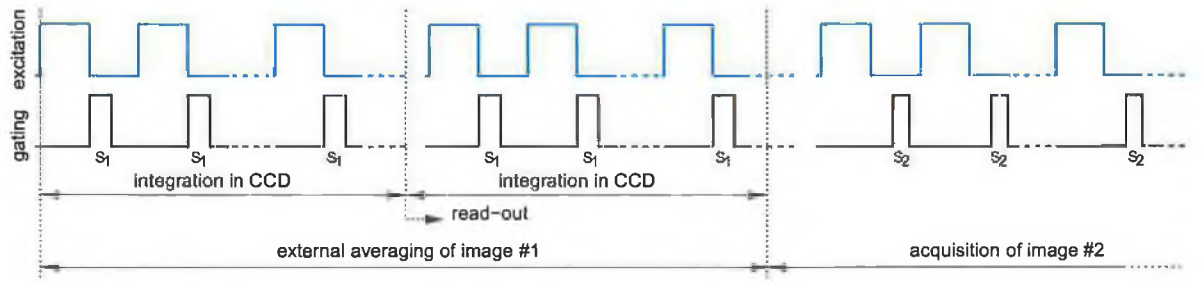

Figure 5.1: Typical image acquisition protocol for lifetime determination.

The numbers of loops and averages are important parameters that influence the noise in the final images. The product of the loops and averages determines the total time needed for image acquisition.

The number of images averaged, m, decreases the error of the resulting image by a factor $\sqrt{m}$. Therefore, in general, both averaging and integration improves the SNR, but the improvement increases only as the square root of the time required for data acquisition. Consequently, no major improvements can be expected in linear time.

The assumption of repeatable luminescence between pulses is very important, as it implies constant conditions during the acquisition of all images. This implies constant temperature and pressure above the test surface and a stable light source and detection system. Therefore, the time needed for image acquisition and the typical timescale for the changes in temperature and pressure should always be taken into account.

5.3.3 Binning

Binning is used to increase the signal level in the case of very small light levels, and when other methods alone are not adequately effective. Binning is the addition of charge collected on the CCD from several adjacent pixels (e.g. from a rectangular area) before converting the charge to a digital signal (Figure 5.2).

It effectively increases the signal, reducing Poissonian noise, while keeping the read out noise the same. At the same time, the spatial resolution of the image is reduced by the binning factor.

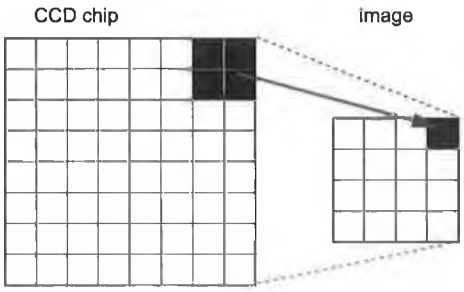

Figure 5.2: Binning in the CCD chip. Intensity from a 2×2 pixel area is integrated into a single super-pixel. Therefore, a CCD chip of 8×8 pixels produces a binned image of $(8 \times 8)/(2 \times 2) = 4 \times 4$ super-pixels.

5.3.4 Paint properties

The total detected signal is proportional to the intensity of luminescence. Therefore, an increase in the luminescence signal itself also contributes to the error reduction.

One approach to achieve this effect is to increase the amount of luminescent dye available per unit area. This can be achieved either by increasing the concentration of the dye, which could have self-quenching consequences (Section 1.2.3), or by increasing the thickness of the paint, which influences the response time and the aerodynamic quality of the surface.

The second approach is to attempt to increase the efficiency of the absorption and emission processes. The model surface can be coated with a white reflective coating, thereby enhancing the effectiveness of the excitation and reflecting the luminescence [1].

5.4 Experimental comparison of noise reduction methods

In order to identify the best measurement protocol for the improvement of the precision of our PSP measurements, a practical evaluation of several noise reduction strategies was undertaken. For example, we know from Section 5.3.2 that averaging will increase the SNR at the cost of increased acquisition time. To keep all improvements comparable, all the following measurements were acquired with approximately the same total data acquisition time of 10 minutes per pressure profile. Four noise reduction strategies were investigated: integration and averaging, binning, variation of the time window and, for co-doped samples, switching of the modulation frequency to optimise measurement of

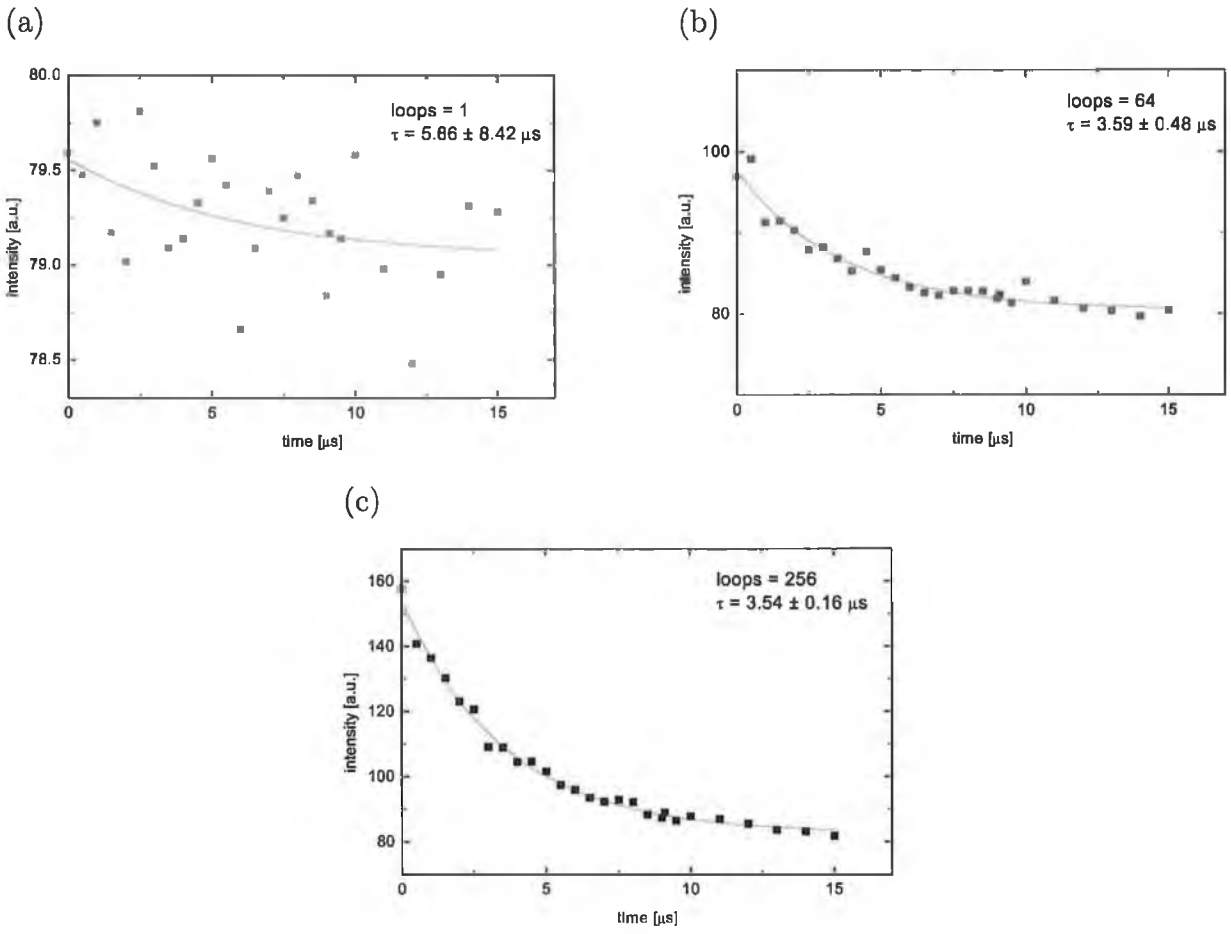

Figure 5.3: Illustration of the error decrease with the integration on the CCD chip. (a) single shot, (b) integrating over 64 pulses (64 loops) and (c) integrating over 256 pulses (256 loops).

short and long lifetimes.

5.4.1 Integration on the CCD chip and averaging

The first method for error improvements is integration on the CCD chip (described in Section 5.3.2). The data which illustrate these improvements are shown in Figure 5.3. Data were acquired from the area of 8×8 super-pixels using 4×4 binning in the CCD and an exposure time of 2 μs. Figure 5.3 (a) shows the data produced by a single exposure. An increase in the number of loops (integrated pulses) reduces the noise of the signal as seen in Figure 5.3 (b) and (c). Relative errors — defined as the ratio of the standard deviation of lifetime between measurements and its average value — are shown in table 5.1.

# of loops	relative error of τ
1	144%
64	13.3%
256	4.5%

Table 5.1: Relative error of lifetime for increasing number of integration loops on the CCD chip.

The integration in the CCD chip dramatically increases signal levels, thereby reducing Poissonian noise in the signal, without introducing additional read-out noise.

The influence of averaging on computer (outside of the CCD) is presented in Figure 5.4 for three sets of averaging cycle, 1 (no averaging), 64 and 256. The same settings were used as for the integration test. The maximum integration (256 loops) is selected, because measurement without integration in the chip is unsatisfactory, as seen in Figure 5.3. The relative errors are summarised in table 5.2.

While the error in lifetime clearly decreases with averaging, the results are not as dramatic as the improvements resulting from integration due to the square-root nature of the noise improvements (Equation 5.3).

# of averages	relative error of τ
1	6.1%
64	1.5%
256	1.1%

Table 5.2: Relative error of lifetime for increasing number of external averages made outside the CCD on computer.

The total improvements must be compared to the cost needed to achieve them. The cost in terms of time needed for the acquisition of a full data set was not influenced by the increasing number of loops (integration on the chip). However, for external averaging, the increase of the acquisition time was not negligible and increased by a factor of approximately 45 between no averaging and 256 averaging cycles (due to the relatively long read-out time of our camera, which makes a significant contribution to the total measurement time).

Finally, we can conclude that the integration in the chip is beneficial and probably

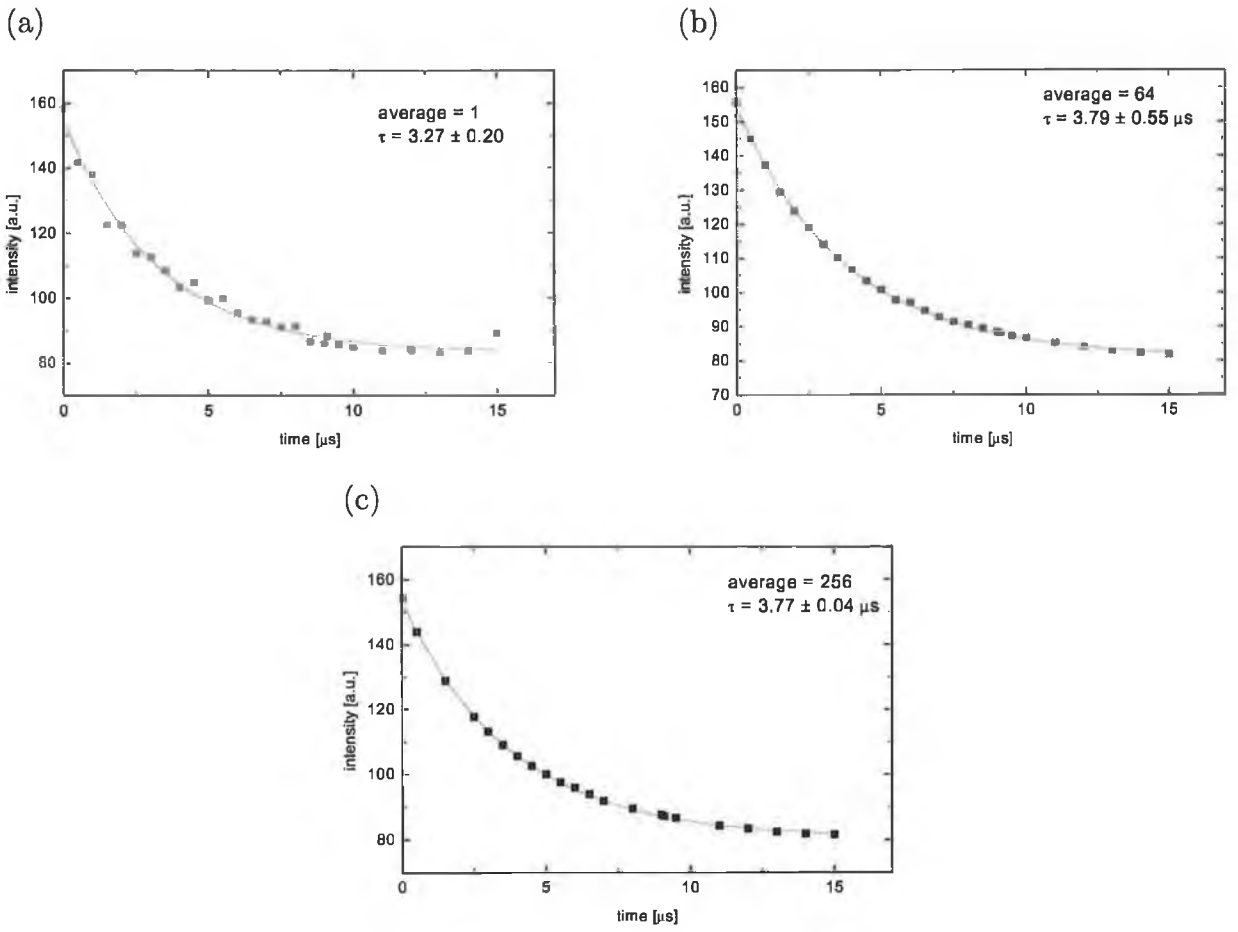

Figure 5.4: Illustration of the error decrease with the external averaging in the computer (outside of the CCD chip). (a) without averaging, (b) with 64 images averaged and (c) 256 images averaged.

necessary in most cases. While external averaging reduces the errors, the improvement must be weighed against the time needed for additional images. The optimal settings were found to be 256 loops and 8 averages. This setting was used for the measurements presented in Chapter 4.

5.4.2 Binning

An investigation of different binning protocols was undertaken. The image pixels are binned either in the CCD chip (while reading the image) or the digital data are binned during data post-processing. We chose a single-doped (ruthenium complex only) sample,

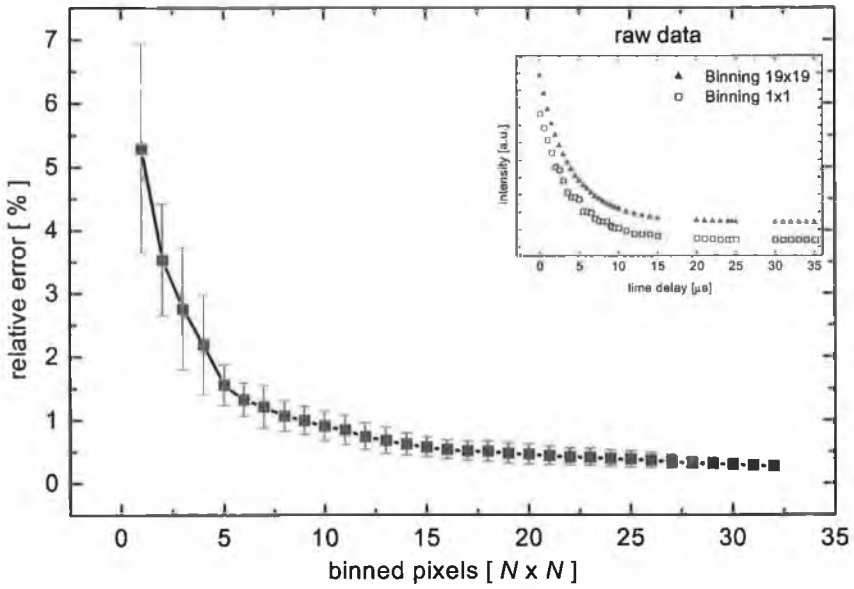

Figure 5.5: Relative error of lifetime variation with increasing binning region (from 1×1 to 32×32 pixels) averaged over 14 oxygen concentrations between 0% and 100% of oxygen.

spray-coated with the standard MTEOS paint, for this experiment. For the purposes of this test, the pixels in a 4×4 area were binned in the camera into a single super-pixel. The data in the resulting image were binned during data processing using binning ranging from 1×1 to 32×32 pixels. The reason for using 4×4 binning in the camera is as follows. The DiCAM Pro camera allows only 256 consecutive exposures during an integration cycle, in which time the pixels cannot fill up fully (to utilise the full well capacity) and binning is chosen to reduce the number of analog-to-digital conversions and, therefore, reduce read-out noise.

For each concentration of oxygen, the measurement was repeated ten times. The data were fitted to Equation 4.1 using a least-squares method. The 10 resulting lifetime values for each configuration were statistically processed to yield an average lifetime and standard error and these were averaged to give a overview of relative error behaviour, including the errorbars. The results are shown in Figure 5.5. As expected, the relative error (in percent) of the measured lifetime decreases with increasing area of binning for all oxygen concentrations. It is clear that the overall trend is the same for all concentrations. The binning significantly decreases the relative error (as well as the absolute error in seconds) up to roughly 8×8 binning (corresponding to binning 32×32 of the physical

a) b)

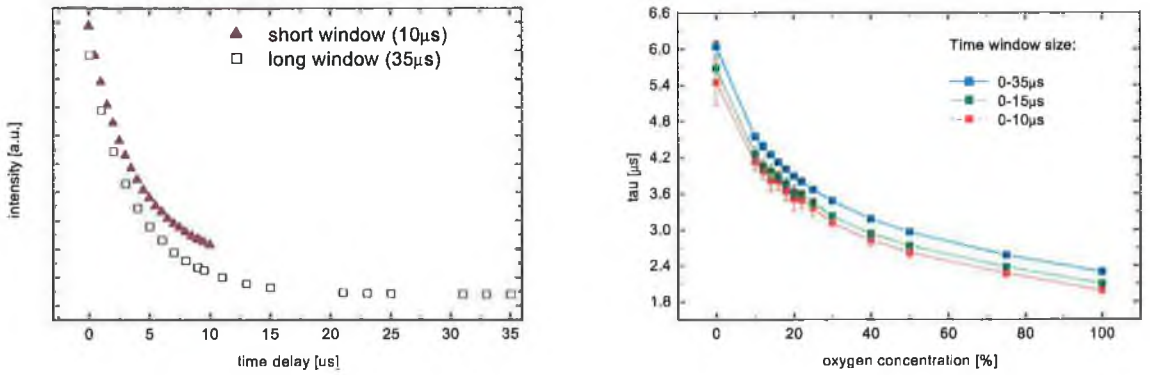

Figure 5.6: Influence of various time window to the quality of the fit. Raw data for short and long time window (a), showing the difference in datasets used for fits. b) resulting lifetime, including the error bars, for window sizes of 10 μs, 15 μs and 35 μs.

pixels). The relative error decreases from around 7% to less than 1%. The decrease of the relative error with further binning is not significant as other sources of variation become more important at this point. Moreover, it can be counterproductive to further increase binning as it reduces the image resolution.

The inset in Figure 5.5 shows the raw data used for fitting, and the clear decrease in noise between the case of no binning (1 × 1 binning) and 19 × 19 binning is illustrated (the curves are shifted in the vertical direction to avoid overlay in the figure).

In addition to the statistical determination of the relative error of lifetime from ten multiple measurements, an estimate of error from the least squares fit can be used. Both methods produce, in general, the same estimation of the experimental error.

5.4.3 Time window

The fitting of data to the exponential function in Equation 4.1 is sensitive to the length of the time window where data are available. This time window is often expressed in units of measured lifetime. It is generally accepted that, for an acceptable fit, the time window should be at least 2–3 times longer than the lifetime. After this time, the luminescence decays to the baseline and the fit becomes stable.

As in the previous section, the total data acquisition time is kept approximately constant by keeping a constant number of acquired data points. This means, that for longer time windows, the density of data points will be smaller (Figure 5.6a).

As in the case of the binning investigation, ten independent measurements of lifetime for an area of 8×8 pixels were taken and the mean lifetime and standard error were calculated. The lifetimes are shown in Figure 5.6b for 10 μs, 15 μs and 35 μs time windows. The calculated lifetimes increase with increasing time window. This is due to the non-single exponential nature of the ruthenium luminescence. The residues are not randomly distributed as would be for an ideal single-exponential decay, further supporting this evidence. The longer the window, the higher the influence of the long components.

a) b)

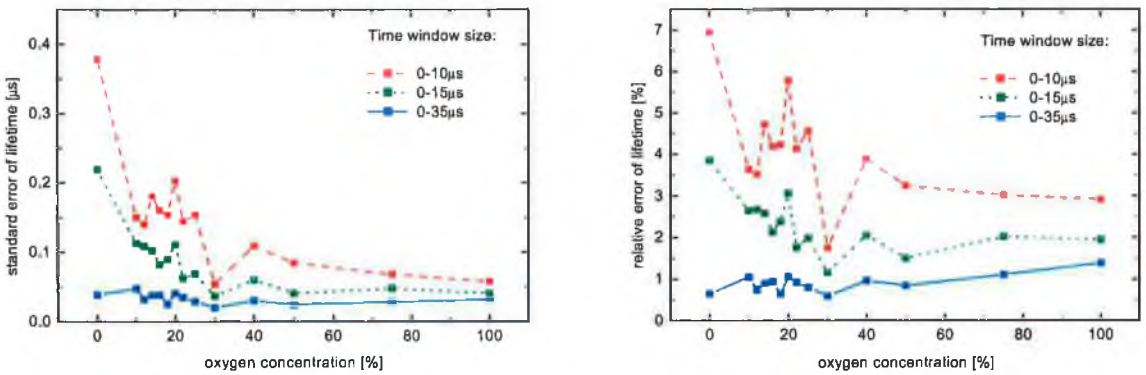

Figure 5.7: Absolute (a) and relative (b) error of lifetime as function of oxygen concentration for three different lengths of the time window.

The absolute and relative errors (measured in seconds and percentages, respectively) are presented separately in Figure 5.7, showing the positive influence of the extended time window on the error. For PSP measurements, the important area on the graphs is around 21% oxygen, when the time windows correspond to 2.5×, 3.75× and 8.75× lifetime, respectively.

The decrease of the absolute error is explained by the relative change of time window in units of lifetime. As the absolute value of lifetime decreases with increasing oxygen concentration, the length of the time window effectively increases and the fit become more stable, removing some of the random error from the results.

5.4.4 Switching of excitation modulation frequency (co-doped samples)

Simultaneous lifetime determination for co-doped samples raises the question of selecting the frequency of the excitation light. When using a simple signal generator typically only

one frequency is selected for data acquisition. This frequency corresponds to the longer of the lifetimes in order to allow the luminescence to decay.

While collecting data for the longer lifetime this frequency is ideal. The exposure is delayed after the short-lifetime luminescence has decayed and the complete light-off half-period is then utilised for data collection.

Short-lifetime data collection occurs at the beginning of the light-off half-period and the larger part of the time is not utilised. It would be desirable to utilise this idle time. The optimum solution is to use a higher excitation frequency while acquiring data for the short-lifetime luminophore. The increased frequency allows for more exposures to be performed in a fixed amount of time. This can be used either to increase the number of averaging cycles in a constant acquisition time or to shorten the total acquisition time.

To keep the data acquisition fully automated, the change in frequency must be computer-controlled. In our case, a computer-controlled trigger circuit was designed (Section 2.4.4 and Appendix B) and was capable of changing frequencies remotely via a parallel port.

In this work, the ratio of long to short lifetime is roughly 1000 but this does not mean that the data acquisition speed will increase by a factor of 1000. The acquisition time consists of the exposure and integration times (which are frequency-dependent) and the time needed for the read out of data (which is fixed). Fixed times contribute a large part to the total acquisition time with increasing exposure frequencies. For our configuration, with the DiCAM Pro camera and standard measurement protocol, the acquisition time can be reduced by as much as a factor of 1.1 or 25, depending on the exact settings. Settings with a higher number of loops benefit most, as the ratio of the time spent while exposing to time spend reading-out the data is higher.

Further possible improvements to the above method would be changing the aspect-ratio of the signal from 50:50 to 10:90 (on:off) and a slight increase in frequency (keeping the off-part of cycle constant), while keeping constant the average intensity of the excitation light. This means increasing the peak power of the excitation light in proportion to the shortening of the duty cycle. The maximum theoretical reduction of the data acquisition time would be 2, while for a 10:90 duty cycle, the maximum theoretical reduction is 1.67. However, in the configuration used, the actual reduction is negligible.

The modification of the excitation frequency for co-doped samples does not have a direct influence on the measurement error, but allows for increased averaging or integration,

the effects of which have been presented in the previous section.

5.4.5 Summary and evaluation of noise reduction methods

This section dealt with the processes responsible for random variations of the measured lifetime and discussed several methods for error reduction in the lifetime. The benefits of integration and averaging are clear from the data presented, which show a reduction in the relative error of ±1%. The use of binning was also shown to reduce the lifetime error.

It was established that the minimum lifetime error was achieved for a measurement time window of at least 8-times the lifetime. Finally, for co-doped samples, the total data acquisition time can be reduced by switching the modulation frequency, while still permitting appropriate time windows to allow analysis of the short and long lifetimes in turn.

The end result of using all of the above strategies simultaneously was an error of 1% in the lifetime, corresponding to an uncertainty in pressure of approximately 3.5%. This translates to ±3.5 kPa in ambient conditions.

5.5 Alternative lifetime measurement methods

5.5.1 Introduction

The previous section focused on improvements in data acquisition protocols compared to that reported in Chapter 4. This section focuses on the use of methods of processing the lifetime data using indirect approaches, when the lifetime is calculated indirectly from a ratio of intensities or a phase shift. The different methods are described and experimentally compared, based on the resulting error in lifetime. For one method, the performances of both the DiCAM Pro camera and another commercial camera system, the Imagex 2000 system are compared. As emphasised in the introduction to this chapter, the evaluation of lifetime errors in the methods discussed here apply to single-point lifetime measurement, and not to two-dimensional lifetime imaging. Finally, a brief discussion will be given of a phase-based, lifetime measurement technique which, while very successful for single point measurement, has not yet been implemented for two-dimensional measurements.

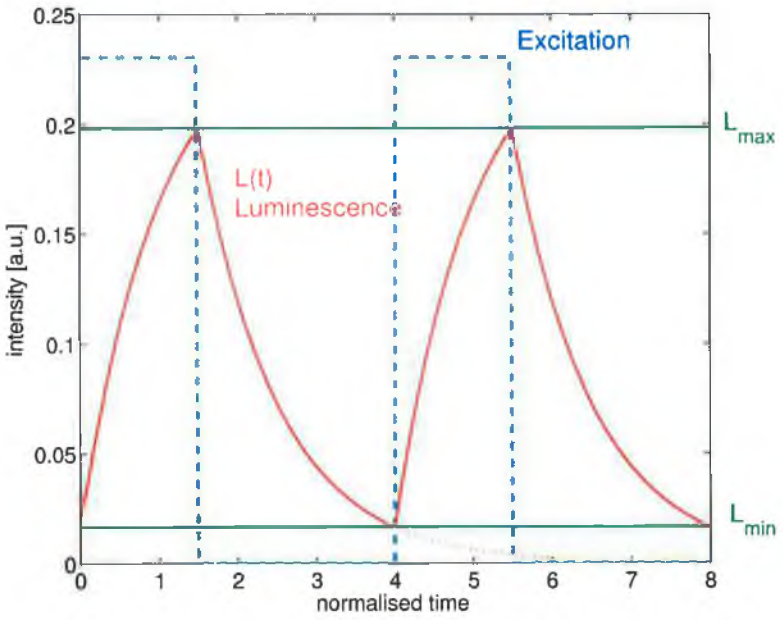

Figure 5.8: Square wave excitation – luminescence decay and rise.

5.5.2 Square wave excitation

For this analysis, we assume that the luminescent material displays a single-exponential behaviour with lifetime, τ. The time dependence of the observed luminescence $L(t)$ can, therefore, be calculated as a convolution of the excitation function and the system response function $I(t)$

$$L(t) = \int_{-\infty}^{t} E(t')\, I(t'-t)\mathrm{d}t' = \int_{-\infty}^{t} E(t')\, \frac{1}{\tau}\, \mathrm{e}^{-\frac{t-t'}{\tau}}\, \mathrm{d}t' , \tag{5.4}$$

where $E(t')$ is the temporal dependence of the excitation rate (which is proportional to the intensity of the excitation light through constants describing the efficiency of excitation of the luminophore molecules, paint thickness, luminophore concentration etc.) and $\frac{1}{\tau}$ is the normalisation factor of the impulse response function. This calculation is valid under the assumption of low light intensities. It implies that the occupation of the excited state is negligible compared to the ground state. This criterion is fulfilled using lamp or LED light sources, but not with focused lasers.

Next, the excitation signal is taken as a square wave of period, T, with an individual pulse duration, t_p, and is defined as

$$E(t) = \begin{cases} A & \text{for} \quad 0 + iT < t < t_p + iT \\ 0 & \text{for} \quad t_p + iT < t < T + iT \end{cases} \tag{5.5}$$

where i is a whole number representing the periodicity of the excitation signal and A is the amplitude of the excitation rate.

The time dependence of the luminescence in the presence of such a square wave (over one period) can be described as

$$L(t) = \begin{cases} L_{\min}\,\mathrm{e}^{-\frac{t}{\tau}} + A(1-\mathrm{e}^{-\frac{t}{\tau}}) & \text{for} \quad 0 < t < t_p \\ L_{\max}\,\mathrm{e}^{-\frac{t-t_p}{\tau}} & \text{for} \quad t_p < t < T \end{cases}, \tag{5.6}$$

where the constants L_{min} and L_{max} are the minimum and maximum levels of luminescence intensity, respectively as shown in Figure 5.8. These can be calculated by evaluating the integral in Equation 5.4, given the excitation light profile from Equation 5.5 to yield

$$L_{\min} = A\frac{\mathrm{e}^{\frac{t_p}{\tau}}-1}{1-\mathrm{e}^{-\frac{T}{\tau}}}\,\mathrm{e}^{-\frac{T}{\tau}}, \qquad L_{\max} = A\frac{\mathrm{e}^{\frac{t_p}{\tau}}-1}{1-\mathrm{e}^{-\frac{T}{\tau}}}\,\mathrm{e}^{-\frac{t_p}{\tau}}. \tag{5.7}$$

The only difference between these two expressions is in the argument of the last exponential factor. The luminescence profile is then

$$L(t) = \begin{cases} A\left(1+\mathrm{e}^{-\frac{t}{\tau}}\frac{\mathrm{e}^{-\frac{T-t_p}{\tau}}-1}{1-\mathrm{e}^{-\frac{T}{\tau}}}\right) = A\left(1+c_1\,\mathrm{e}^{-\frac{t}{\tau}}\right) & \text{for} \quad 0 < t < t_p \quad \text{(exc. on)} \\ A\frac{\mathrm{e}^{\frac{t_p}{\tau}}-1}{1-\mathrm{e}^{-\frac{T}{\tau}}}\,\mathrm{e}^{-\frac{t}{\tau}} = Ac_2\,\mathrm{e}^{-\frac{t}{\tau}} & \text{for} \quad t_p < t < T \quad \text{(exc. off)} \end{cases} \tag{5.8}$$

For a particular measurement, the excitation frequency (period T), pulse duration, t_p, and lifetime, τ, are constants and the expression can be written in terms of the constants c_1 and c_2.

It is worth noting that the luminescence intensity never reaches a zero value. Moreover, during both on and off periods of the excitation, the luminescence follows an exponential curve with decay constant $-1/\tau$ (see Figure 5.8). Therefore, both the rising and falling parts of the curve could be used for determining the lifetime.

When the luminescence profile over time is known, the amount of light that will be captured within a finite exposure time can be evaluated. The number of different gating strategies is very large.

For dual lifetime paints, the question of the influence of the second luminescence decay on the latter expression is relevant. Fortunately, as the system is linear in nature and, assuming that the luminophores do not influence each other, it can be quickly shown

that the contribution of both can be simply added yielding $L(t) = L_1(t) + L_2(t)$, where L_1 and L_2 are the temporal profiles of the luminescence of each individual lifetime from Equation 5.8.

5.5.3 Detection: two-shot exposures

An alternative method (compared to that used in Chapter 4), for the determination of lifetime-related information from luminescence relies on calculation ratio of two intensities both exposed during the 'off' part of the excitation cycle. The method is sometimes called the *dual gate* method, which belongs to the family of rapid lifetime determination methods (RLD) and its principle is depicted in Figure 5.9. The advantage is that the two independent exposures have the same duration, t_{exp}, and the data can be acquired without any optical filters (exposures happen when the excitation light is switched off), which is advantageous. The intensity acquired during each exposure can be written as the integral over the exposure time from the decaying exponential functions

$$I_1 = \int_{t_{\mathrm{delay}}}^{t_{\mathrm{delay}}+t_{\mathrm{exp}}} A' \mathrm{e}^{-\frac{t}{\tau}} = \tau A' \mathrm{e}^{-\frac{t_{\mathrm{delay}}}{\tau}} \left(1 - \mathrm{e}^{-\frac{t_{\mathrm{exp}}}{\tau}}\right), \tag{5.9}$$

$$I_2 = \int_{t_{\mathrm{delay}}+\Delta}^{t_{\mathrm{delay}}+t_{\mathrm{exp}}+\Delta} A' \mathrm{e}^{-\frac{t}{\tau}} = \tau A' \mathrm{e}^{-\frac{t_{\mathrm{delay}}}{\tau}} \left(1 - \mathrm{e}^{-\frac{t_{\mathrm{exp}}}{\tau}}\right) \mathrm{e}^{-\frac{\Delta}{\tau}}, \tag{5.10}$$

where t_{delay} is the time when the exposure of the first image starts (usually measured as a time delay after switching off the excitation light), A' is a pre-exponential factor including the efficiency of excitation and the sensitivity of the detection system, and Δ is the delay between the individual shots. Dividing these two values removes the dependence on the usually unknown constant A' and the other terms in equations 5.9 and 5.10 giving $I_1/I_2 = \mathrm{e}^{\frac{\Delta}{\tau}}$. Using a simple logarithm, this gives

$$\tau = \frac{\Delta}{\ln \frac{I_1}{I_2}} \tag{5.11}$$

as the value of the lifetime.

A lifetime measurement using this method depends only on the two intensities and the delay time, Δ, between the individual shots. The value of the resulting lifetime is independent of t_{exp} and t_{delay}, but it can be shown that the precision of the lifetime estimation depends on all the parameters t_{exp}, t_{delay} and Δ. However, in general, there is no reason for the two integration periods t_{exp} to be equal and the intervals do not have

to be discrete. The optimum parameter settings depend on the exact system setup and the value of the expected lifetime as is shown in the literature [2, 3]. The parameters can be varied; for example, the gate can be moved to the "on" part of the cycle. In this case, Equation 5.11 is no longer valid. A special case of this arrangement is discussed in Section 5.5.5.

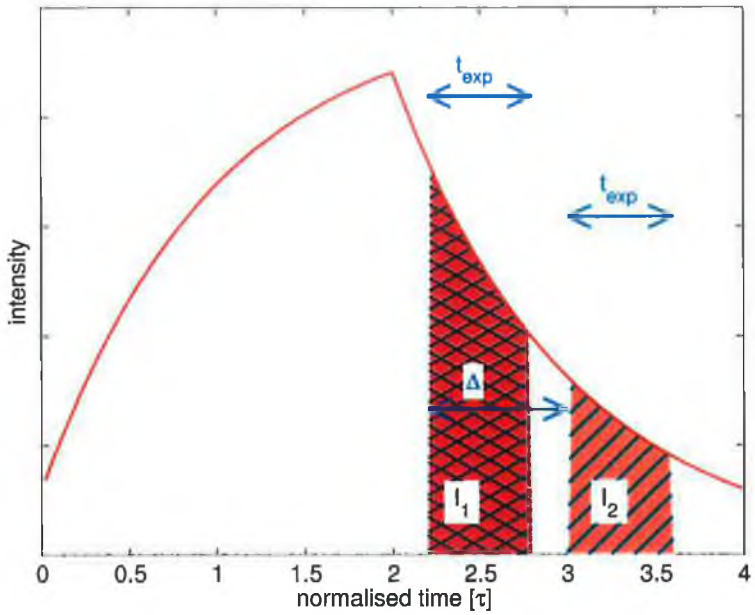

Figure 5.9: Capture of luminescence during the "off" part of the excitation cycle using two exposures (gates).

The two-shot exposure method is relatively simple and popular for lifetime detection. Complications occur when either the background can not be subtracted from the intensities I_1 and I_2, or in the case of multiple exponential decays. In the case of multiple decays the long-lived luminophores contribute to the background seen during the image exposures for short-lived species. In the case of the dual luminophore paint, when the short and long lived luminescence signals are independent, the background is not known *a-priori*. It can be extrapolated from the intensities and the lifetime measured for the long lived luminophore.

For our combination of luminophores, the reading of the MFG lifetime can be used to (a) read the temperature and (b) employ background correction of the reading of the ruthenium complex lifetime. The ruthenium complex lifetime is then converted to the pressure reading and corrected for the second time by the MFG lifetime reading of

temperature.

The two-shot exposure method for dual luminophore paint was not investigated, but the reproducibility for paint containing the only ruthenium complex was evaluated. The same configuration as in Section 5.4.3 was used to allow direct comparison of the results.

The data shows that the lower limit for the experimental error in lifetime using the dual gate strategy is between 0.5 – 0.25 %. Another important finding, presented in Figure 5.10, is that the total time needed for the acquisition of the data with reasonable precision is one order of magnitude shorter (less then a minute) compared to the total time for the measurement presented in Section 5.4 (~10 minutes).

The decreased level of random error in the case of the two-shot exposure method is attributed to the missing step in data processing, i.e. the data fitting stage. The decreased data acquisition time needed for improvement in error is due to the need for just 2 images, as opposed to the set of images required for fitting.

In conclusion, the two-shot exposure method is roughly 2–3-times better than the multi-shot exposure method used in Chapter 4 (and further improved on in the Section 5.4) in terms of experimental error, while significantly decreasing the total data acquisition time.

5.5.4 Detection: multiple shots exposure

Extending the idea of two exposures detailed in the previous section to that of the multiple exposures with increasing delays between shots ($\Delta_i = i\,\Delta$; $i = 1, 2, 3, \ldots$) gives a series of intensities where the consecutive values differ by a factor, $e^{-\frac{\Delta}{\tau}}$. This is a series which follows an exponential decay with the same constant, τ, as the original luminescence and, therefore, could be used for direct fitting of the data with an exponential decay curve to yield the original decay constant τ.

It is worth mentioning that the step in the delay, Δ, does not have to be bigger than the exposure time t_{exp} (Figure 5.11). The longer exposure time helps to increase the SNR as the lifetime data are typically collected by averaging over many cycles.

Such a protocol was used for the dual lifetime measurements presented in Section 5.5.3 and in Chapter 4. It is explained in more detail here for comparison with the protocol discussed in the previous section. The advantage of this approach is that, unlike the previous dual gate detection method, the multiple shot exposure is not susceptible to the problems associated with the unknown background light level. Therefore, it can be used

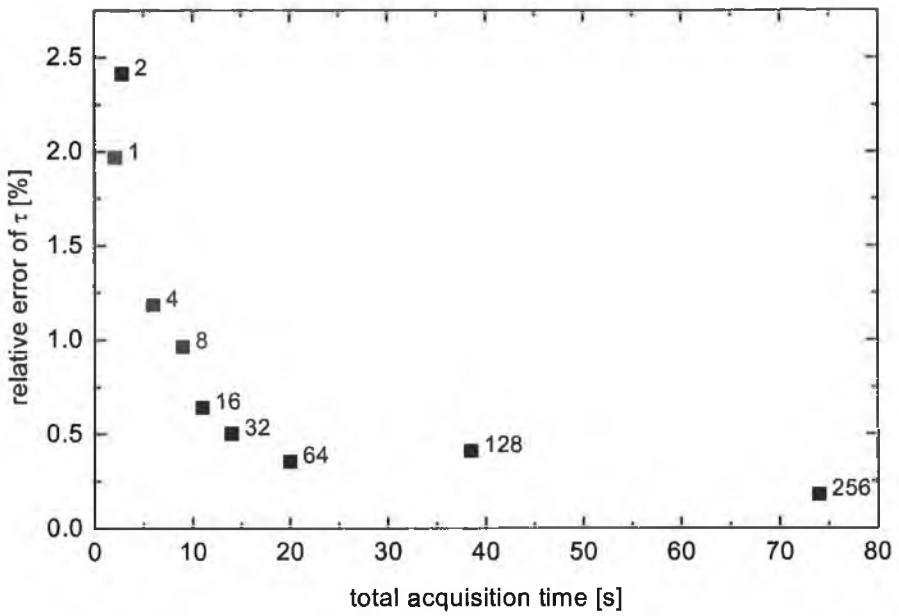

Figure 5.10: Two-shot exposure method. The relative error of the calculated lifetime as a function of the duration of data acquisition (increasing number of averaging cycles from 1 to 256 are shown next to the data points).

without any modification to measure multiple lifetimes from a single sample, where the longer-lived luminophore contributes to the "background" seen while fitting the short-lived lifetime. Such a background is then included in the constant C in Equation 4.1.

5.5.5 In-phase/out-of-phase detection (Imagex 2000)

An alternative lifetime detection method is that of *in-phase/out-of-phase* detection, which is implemented in the commercially available lifetime system Imagex 2000. The principle is shown in Figure 5.12. The sample is excited by the square wave of period T and pulse duration t_p. Two sets of images are acquired – first, the image noted as "on" is acquired during the time when the excitation light is on. The second image is acquired while the excitation light is off. As the images are acquired in phase or out of phase with the excitation light, the images are often called in-phase and out-of-phase images, respectively. Therefore, the camera and the excitation light source can be triggered from a single source without any extra time delay circuits, as was the case in the multi shot method and dual-shot method.

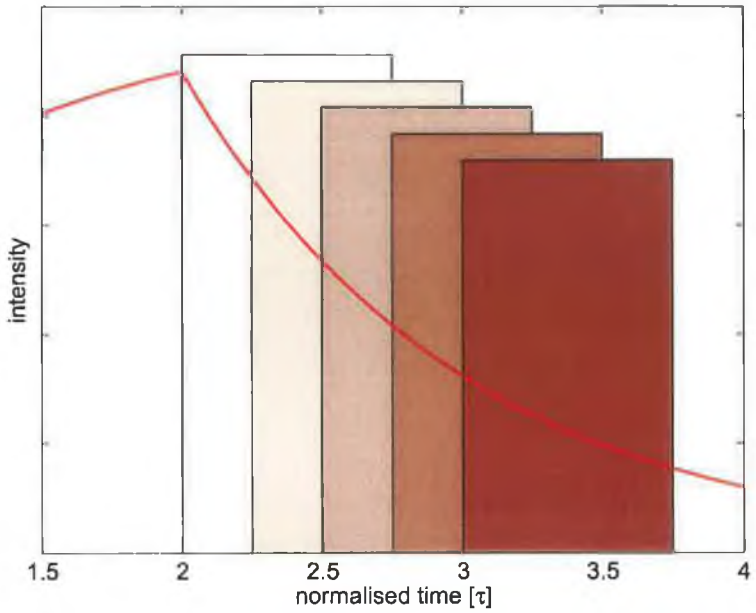

Figure 5.11: Multiple exposures during the single exponential luminescence decay yield integrated intensities having the same exponential decay as the original decay. Filled rectangular boxes represent the constant exposure time $t_{\mathrm{exp}} = 1.5\tau$, while the start of each exposure is delayed by $\Delta = 0.25\tau$ from the previous.

Using ideally crossed optical filters on the light source and camera, the intensity captured in the on and off cycle can be calculated as an integral of the temporal luminescence profile (Equation 5.8) over intervals $\langle 0; t_p \rangle$ and $\langle t_p; T \rangle$:

$$\begin{aligned} I_{\mathrm{ON}} &= \int_0^{t_p} L(t)\,\mathrm{d}t = A\left[t_p + \tau\frac{(\mathrm{e}^{-\frac{T-t_p}{\tau}} - 1)(\mathrm{e}^{-\frac{t_p}{\tau}} - 1)}{1 - \mathrm{e}^{-\frac{T}{\tau}}}\right] \\ I_{\mathrm{OFF}} &= \int_{t_p}^{T} L(t)\,\mathrm{d}t = \tau A\frac{(\mathrm{e}^{\frac{t_p}{\tau}} - 1)(\mathrm{e}^{-\frac{t_p}{\tau}} - \mathrm{e}^{-\frac{T}{\tau}})}{1 - \mathrm{e}^{-\frac{T}{\tau}}} \end{aligned} \tag{5.12}$$

Calculation the ratio of the outputs should give an intensity-independent value, in our case dependent on the timing parameters T (period of excitation signal), t_p (length of single excitation pulse) and τ (lifetime):

$$R = \frac{I_{\mathrm{OFF}}}{I_{\mathrm{ON}}} = \frac{\tau(\mathrm{e}^{\frac{T}{\tau}} - \mathrm{e}^{\frac{t_p}{\tau}})(\mathrm{e}^{\frac{t_p}{\tau}} - 1)}{(t_p - \tau)\,\mathrm{e}^{\frac{T+t_p}{\tau}} + \tau\,\mathrm{e}^{\frac{T}{\tau}} + \tau\,\mathrm{e}^{2\frac{t_p}{\tau}} - (t_p + \tau)\,\mathrm{e}^{\frac{t_p}{\tau}}} \tag{5.13}$$

Such an equation looks rather complicated, but in the case of $T = 2t_p$ (50% duty

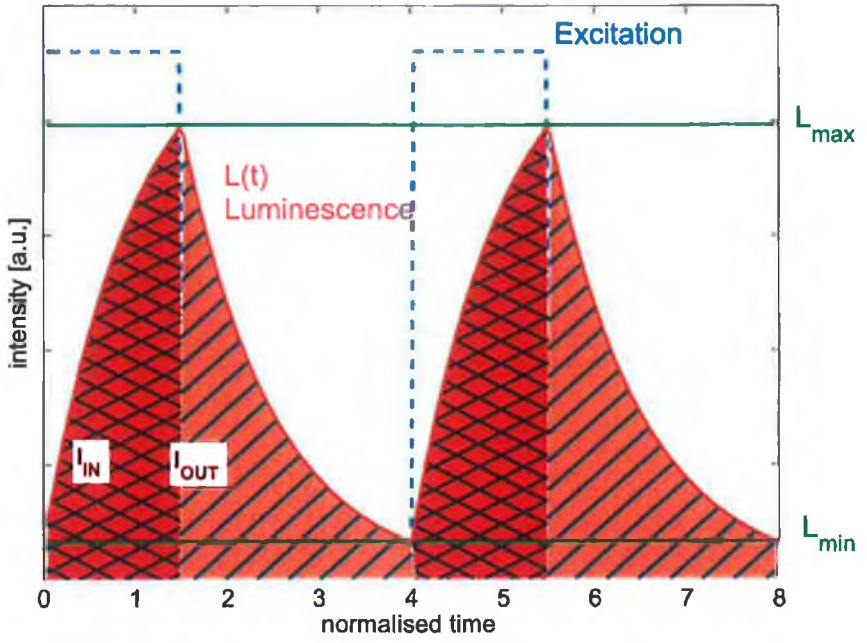

Figure 5.12: Capture of luminescence during "on" and "off" parts of the excitation cycle.

cycle) it can be simplified into the more compact form

$$R = \left[\frac{e^{-\frac{T}{4\tau}} + e^{\frac{T}{4\tau}}}{e^{\frac{T}{4\tau}} - e^{-\frac{T}{4\tau}}} \cdot \frac{T}{2\tau} - 1 \right]^{-1} = \left[\frac{T}{2\tau} \coth\left(\frac{T}{4\tau}\right) - 1 \right]^{-1} . \tag{5.14}$$

The behaviour of the ratio, R, for different lifetimes is captured in Figure 5.13, using normalised units of lifetime at ambient conditions when $\tau = 1$. The maximum change of the R value versus lifetime, which yields the maximum resolution of measurement, is found by numerical solution for a period $T \approx 4.72332\tau$ around the point where $\tau = 1$ (the region of PSP interest). This corresponds to an optimum ratio $R = 0.5396$. In the real world we want to keep the ratio R close to 1 in order to be able to utilise the full dynamic range of the CCD chip, thereby shortening the period of the excitation light. Alternatively, if the image is obtained by integrating over several pulses, the exposures can be set independently for each image in order to utilise the full dynamic range, followed by normalising to the number of integration cycles.

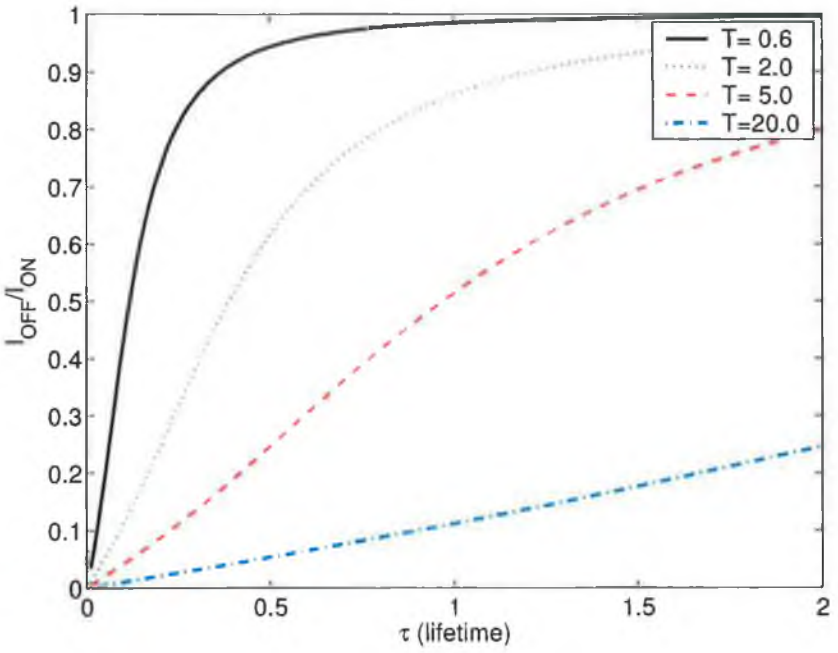

Figure 5.13: Ratio of I_{ON}/I_{OFF} versus lifetime for four different periods of excitation pulses. Lifetime τ and period T are normalised to lifetime at ambient conditions.

5.6 Lifetime measurement using the Imagex 2000 system

The Imagex 2000 system (described in Section 2.4.3) was used to measure the lifetime of two different luminophores; (i) the $[Ru(dpp)_3]^{2+}$ complex previously measured with the DiCAM Pro system and (ii) a reference sample from Photonic Research Systems (PRS). The results obtained are shown in Figure 5.14. Clearly, the measured "lifetime" is a function of the modulation frequency for both samples. This result is correlated with the non-single-exponential nature of the luminophore lifetime. For a single exponential decay, the Imagex 2000 measurement protocol of obtaining ratio of the I_{OFF} and I_{ON} intensities should give an intensity-independent value of lifetime which is independent of modulation frequency. In the case of non-single-exponential decays, the lifetime reported by this method is the weighted average of all lifetimes. The change in the modulation frequency changes the weighting factors for different lifetimes, thereby yielding a different value for the intensity ratio, R, and the resulting averaged lifetime displayed in the graph. In Figure 5.14 the effect is present for the lifetime measurements of both samples. It is known from other measurements that the luminescent decays of both samples are not single-exponential, as the $[Ru(dpp)_3]^{2+}$ complex is immobilised in an amorphous glass

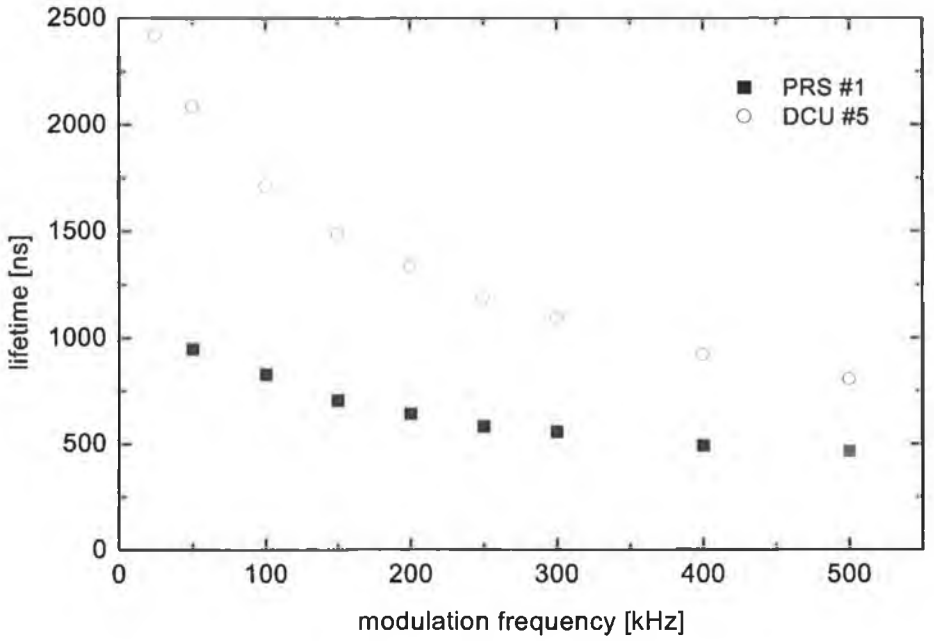

Figure 5.14: Lifetime measurements with Imagex 2000 system.

matrix.

Apart from the problem discussed above, it was found that the Imagex 2000 system did not cope very well with the lower modulation frequencies ($< 100\,\text{Hz}$) required to measure the MFG lifetime ($\sim 2\,\text{ms}$). The modulation frequency was not stable at low frequency settings. Therefore, we were discouraged from using this system for our primary investigation. However, it was possible to configure the DiCAM Pro camera to use the same detection method as the Imagex and the results obtained are discussed below.

The gated DiCAM Pro camera is very flexible with regard to setting up various exposure times and delays and allows for partial external control through its trigger input (`TRIG`) and input disabling gate (`GATE DIS`). The DiCAM Pro is capable (when used with our trigger box (Appendix B)) of being configured in the same way as the Imagex 2000 and, therefore, we decided to carry out measurements for the purposes of comparing the two systems in this configuration.

As for the previously described methods, the experimental error evaluation was carried out using similar settings as in Section 5.4.3 and using a standard ruthenium complex-based PSP paint. To rule out the effects of different detection systems and allow for direct comparison, the DiCAM Pro camera was used again as in the previous sections.

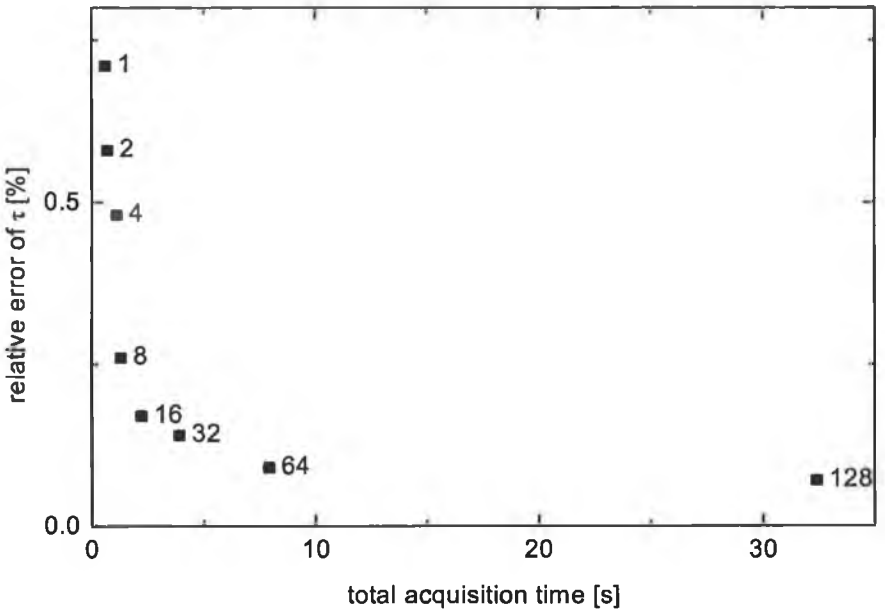

Figure 5.15: In– and out– of phase method using the DiCAM Pro camera. The relative error of the calculated lifetime as a function of the duration of data acquisition (increasing number of averaging cycles from 1 to 128 shown next to the data points).

The `GATE DIS` input on the camera was used to directly synchronise the detection gate and excitation light without the use of internal timing circuits of the camera. An exposure time of 20 ms was used and integration on the chip was achieved using a single integration loop — multiple loops were not necessary to achieve reasonably intense images as in Section 5.4.1. The effective increase of the detected light, compared to the previous methods, allowed us to take the measurements without on-chip binning.

The achieved error was on the order of 0.1% of the lifetime, again including a large decrease in the total acquisition time (necessary for the reduction of error values), as shown in Figure 5.15.

When a similar measurement was made using the Imagex 2000 system, the minimum error was approximately 1%. The Imagex 2000 system does not have averaging options and therefore does not facilitate the improvement of performance through averaging. The total acquisition time is in the range of seconds.

The in-phase/out-of-phase method is potentially capable of improving the experimental error of the data by an order of magnitude compared to the errors in Chapter 4 with multiple exposures. The gating used here captures a relatively large amount of the lu-

minescent light (up to 50%), hugely improving the Poissonian noise in the system, which explains the very promising results.

5.7 Phase based lifetime detection

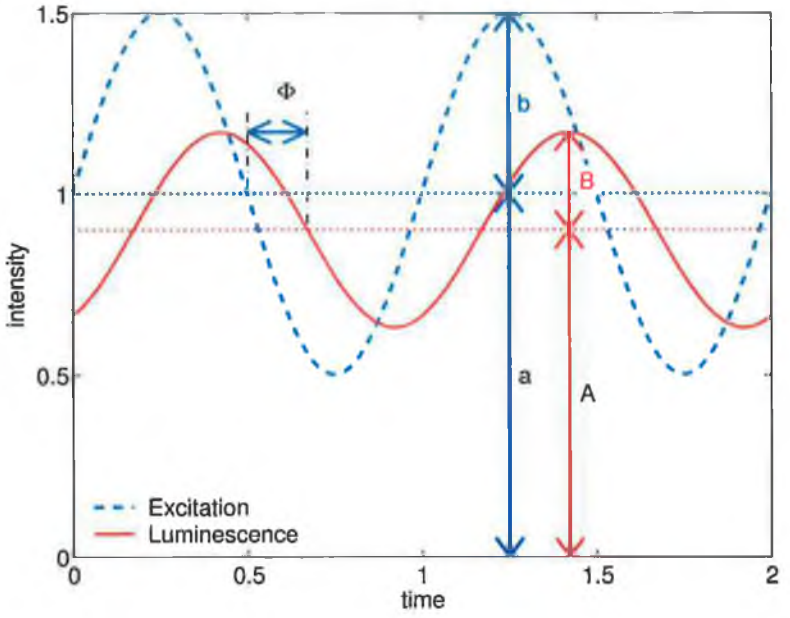

Figure 5.16: Phase and modulation of luminescence.

This is an alternative method of measuring lifetime where the light is modulated ideally by a harmonic (sine) function. It can be shown [4] that, if the luminophore with a single exponential lifetime τ, is excited with a harmonic (sinusoidal) signal of frequency f, then the resulting luminescence will be at the same frequency and shifted by a phase, Φ, relative to the excitation signal*:

$$\Phi = \arctan(2\pi f\tau)\,. \tag{5.15}$$

Inverting this equation to get lifetime τ gives

$$\tau = \frac{\tan\Phi}{2\pi f},. \tag{5.16}$$

*Assuming an excitation intensity in the form of $I_{\mathrm{exc}}(t) = a + b * \sin(\omega t)$, where $\omega = 2\pi f$, and using a convolution integral, the resulting luminescence yields $L(t) = \int_{-\infty}^{t} I_{\mathrm{exc}}(t)\frac{1}{\tau}\,\mathrm{e}^{-(t-t')/\tau}\mathrm{d}t' = a + [b\cos(\omega t - \Phi)]/m$, where $\Phi = \arctan(2\pi f\tau)$ and $m = \sqrt{1+(\omega\tau)^2}$ yielding the results shown above.

The change in modulation is also helpful for lifetime determination, as the unit-less demodulation, m, is also lifetime dependent:

$$m = \frac{A/B}{a/b} = \frac{1}{\cos\Phi} = \sqrt{1 + 4\pi^2 f^2 \tau^2}\,, \tag{5.17}$$

$$\tau = \frac{\sqrt{m^2 - 1}}{2\pi f}\,, \tag{5.18}$$

where a and A are the mean values of the intensities (DC component) of excitation and emission, respectively, and b and B are the amplitudes of the harmonic part of the excitation and luminescence, respectively, as defined in Figure 5.16.

In a practical configuration, phase measurements are typically used as such measurements are not sensitive to the offset of detectors, amplifiers or background light.

To achieve exact harmonic (sinusoidal) excitation can be difficult, taking into account the non-linear response of the light source to the driving voltage (for example the non-linear response of LEDs). However, due to the fact that the luminescent system is a linear system, the excitation can be treated as a sum of Fourier components $a + \sum_{j=1}^{\infty} b_j \cos(j\omega t)$ and the resulting luminescence is again a sum of harmonic components with different changes in the amplitudes and in the phases. As phase detection is usually performed with lock-in detection, only the first term corresponding to the fundamental frequency, ω, is detected and Equation 5.16 is used [5]. This conclusion is not valid for demodulation of the signal (Equation 5.17).

This method, called *phase detection*, is very popular in optical sensor systems as it is very robust. The implementation for a PSP camera system is not straight-forward, as a lock-in amplifier for each pixel would be needed or harmonically modulated image intensifiers must be used. To our knowledge, this has not yet been used in PSP systems. However, phase bdetection using a camera with modulated gain and modulated excitation light source for FLIM measurements was demonstrated a patented by Morgan [6]. For single point measurements, the phase detection method yields excellent signal-to-noise ratios.

For multiple-component lifetime samples, the method does not produce correct lifetimes. However, the method can be slightly extended to produce useful results. Specifically, the phase can be measured for several frequencies and the dependence of the phase versus frequency is fitted to yield the pair of lifetimes [4].

5.7.1 Summary

The three alternative methods for lifetime measurement discussed in this chapter demonstrated improved noise reduction for single-point lifetime measurement compared to the results reported in Chapter 4. The dual gate exposure technique achieved a random error in lifetime of 0.25%, while the error for the in-phase/out-of-phase method was 0.1%. The two methods above involve fewer data manipulation steps, as well as making more effective use of the available luminescence signal. Unfortunately, the reported lifetime is not accurate in absolute values. However, the true value of the lifetime is not important for PSP users as long as the reported parameter is reproducible and repeatable and can be calibrated against pressure. The phase detection method as described in Section 5.7, while yielding high precision oxygen pressure data for single point measurements, cannot be used for spatial measurements using current technology. However such measurements could be achieved by employing sinusoidal modulation in conjunction with a square wave gate and varying delay.

5.8 Overall conclusion of this chapter

5.9 Conclusions

In the first part of the chapter, several methods for error reduction in the lifetime were discussed. These included averaging and binning techniques as well as optimisation of the measurement time window for direct lifetime measurement method. These methods, when used simultaneously, yielded a lifetime error of $\pm 1\%$ corresponding to an uncertainty in pressure of approximately $\pm 3.5\,\mathrm{kPa}$. In the second part of the chapter, alternative techniques for lifetime measurement were considered. The optimum technique was the in-phase/out-of-phase technique, which yielded a lifetime error of 0.1%, for single point measurement, corresponding to $0.35\,\mathrm{kPa}$. The spatial behaviour of the lifetime will be considered in the next chapter.

5.10 References

[1] W. M. Ruyten, "Self-illumination calibration technique for luminescent paint measurements," *Rev. Sci. Instrum.*, vol. 68, no. 9, pp. 3452–3457, 1997.

[2] L. Hand and J. Bell, "Optimum timing for excitation and detection gates in luminescence lifetime measurements," in 9^{th} *Annual PSP Workshop*, (Washington DC, USA), p. unpublished, 7 – 11 April 2002.

[3] S. P. Chan, Z. J. Fuller, J. N. Demas, and B. A. DeGraff, "Optimized gating scheme for rapid lifetime determinations of single-exponential luminescence lifetimes," *Anal. Chem.*, vol. 73, no. 18, pp. 4486–4490, 2001.

[4] J. R. Lakowicz, *Principles of Fluorescence Spectroscopy.* New York: Kluwer Academic/Plenum Publishers, second ed., 1999.

[5] H. Rowe, S. P. Chan, J. Demas, and B. DeGraff, "Elimination of fluorescence and scattering backgrounds in luminescence lifetime measurements using gated-phase fluorometry," *Anal. Chem.*, vol. 74, no. 18, pp. 4821–4827, 2002.

[6] C. G. H. MORGAN, "Measurement of luminescence," 1992. European paten application – EP0519930B1, US patent application – US 5.459.323.

Chapter 6

Wind tunnel measurements and spatial variations

6.1 Introduction

The data discussed in chapters 4 and 5 dealt exclusively with single point measurements, where the oxygen response was measured from a small area of the test surface. This chapter deals with measurements on the complete two-dimensional test surface. Firstly, the wind-tunnel testing of the PSP is described. Laboratory-based characterisation of a range of test surfaces is then presented. Finally, results of non-camera-based lifetime studies of the paint surface are reported.

6.2 Wind tunnel measurements

Following the laboratory testing of the PSP system and the paint described in Chapter 4, the system was tested in real wind tunnel conditions. This measurement was carried out at the wind tunnel facility of the Stokes Research Institute in the University of Limerick [1] in collaboration with Dr. Tara Dalton and David McGuire.

The aerodynamic object selected to test was an airfoil made from aluminium, machined into a shape specified by the National Advisory Committee for Aeronautics (NACA) as NACA 0012 [2]. The transverse dimension of the test piece was 30 cm and the longitudinal dimension was 26 cm. The aerodynamic characteristics of this particular shape are well documented and it has been used over many years as the test case for various

techniques [3]. The variation of the surface pressure is reported to be relatively high, promising a good chance of pressure measurements using the PSP method.

The test piece of airfoil was pressure profiled using both the conventional and PSP&TSP methods. For the conventional pressure measurement, the test piece was instrumented (pressure-tapped) with 9 pressure taps, facilitating pressure distribution measurements using direct methods. The airfoil was then spray-painted with a stripe of standard PSP&TSP paint (ruthenium complex and MFG based) and was cured overnight in the oven at 70 °C. Figure 6.1 shows the airfoil after spray-coating ready to be installed in the wind tunnel.

Figure 6.1: Left: NACA 0012 airfoil before the wind tunnel test. The black dots in the middle are the inlets to the pressure taps and on the right-hand side of the image is the plastic tubing used for the connection of manometers. To the left of the pressure taps is the yellow strip of the PSP&TSP paint (on the right of this is a black strip of paint from another experiment). Right: Cross section of NACA 0012 airfoil at a positive angle of attack. Arrows show the approximate position of the pressure taps shown in the photograph on the left.

Wind tunnel

The wind tunnel experiments were carried out in an open-circuit*, medium speed wind tunnel capable of running at speeds up to 100 ms^{-1}. The overall length of the complete tunnel, including the suction entrance, fan, stabilising honeycomb section, test section and the diffuser was approximately 12 metres. The working area (test section) of the tunnel consisted of perspex walls to allow optical access to the model. The cross-section

*The air is discharged and up-taken from the laboratory.

of the test section was 30×30 cm and length was 1 m. The airfoil was mounted in the wind tunnel vertically; therefore the painted stripe was oriented horizontally and was optically accessible from the side. The overall configuration of the system consisting of the DiCAM Pro camera, blue LED bank and the wind tunnel is shown in Figure 6.2.

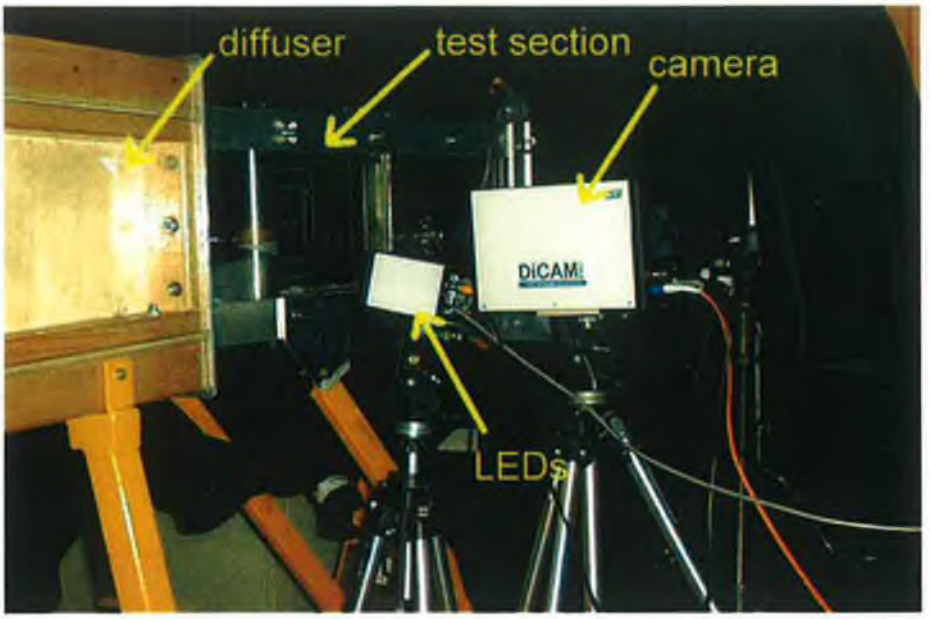

Figure 6.2: The PSP&TSP system at the medium speed wind tunnel — the DiCAM Pro gated CCD camera and blue LED bank are in front of the window of the wind tunnel.

6.2.1 Results from wind tunnel measurements

The image of the luminescent strip is shown in Figure 6.3. The data were recorded using a similar protocol as in Chapter 4 (multiple shot exposure, Section 5.5.4). The raw images were cropped to fit the stripe of PSP paint and divided into 30 vertical slices. It was expected that variations in air pressure would be observed in the horizontal direction only (i.e. the direction of wind flow) and therefore the variation of signal in the vertical direction was not studied in detail. The brief investigation which was carried out supports this assumption. The intensity in all pixels in each slice was integrated over the slice area and these data were fitted to a single exponential function (Equation 4.1). The resulting lifetime and corresponding error bars of 1σ are represented in figures 6.4 and 6.5.

The lifetime data represent a positive angle of attack, $\alpha = 12°$ and four different

air speeds. For this value of the angle of attack (AoA) and available air speeds, the lift is large and the airflow is still laminar over the entire top surface of the airfoil. The graphs represent two independent measurements taken on two different days under similar conditions.

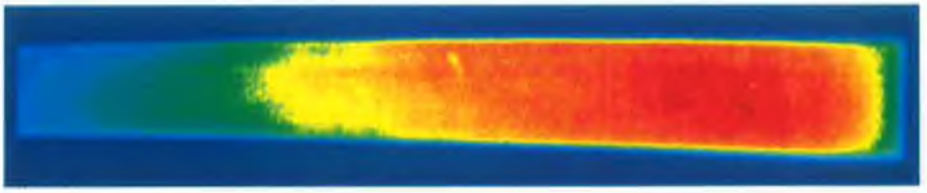

Figure 6.3: Raw image of the strip of PSP before processing. False colours represent luminescence intensity, increasing from blue through green, yellow to red.

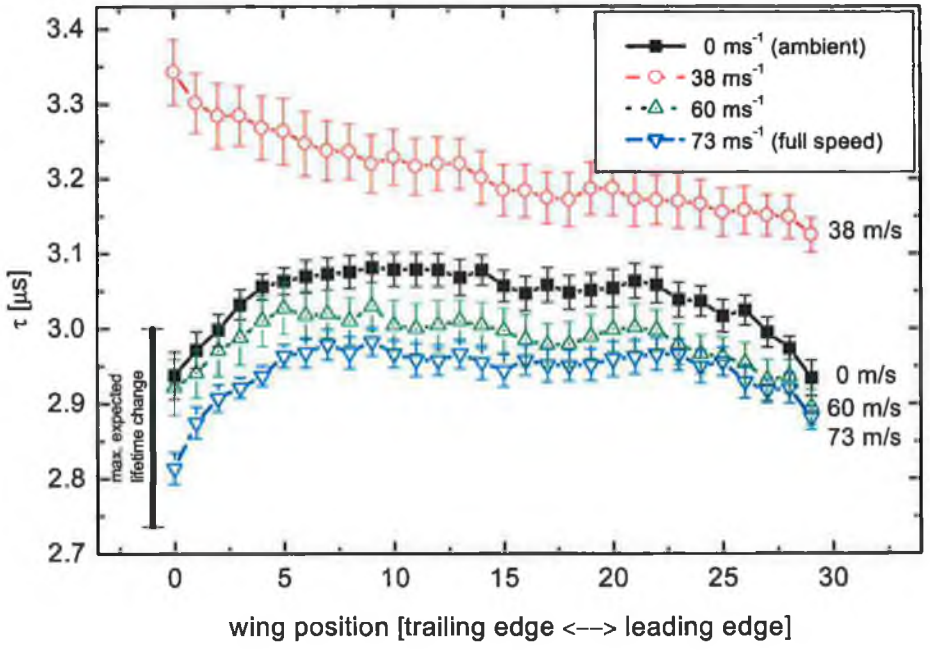

Figure 6.4: Ruthenium-complex lifetime data from the wind tunnel test (16^{th} Nov) with error-bars representing standard error σ. Vertical bars represent the maximum expected lifetime change, predicted from the calibration curve (Figure 4.5).

In parallel with the lifetime PSP measurements, pressure measurements using the manometer and 9 available pressure taps were carried out. The pressure values in each pressure tap are shown in Figure 6.6.

The standard NACA 0012 airfoil profile and its aerodynamic properties are well under-

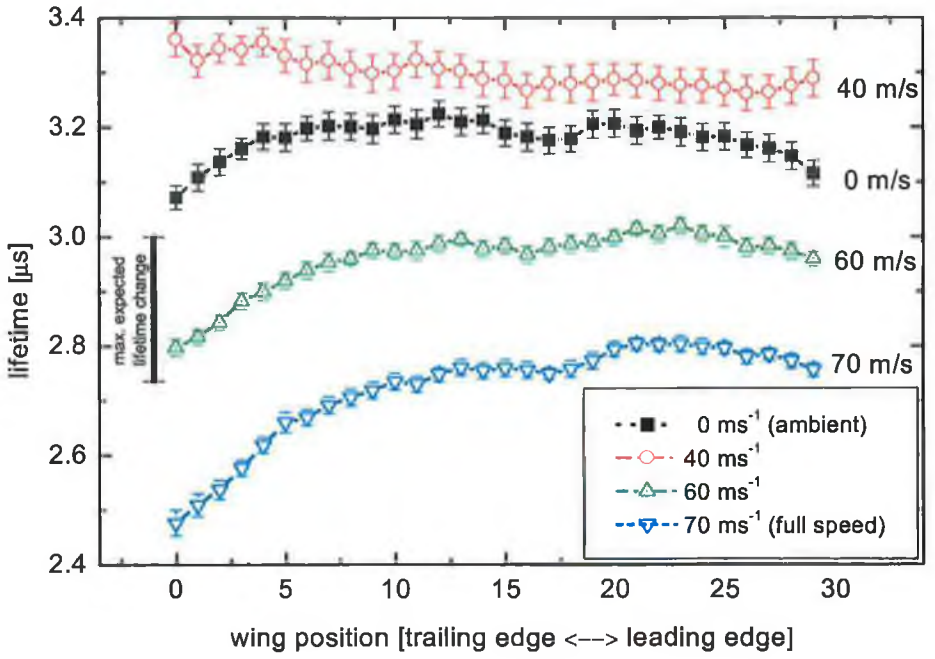

Figure 6.5: Ruthenium-complex lifetime data from the wind tunnel test (14th Nov) with error-bars representing standard error σ. Vertical bar represents the maximum expected lifetime change, predicted from calibration curve.

stood and, in general, the measured values of total surface pressure from the pressure taps (traditional method) followed the expected spatial profile. The pressure values decreased monotonically with increasing wind speed, causing increasing lift.

From the maximum pressure difference measured by the conventional method, the estimated maximum relative change of the lifetime was estimated and is shown in Figure 6.4 and Figure 6.5 as a bar on the left hand side. For the reasons discussed below, the lifetime is not converted into pressure. However, in general, the pressure in pascals is inversely proportional to the lifetime and this guide should be remembered when comparing lifetime and pressure data.

The variation of the temperature sensitive MFG lifetime was very large, due to large level of Poisson noise in the data at low recorded levels of luminescence, giving a temperature uncertainty of over 20 degrees (higher than the maximum expected temperature difference in the wind tunnel measurement). Therefore, the MFG lifetime was not acquired and temperature corrections were expected to be realised by using the temperature measured by a single thermocouple mounted on the wing.

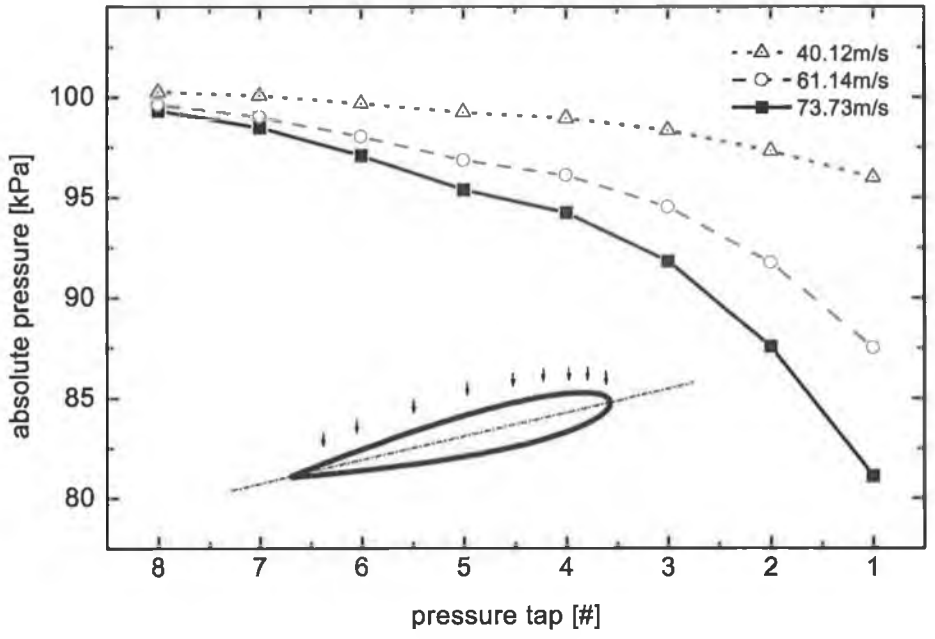

Figure 6.6: Absolute pressure distribution over the surface of the airfoil (NACA 0012 at a 12° angle of attack), the errorbars are of size of the data points. The inset shows the shape of the foil and the approximate position of the pressure taps.

6.2.2 Integrity tests

When the lifetime data and pressure taps data are examined in detail, a discrepancy between the PSP data in figures 6.4 and 6.5 and the pressure tap data in Figure 6.6 become visible. The pressure tap data follow the expected profile with pressure decreasing with increasing wind speed. Figures 6.4 and 6.5 on the other hand, contradict this trend where, for most speeds, the lifetime decreases with increasing speed, which corresponds to a pressure increase.

The principal discrepancies are summarised below:

1. The absolute values of the lifetime do not fit the expected lifetime range from the calibration (the expected values were 2.5–3 μs).

2. The sequence of the lifetime curves for various wind speeds does not increase monotonically as was expected.

3. The lifetime variation between the individual runs is higher than the maximum change estimated from the calibration curve in Figure 4.5.

4. The overall trend of the lifetime profile, which is indirectly proportional to the total pressure, does not follow the measured total pressure from the pressure taps.

5. Data for the ambient conditions shows a spatial variation, where none should be evident.

There are several sources of these discrepancies, ranging from the humidity sensitivity of the paint, the sensitivity of the lifetime of ruthenium complex to the coating technique and coating conditions, non-ideal optical access to the paint strip, the unsteady conditions during the tests and missing temperature corrections. These issues are discussed below.

6.2.3 Humidity effects

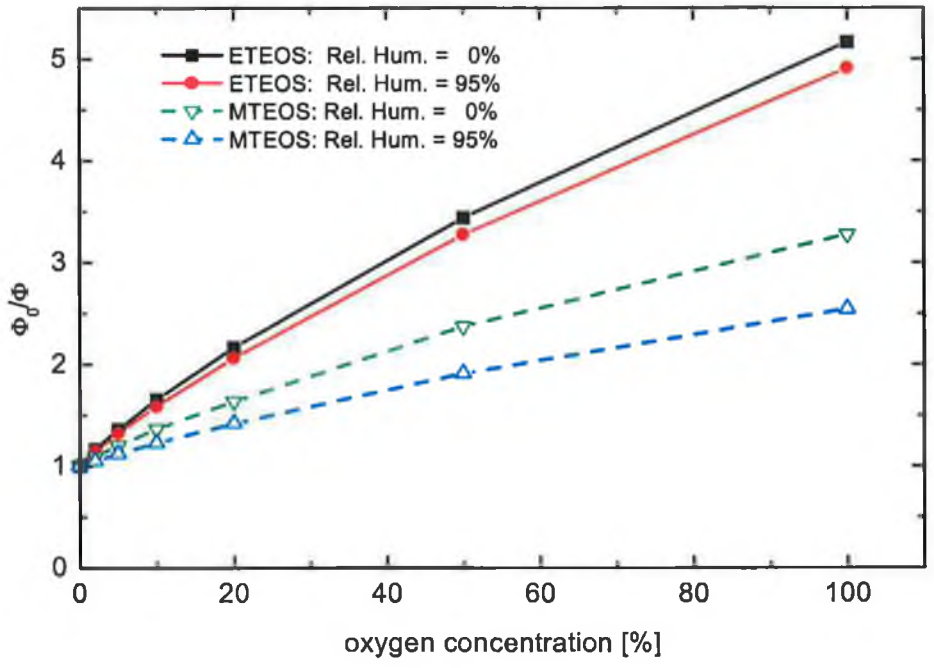

Figure 6.7: Humidity sensitivity of MTEOS and ETEOS (EthylTEOS) shown in a Stern-Volmer phase plot.

Firstly, as was later discovered, the laboratory-based a-priori calibration* that was taken with dry gases (Figure 4.5) cannot be directly applied to the wind tunnel measurements due to the fact that the paint itself is humidity-sensitive (this was established after

*a-priori calibration — calibration curve is constructed from the data collected independently of the wind tunnel measurement data.

the wind-tunnel test). The increasing humidity reduces the oxygen sensitivity of the paint, making the laboratory calibration with dry gases unsuitable for paint characterisation, as the air in the wind tunnel was at ambient humidity. This explains the long lifetimes observed in the wind tunnel data. Since this measurement was carried out, it has become clear that more hydrophobic ORMOSILs (Section 2.1.5), for example EthylTEOS, have minimal or no humidity sensitivity [4]. This is shown in Figure 6.7.

The issue with the humidity sensitivity of MTEOS-based paint could, in principle, be improved by using in-situ calibration*. However, whilst in-situ calibration could correct for the significantly longer lifetimes observed it would not resolve the other discrepancies.

6.2.4 Possible effects of the temperature corrections

As the lifetime data are not temperature corrected, the previous discrepancies can be potentially explained by temperature effects. From the calibration curve, the temperature sensitivity of the ruthenium complex lifetime is 0.6–0.65 % of lifetime value per °C in conditions close to ambient conditions (25 °C and atmospheric pressure). The temperature of the air in the wind tunnel between runs, as recorded by the thermocouple,varied between 22 °C and 26 °C and this corresponds to a maximum shift in lifetime of 2.5% ($\sim 0.075\,\mu$s). Therefore, this cannot explain the discrepancies in the data.

6.2.5 Unsteady conditions

For reliable results, the PSP data acquisition protocol assumes constant conditions (pressure and temperature) during a single data acquisition (at a particular wind speed). For the protocol used here, the full data acquisition time lies between 10 and 15 minutes and the temperature in that time interval rises, depending on the wind speed and ventilation status of the wind tunnel facility, by up to 3 °C. As the lifetime images were recorded with decreasing time delay t_{delay}, the increase in the temperature during the measurement would cause a slow decrease in the intensity (efficiency) of luminescence and lifetime during the single data acquisition. For co-doped paint the background is also temperature dependent due to the fact that the time-resolved intensity of the ruthenium complex sits on the background signal level of MFG luminescence, which is temperature dependent.

*in-situ calibration — calibration using auxiliary data from the wind tunnel measurement, typically pressure taps data with temperature information.

However this signal is almost negligible.

As the effects of the increasing temperature of the airflow are similar for the whole wing, all zones (pixels) in the image are influenced in a similar manner with the final fitted lifetime being somewhere between the true lifetime at the beginning and end of measurement. Even the varying temperature cannot explain all the issues mentioned earlier and again the in-situ calibration can reduce the effect of the unsteady temperature in the wind tunnel.

Small vibrations of the airfoil, observed at the air speeds $> 50\,\mathrm{ms}^{-1}$ presented movement of the airfoil in the picture of less than 0.3 pixels which is almost negligible in terms of the size of super-pixels used for lifetime fitting.

6.2.6 Alternative fitting model

The temporally resolved intensity of luminescence of the ruthenium dye is superimposed on top of the background light intensity. The background consists of ambient background (constant in time) and background light originating from the long-lifetime MFG phosphor. In the first approximation, the MFG component can be taken as constant and included in the constant C in Equation 4.1 ($A\,\mathrm{e}^{-t/\tau} + C$). A second approximation of the MFG component yields a linear dependence of the background level. Therefore, the background is represented in the form of $C + Dt$, giving a final function

$$I(t) = A\,\mathrm{e}^{-t/\tau} + C + Dt\,. \tag{6.1}$$

Such an improved fitting function contains one extra parameter to fit, and could possibly describe the data in better way and, therefore, remove some of the discrepancies mentioned earlier.

Unfortunately, when this model is applied to the previously discussed data, it does not yield any major improvements. Indeed, the additional parameter did not improve the quality of the fit and even worsened the correlation coefficients. The error bars on the lifetime increased by a factor of five due to the instability of the fit. The final values of the parameter D are relatively low, resulting in maximum values of the term Dt on order of single units (around 1 a.u.), which is comparable with the noise and negligible compared to the measured time resolved intensities (which range in value up to 4000 a.u.).

So we have to conclude that the model described by the single exponential and constant background in Equation 4.1 is a more suitable model for our PSP data.

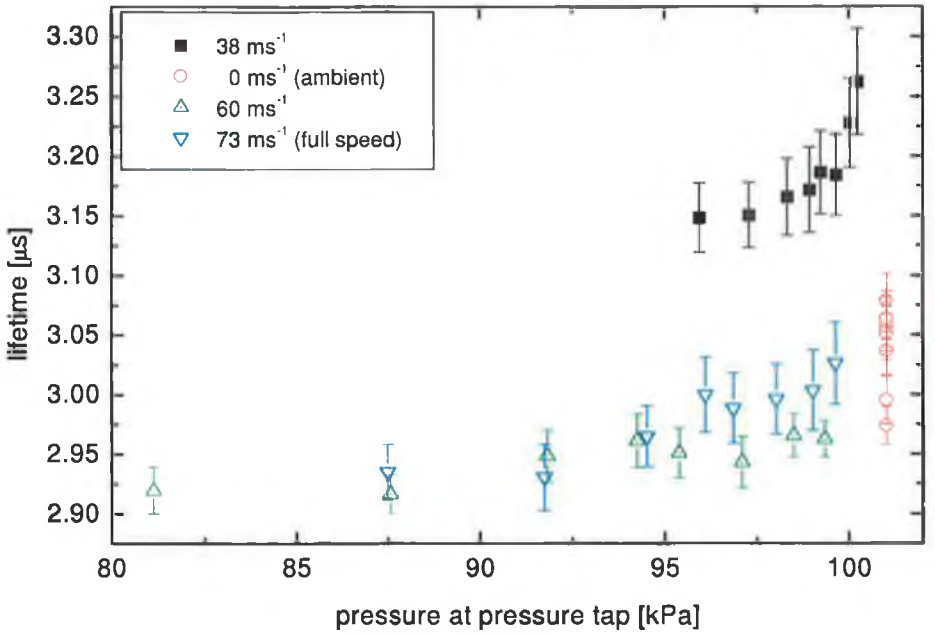

Figure 6.8: Lifetime versus pressure at pressure taps, yielding the in-situ calibration curve corresponding to the data in Figure 6.4.

6.2.7 In-situ calibration

Suggested in-situ calibration, which relates the measured lifetime versus data with the pressure reading recorded by the pressure taps, is plotted in Figure 6.8. Clearly the data at wind speed 38 ms^{-1} show a surprising shift in measured lifetime compared to other data — the same behaviour is observed for both wind tunnel measurements in figures 6.4 and 6.5. The reason for this shift is unknown and its appearance was unexpected as the wind speed control is totally independent of the luminescence data acquisition system.Data were examined several times but no flaws in the processing were revealed.

The in-situ calibration using data at wind speeds of 0 ms^{-1}, 60 ms^{-1} and 73 ms^{-1} show a greater degree of correlation ($R = 0.9$). However, the large error-bars (compared to the total maximum change) are not promising for precise measurement at low wind speeds in the wind tunnel.

6.2.8 Interim summary

In the previous sections, several explanations for the 5 major discrepancies (listed on page 119) observed in the data were presented. Some effects can, potentially, be success-

fully explained and corrected (for example by applying an improved a-priori calibration). However, some effects are still unexplained and this points to more serious issues with the system. Firstly, the lifetime data at ambient conditions must correspond to constant pressure over the surface of the sample. This means that the plotted data should be flat with fluctuation in the range of the error-bars. This is clearly not the case in figures 6.4 and 6.5 (for wind speeds $0\,\mathrm{ms}^{-1}$). Section 6.3 addresses this issue in more detail and suggests possible solutions.

The second area to investigate is the issue of the unexpected sequence of the measured curves. The a-priori laboratory calibration curve (in Figure 4.5) displays a monotonic dependence of the ruthenium complex lifetime on oxygen concentration (and, hence, pressure). This monotonic behaviour would be conserved when the corrections mentioned earlier are applied (at least for the range of conditions occurring during the medium speed wind tunnel tests). Therefore, the incorrect sequence of the curves in figures 6.4 and 6.5 cannot be explained, unless when the temperature of the air between runs differs by an order of magnitude from the measured difference, which was not observed.

6.2.9 Rapid lifetime determination and intensity approach

Having observed large discrepancies in the direct lifetime-based PSP data, it was decided to carry out some alternative data processing using the current data. The raw data from Section 6.2.1 were processed by two other methods. First, the two-shot exposure approach (rapid lifetime determination method described in Section 5.5.3) was applied to the data. The resulting lifetimes are theoretically proportional to the pressure but were not calibrated. However the lifetime profiles did not pass the integrity tests detailed in Section 6.2.2 and did not produce a flat profile for ambient conditions.

The final attempt to use the data (initially recorded for lifetime extraction) to calculate pressure profiles based on the ratio I_{ref}/I (Section 3.1.1) failed as the noise levels exceeded the possible pressure differences. Unfortunately, intensity ratioing was not employed during this wind tunnel test as the lifetime method was expected to be sufficient to yield reasonable results and it was not possible to reserve wind tunnel for a second experiment at that time.

6.2.10 Conclusion from wind tunnel measurement

While some of the discrepancies in the data can be explained by the wind tunnel environment conditions as discussed above, it has been concluded that there are fundamental problems with the data that are not associated with the wind tunnel measurement. Specifically, the widely varying absolute value of lifetime and the varying spatial profile at ambient conditions. These effects are investigated in the next section and attempts are made to improve the data.

However, in spite of the poor quality of the data, the wind tunnel measurement was a valuable experience in highlighting the real problems encountered by PSP users, which are widely different from the problems encountered in small-scale laboratory experiments.

6.3 Spatial variations

In the previous section, problems detected during wind tunnel testing were reported. These included the spatial variation of lifetime across the test surface in wind-off conditions, as well as unexplained variations in the absolute value of the lifetime. Subsequent

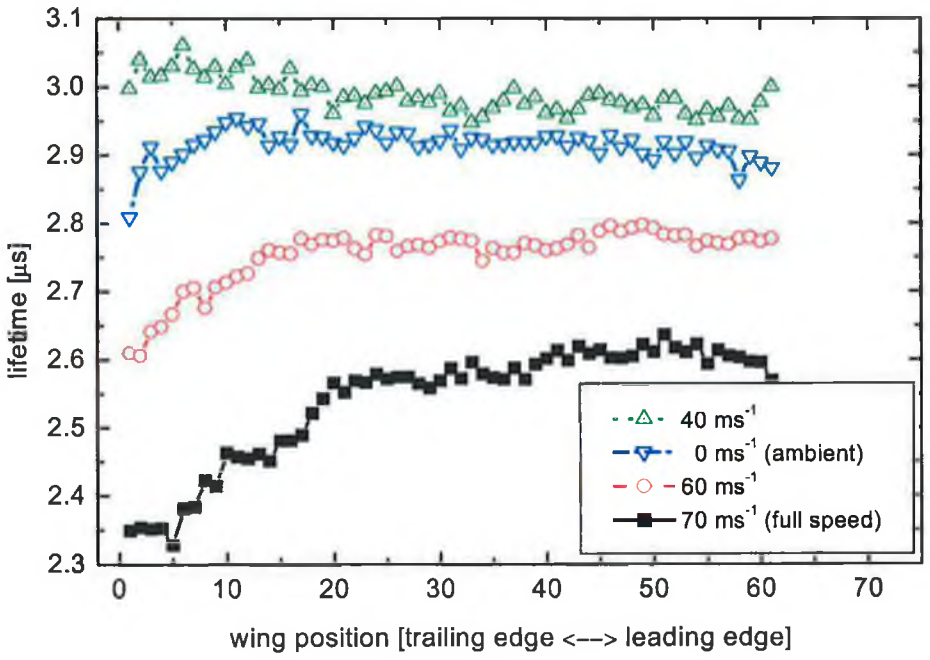

Figure 6.9: Rapid lifetime determination (RLD) method applied to the data from 14th Nov (Figure 6.5).

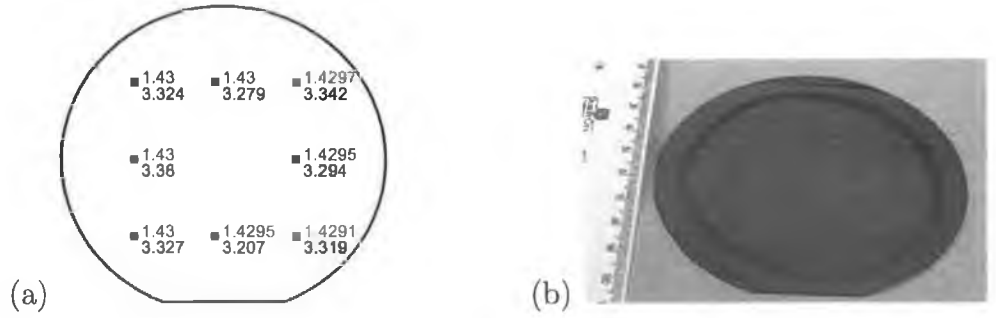

Figure 6.10: (a) Spatial distribution of thickness (black, in μm) and refractive index (wine) of the PSP spin-coated film on 4" wafer, measured with a prism coupler Metricon Model 2010 (Metricon, USA). (b) Photography of the coated wafer, interference fringes are visible on the surface.

to the wind tunnel tests, these problems were also encountered with laboratory-based testing. Accordingly, a comprehensive investigation of these effects was carried out. In this section, the source of the varying spatial profile of the lifetime measurement under ambient conditions is investigated.

So far in this work, sample homogeneity was not considered to be an important criterion, since, in principle, lifetime imaging should be immune to sample inhomogeneities. It was for this reason that spray-coated test samples used up to this point despite the nonuniform layers resulting from such a deposition technique. It should also be noted that lifetime variations over a surface were reported with other paint formulations using spray coating [5]. For this study of the spatial variations in lifetime, it was decided to optimise the sample homogeneity. Consequently, it was decided to employ spin-coating to produce a homogeneous surface, as this technique facilitates the deposition of highly uniform thin films [6]. A polished silicon wafer was chosen as the substrate. To simplify the system and to avoid any interference from the MFG luminophore, it was decided to use a sample doped with the ruthenium complex only.

6.3.1 Sample preparation

The data were obtained using a sample prepared by spin coating a 4" silicon wafer with single doped (ruthenium complex only) standard MTEOS-based PSP paint. The area in the centre of the wafer was highly homogeneous in thickness ($3.31 \pm 0.05\,\mu$m) within a circle of approximate radius 7.5 cm (Figure 6.10) as recorded with a prism coupler

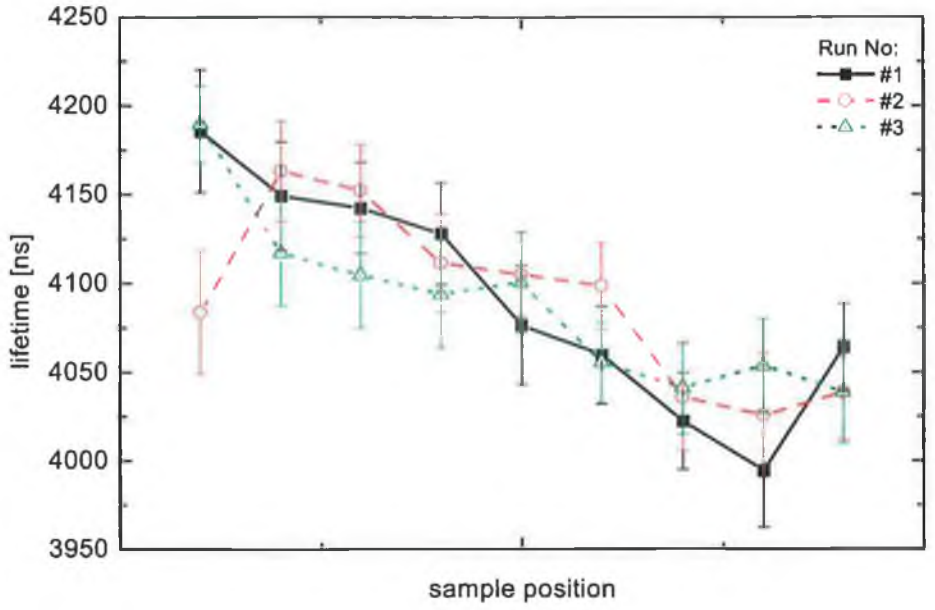

Figure 6.11: Ruthenium complex lifetimes measured by a standard method (fitting single exponential function to the temporally resolved luminescence intensity). The area under test is similar to the area shown in figures 6.12 and 6.13.

Metricon Model 2010 (Metricon, USA). The region approximately 1 cm from the edge is a thicker layer of the paint caused by the excess paint which was not centrifuged off the wafer and, flowing back from the edges, created a small rim, visible in figures 6.12 and 6.13. The ring itself is inhomogeneous in thickness, thicker than the central part, therefore showing higher luminescence intensity and causing corresponding pixels in camera to be over-exposed. Consequently, the ring has been omitted from the final data interpretation.

6.3.2 Standard lifetime measurement

The spin-coated silicon wafer, was examined under ambient conditions and the lifetime data were taken following the procedure described in Chapter 4. The resulting spatial lifetime profiles are shown in Figure 6.11 for 3 independent runs. The measurement shows reproducibility of the lifetime measurements within the random experimental error shown by error bars. However, the absolute value of the lifetime is showing approximately a 3-times bigger variation than the error bars across the observed surface. This trend is unexpected as the lifetime profile across the surface should be flat. On the other hand, it confirmed the observation from the wind tunnel tests, where the lifetime profiles also

showed the unexplained spatial dependence during wind-off conditions.

6.3.3 Alternative camera and acquisition protocol

To rule out the possibility that the standard data acquisition protocol is prone to spatial drift, the in-phase/out-of-phase method (Imagex-like approach, described in Section 5.5.5) was also tested. Both the DiCAM Pro and Imagex 2000 are capable of making in-phase/out-of-phase measurements and the results were compared. The choice of single-luminophore paint eliminate the need for additional compensations which would be required for co-doped paint. Averaging and binning over large areas, necessary for the standard lifetime measurement, are also not needed and reasonable experimental error is achieved while maintaining large spatial resolution.

(a) (b)

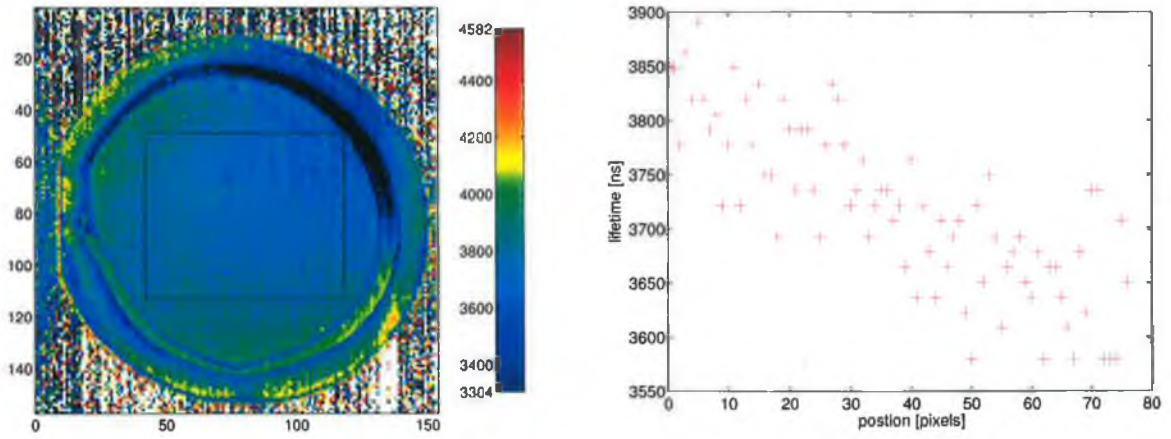

Figure 6.12: Imagex 2000 results. (a) the lifetime map of the silicon wafer (lifetime in nanoseconds). The area inside the rectangular box has average lifetime 3730 ± 65 ns (1.75%). (b) the distribution of the lifetime values alongside the top edge of the rectangle from the left figure.

The spin-coated sample, which was described previously in Section 6.3.1, was illuminated with the single blue LED bank in pulsed mode at 50 kHz, and the luminescence was recorded in sequence by each camera system. The cameras were positioned next to each other to cover approximately the same area on the sample and experience similar viewing conditions. The DiCAM Pro camera was configured to use the same measurement protocol as the Imagex 2000 system and the ratio, R, of out-of-phase and in-phase intensities was converted to lifetime via a numerical solution of Equation 5.14.

The lifetime results from the Imagex 2000 system are shown in Figure 6.12 and the data acquired with the DiCAM Pro camera system using the in-phase/out-of-phase acquisition protocol are shown in Figure 6.13. Immediately, we can note several differences between the lifetime pictures acquired with these two systems. The Imagex 2000 system with lower image resolution also produces larger experimental errors in the lifetime data than the DiCAM Pro system. This is due to the higher number of averages in the case of images recorded using the DiCAM Pro camera.

When the total measurement times are levelled for both systems (averaging with the DiCAM Pro camera is removed), the noise in the data is lower for the Imagex system. This is the consequence of the noise introduced into the system by the image intensifier.

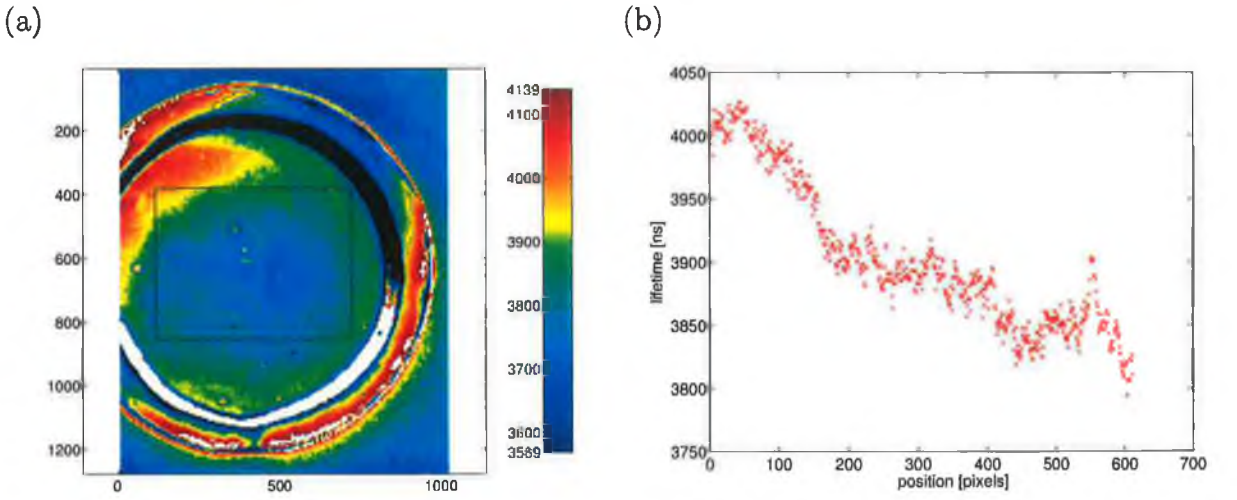

Figure 6.13: DiCAM Pro in Imagex-like configuration. (a) the lifetime map of the silicon wafer (lifetime in nanoseconds). The area inside the rectangular box has average lifetime 3789 ± 56 ns (1.49%). (b) the distribution of the lifetime values alongside the top edge of the rectangle from the left figure.

As the air pressure over the whole surface was ambient, the lifetime over the surface should be constant. Observation of the data in both figures reveals that the lifetimes over the surface are not constant (within the range of experimental error), but clearly follow some spatial trend. It is again another independent confirmation of the problems with an unexplained spatial dependence of the lifetime for wind-off measurements. Data from both systems show a similar trend. The DiCAM Pro data, with lower error, reveals some additional features best seen in Figure 6.13(b).

When comparing results obtained with the Imagex 2000 system in Figure 6.12 and

the in-phase/out-of-phase measurements with the DiCAM Pro shown in Figure 6.13 a slight difference in absolute value of lifetimes is apparent. This may be due to the fact that the duty cycle of the signal produced by the trigger box (Appendix B) in DiCAM Pro experiment, is not exactly 50%, but varies between 40–50% depending on the set frequency. Therefore the lifetime calculated from Equation 5.14 is not correct in absolute numbers, but the global trends, along with the relative comparisons and conclusions in the previous paragraph are still correct.

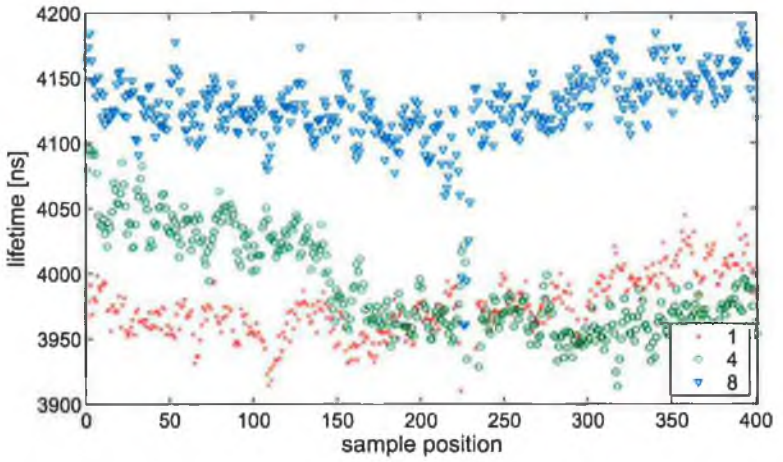

Figure 6.14: Lifetime across the wafer measured using Imagex-like strategy. Data represents approximately the same line at sample, while sample is positioned in (1) basic position, (4) upside-down relative to previous and (8) basic position with excitation source shifted to side (the profile of illumination intensity is altered).

In order to investigate any lifetime dependence on sample shape or orientation, the sample was rotated and the data was measured in a number of different orientations and the relative position between sample, LED light source and the camera was also altered. Three representative lifetime curves are shown in Figure 6.14. The lifetime profile changed for different sample orientations but was not flat under any circumstances. The lifetime values of two consecutive measurements are overlapping within the limitation of the Poisson noise. However, the lifetime measured for alternating positions of the sample, the light and the camera resulted in randomly changing lifetimes on the order of 5%. Figure 6.14 shows not only a shift in the absolute value of lifetime, but also the overlap of the two curves. One cannot attribute such effects to changes in the ambient condition between tests. The experiments were carried out in the interval of several

minutes at undisturbed ambient conditions. The presence of a local gradient of pressure or temperature, which would explain the crossing curve (curve (4) in Figure 6.14), is highly unlikely.

The dip in the lifetime in the middle of the Figure 6.14 (around position 230) appears at a position where the sample thickness is inhomogeneous, an area that is also visible in Figure 6.13.

Although these data show only the in-phase/out-of-phase approach, similar behaviour was observed with other samples and using the standard method of data fitting to a single exponential curve.

Extensive effort was invested in examining the possibility of spectral leakage of the optical filters, which was one suspected source of the problems. Both the light source and the camera objective were fitted with additional spectral filters. However, no improvement in terms of elimination of the spatial trends was observed.

6.3.4 Pressure sensitivity of spatial variations

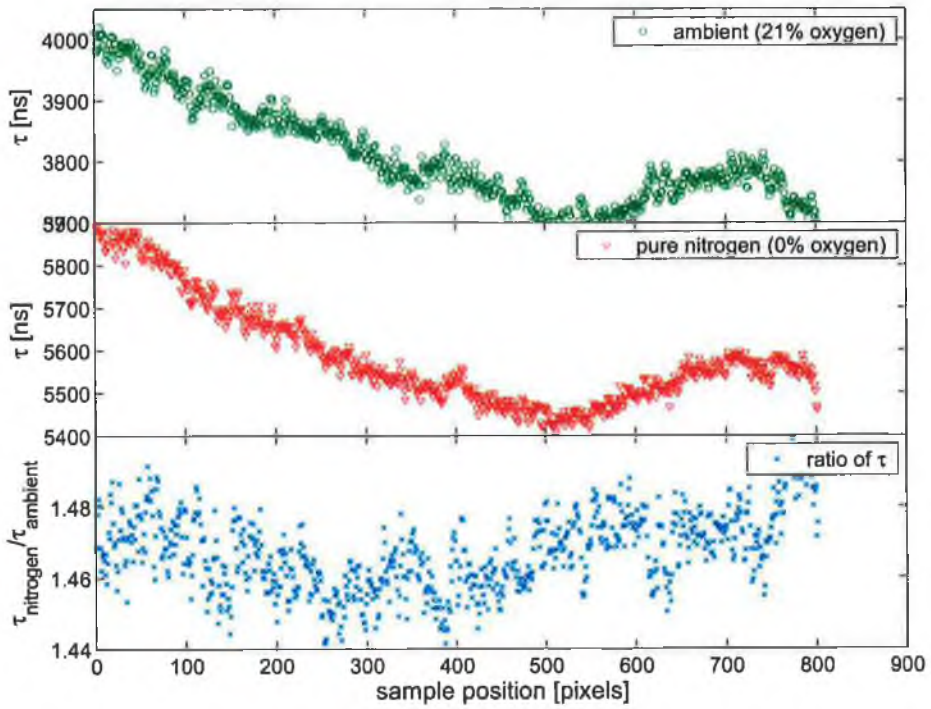

Figure 6.15: Lifetime profile (in-phase/out-of-phase approach) at 0% and 21% (ambient) oxygen concentration and ratio of previous two.

Numerous investigations were focused onto solving the problem of spatial variations of the lifetime at ambient conditions. Here we look at the behaviour of the lifetime profile while varying oxygen concentration (i.e. emulating pressure changes in the wind tunnel).

Figure 6.15 shows two lifetime profiles collected using the in-phase/out-of-phase technique under pure nitrogen (0% oxygen concentration) and at ambient conditions (21% oxygen concentration) at room temperature (24 °C). As in the previous measurements, the lifetime data exhibit a trend exceeding random error. In this case the trend results in variations of up to 5% in lifetime.

The bottom curve in Figure 6.15 represents the ratio of both lifetime profiles. Clearly the random error now dominates the slope of the profile. In this case, the relative total error was reduced down to 2%. This is a good improvement at the cost of introducing a wind-off image. However the standard $I_{\text{off}}/I_{\text{on}}$ profiles give better results and, consequently the introduction of wind-off images to improve the data was not pursued in this work. It would also have all the disadvantages associated with ratiometric measurements in wind tunnels, such as the need for image registration and correction for temperature changes during wind-on/wind-off tests, described in detail in Section 3.1.1.

6.3.5 Correlation of lifetime and recorded intensity

The investigation in the previous sections did not reveal the source of the spatial variations of the lifetime. The transformation of the data in an empirical attempt to find a solution is presented here.

A set of data acquired with a spin-coated sample is presented. The data were acquired using the in-phase/out-of-phase method with the DiCAM Pro camera under ambient conditions. Two intensity images were acquired, one in phase with the excitation light with intensities, $I_{\text{ON}}(x, y)$, where (x, y) represent the position on the sample, the second containing the out-of-phase intensities, I_{OFF}. Before further manipulation, the value of the background image, $I_{\text{BG}}(x, y)$ was subtracted from both images. The background image $I_{\text{BG}}(x, y)$ was acquired when the excitation light was off and the image was exposed with the same exposure times as images I_{ON} and I_{OFF}. I_{BG} was always flat with 1–2 counts of random noise as these measurements were carried out in a dark room. In the text that follows, I_{ON} and I_{OFF} are understood to be corrected for background.

The next step in the process of lifetime recovery was to divide the values of $I_{\text{OFF}}(x, y)$ and $I_{\text{ON}}(x, y)$ in each pixel and convert it to the lifetime following the inverse transforma-

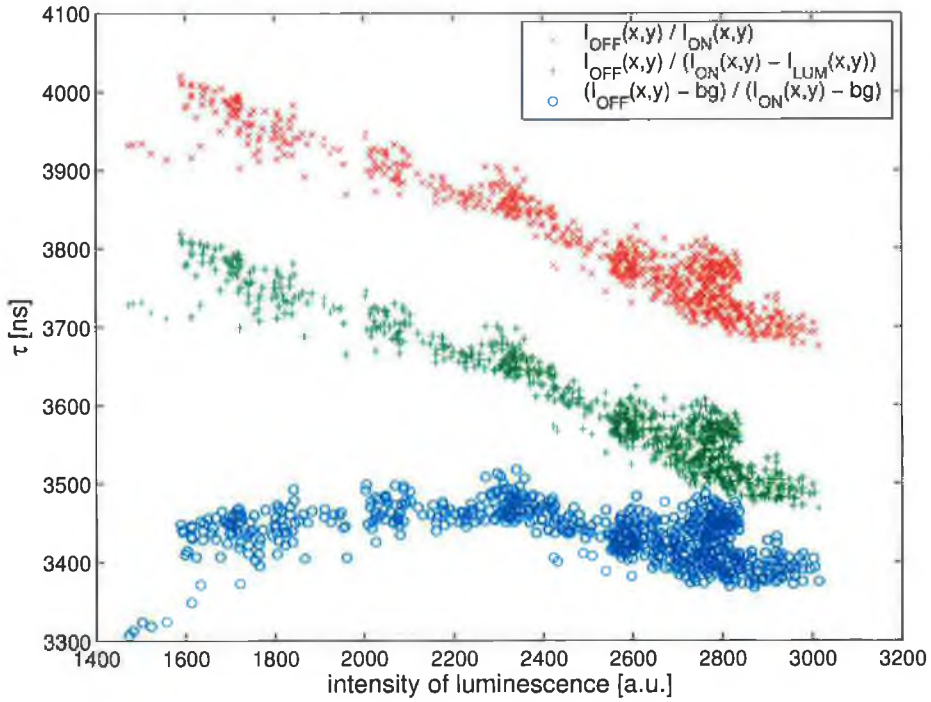

Figure 6.16: The correlation of lifetime values and luminescence intensity for data recorded using in-phase/out-of-phase method. Lifetime calculated without corrections from ratio $R = I_{\mathrm{OFF}}(x,y)/I_{\mathrm{ON}}(x,y)$ (×), with correction in Equation 6.2 (+) and using correction in Equation 6.4 (○).

tion to Equation 5.14. The transformation is nearly linear for the typical range of values of R and therefore all trends in lifetime are not significantly different from trends in ratios $R(x,y)$.

The theory of the lifetime measurements predicts that the true lifetime is independent of intensities of excitation light, thickness of the sample etc. Therefore the data of lifetime plotted versus intensity of luminescence $I_{\mathrm{LUM}} = I_{\mathrm{ON}} + I_{\mathrm{OFF}}$ should, ideally, be uncorrelated. This is not the case as is shown in the top curve in Figure 6.16 (the data displayed represent a single line of the image to keep the number of points reasonably low). The correlation of the lifetime and intensity of luminescence is clearly visible and an approximately linear trend is shown.

It was assumed that the optical filters exhibited some leakage of excitation light into the detection system. As the sample is highly homogeneous, the emitted luminescence intensity is proportional to the excitation intensity with the same constant of propor-

tionality for each sample position. If this is the source of the correlation, then the ratio $R(x, y)$ should be calculated as

$$R(x,y) = \frac{I_{\mathrm{OFF}}(x,y)}{I_{\mathrm{ON}}(x,y) - fI_{\mathrm{LUM}}(x,y)}, \tag{6.2}$$

where f is a measure of the hypothetical spectral leakage. However, this correction does not improve on the correlation of the lifetime versus intensity as shown by the middle (green) curve in Figure 6.16.

It is obvious (if it is assumed that I_{OFF} is proportional to I_{ON}) that the values of $R(x, y)$ are just multiplied by a constant factor:

$$R(x,y) = \frac{I_{\mathrm{OFF}}(x,y)}{I_{\mathrm{ON}}(x,y) - f'I_{\mathrm{ON}}(x,y)} = \frac{I_{\mathrm{OFF}}(x,y)}{I_{\mathrm{ON}}(x,y)} \frac{1}{(1-f)} \tag{6.3}$$

Several other correction functions were examined with a view to removing the observed correlation and an apparent solution was presented by Equation 6.4:

$$R(x,y) = \frac{I_{\mathrm{OFF}}(x,y) - bg}{I_{\mathrm{ON}}(x,y) - bg}. \tag{6.4}$$

Here bg is a single constant value common for the whole sample. When such a correction is applied to the data with $bg = 65$, the correlation is removed as is shown by the bottom (blue) curve in Figure 6.16. There is currently no explanation for this behaviour but it was thought to be associated with the method by which the background image is acquired.

As the gating signals for the LED bank and camera are hardware-connected and one cannot be switched completely off while the second is gated, the image intensifier is not gated during normal background image acquisition, which could lead to incorrect background images. This was tested by manually disconnecting the LED bank, and leaving the image intensifier connected to the gating signal but no difference between background images was observed.

A second, perhaps more likely, explanation for this result is the presence of autofluorescence in the detection system which could result in a uniform light intensity across the acquired images and would, furthermore, explain the effectiveness of Equation 6.4 in removing the observed correlation.

It was found that the red OG550 emission filter exhibits weak, short-lived luminescence under blue illumination. Efforts were made to eliminate this effect through the introduction of additional, alternative filters into the detection channel but the results were not conclusive. Further investigations are required to resolve this matter.

Although Equation 6.4 removes the correlation between the lifetime and the intensity, the value of the constant *bg* required to remove the correlation varies between measurements under different conditions. Equation 6.4 cannot be derived in an analytical manner from first principles but its shape can, in principle, suggest its origin. A similar correlation was discovered for a sample that was doped with just the MFG phosphor, which suggests that the source of the problem is not the luminophore itself.

6.3.6 Interim summary

A problem was identified whereby the spatial variation of the lifetime across the surface of a spin-coated film does not yield a flat and reproducible lifetime profile at ambient conditions. This result confirms the results of the wind tunnel tests and also indicates that the trend is not associated with a non-homogeneous spray-coated sample.

In order to investigate whether this effect was associated with the data acquisition protocol of the DiCAM Pro camera, the camera was configured to collect data in a different mode and also an alternative camera (the Imagex 2000) was used to measure the lifetime profile. The same profile was still obtained under these conditions. It was concluded that the current experimental setup yields lifetime data which is correlated with the intensity of recorded luminescence and this issue remains to be resolved.

6.4 Spatially resolved phase detection

In order to investigate the inconsistency in the lifetime measurements in the previous section, an alternative and well established method for lifetime measurement was used to characterise the sample. This was expected to rule out any bias in the gated CCD camera-based methods previously presented. Phase fluorometric detection was selected as a suitable candidate because of the very high achievable precision (routinely under 0.04% of the lifetime) and repeatability as well as its widespread use in the Optical Sensors Laboratory at Dublin City University.

The experimental setup used for single point lifetime measurements uses a blue LED and photodiode with built-in amplifier connected to a lock-in amplifier. A sample with typical surface area of $\sim 1\,\mathrm{cm}^2$ is examined in a flow cell. Such a setup does not facilitate spatial resolution.

A new setup, based on optical fibres, was built to facilitate spatially resolved lifetime measurements. A schematic diagram is shown in Figure 6.17 and consists of a Nichia blue LED (type NSPB500S) coupled through a blue optical filter (Lee #168) into an bifurcated optical fibre bundle which is terminated by a reflectance probe. The luminescent light is collected through the reflectance probe back into the fibre bundle, then is filtered by the orange optical filter (Lee #135) and is detected at the other end of the fibre by a photodiode with built-in amplifier (IPL-10530DAL, Radionics, Ireland, RS: 194-290). The phase signal is processed in the lock-in amplifier (Signal Recovery, model 7225), which also generates a reference signal for the excitation LED.

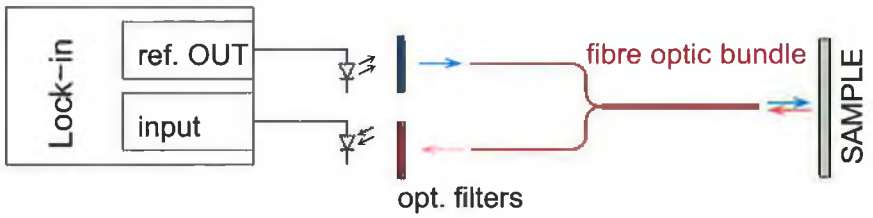

Figure 6.17: Diagram of the fibre optic phase sensitive setup.

The fibre bundle illuminates the sample over an area of approximately $2\,\mathrm{mm}^2$, determining the spatial resolution of the probe. The probe connected to the position stage can measure the phase shift of the luminescence signal relative to the reference signal, as described in Section 5.7. The lifetime corresponding to the measured phase shift and selected excitation frequency is calculated according to Equation 5.16.

The resolution of the fibre-based phase detection system was determined to be two orders of magnitude worse than the resolution of the standard phase detection system, i.e. the resolution was around 1.5% of lifetime for the measured lifetime of $3-4\,\mu\mathrm{s}$, with optimum excitation frequency of 20 000 Hz. This is the frequency that yields maximum phase sensitivity to changes in lifetime. The reduced resolution of the fibre system is due to the smaller sample area measured and high coupling loses into the fibre bundle, both of which translate into low signal levels, introducing noise into the phase signal.

Subsequent spatially resolved measurement of lifetime across the wafer surface proved inconclusive. The data yielded a lifetime around $4.1\,\mu\mathrm{s}$ and variations over the surface did not exceed the previously determined resolution of the system of 1.5 %. Consequently, it was not possible to observe any spatial variations of the lifetime that may have been present.

6.5 Evaluation of PSP system

During the course of the work focused on resolving the problems with lifetime measurements, several potential reasons were suggested and all were investigated.The non-reproducible lifetime measurements were observed using several independent data acquisition methods and across several samples prepared on various substrates (aluminium, silicon wafers) and using various coating techniques (e.g., spray coating and spin coating). Not all the data measured are presented here but all manifest varying measured lifetime with relative position of sample, light source and camera system. The analysed suggestions are summarised as follows:

- Light source not operating (switching off) correctly — checked with DiCAM Pro camera, which showed that switching times are under 100 ns relative to the trigger pulse, which is acceptable for our application as the expected measured lifetime is in the microsecond region (if the images acquired with zero delay are not used for exponential fittings).

- Spectral leakage of filters — for standard data acquisition, filters are not needed at all as luminescence is temporarily filtered using the gates only while the light source is switched off. This can be an issue for in-phase/out-of-phase acquisition. Nevertheless, the filters used exhibit no measurable spectral leakage and using additional filters did not improve on the results.

- Variation of lifetime on the sample itself — this was not completely ruled out. Spatial variation was confined under 1.5% (Section 6.4) and it is reasonable to expect the sample to have constant properties at constant external conditions (ambient laboratory environment) over a short time scale. Previous experience with sol-gel based ruthenium complex-doped films for sensors suggests very good temporal stability over a timescale of several months [7, 8]. Lifetime profiles acquired with the camera systems exceed even these maximum potential variations and, therefore, cannot be the only source.

- Autofluorescence in the filters — as mentioned in Section 6.3.5 the OG550 emission filter exhibits autofluorescence and further work is required to eliminate this effect.

- Multi-exponential luminescence decay — as is known, the luminescence decay of

the ruthenium complex is not single-exponential and, therefore, the absolute value of lifetime recovered from the sample using the above methods is not correct in principle. Nevertheless, the luminescence processes remain in the linear regime using low power densities even of ultra-bright LED light sources (i.e., not using lasers). Therefore changes in illumination should not influence such measurements if the detection system is linear and the non-linearity of the DiCAM Pro has been evaluated experimentally as less than 1%.

6.6 Conclusion

In this chapter, the PSP system developed and described in previous chapters was deployed for the test of a NACA 0012 airfoil in a medium speed wind tunnel. Wind speeds up to $73\,\mathrm{ms}^{-1}$ provided pressure differences of up to 18 kPa over the airfoil. Measured lifetime profiles showed poor agreement with the pressure profiles determined by the standard pressure-tap technique. Several potential explanations for such discrepancies were evaluated, including the sensitivity of the paint to humidity and the necessity for in-situ calibration was apparent. It appears that the observed irregularities and the varying absolute value of lifetime are not exclusively caused by the wind tunnel environment and are also observed repeatedly in small-scale laboratory tests.

Spatial variations of lifetime were observed using carefully prepared homogeneous samples with several data acquisition techniques and camera systems. The possibility of spatial variations in the lifetime was probed with a custom-designed phase-based fibre-optic system and a single point measurement. This reduced the variation of lifetime under the limit observed in the camera based measurements. The subsequent two-dimensional measurements showed poor repeatability between different sample positions and configurations of the illumination source and collection optics. However, the lifetime for individual points at fixed system configurations can produce data that are locally reproducible.

None of the systems and approaches yielded global repeatability lower then 5%, which points to the necessity for further investigations into the system in order to improve its performance.

6.7 References

[1] Stokes Research Institute, University of Limerick, Limerick, Ireland. `http://www.stokes.ie/`.

[2] J. Trapp and R. Zores, "NACA 4 digits series," 2001. `http://www.pagendarm.de/trapp/programming/java/profiles/NACA4.html`.

[3] A. De Bortoli, "Multigrid based aerodynamical simulations for the NACA 0012 airfoil," *Applied Numerical Mathematics*, vol. 40, no. 1-2, pp. 337–349, 2002.

[4] D. Wencel, C. Higgins, A. Guckian, C. McDonagh, and B. D. MacCraith, "Novel hybrid materials for smart sensor windows," in *Opto Ireland*, vol. 5826, (Dublin, Ireland), SPIE, 2005.

[5] J. Bell, "Accuracy limitations of lifetime-based pressure-sensitive paint (PSP) measurements," *Instrumentation in Aerospace Simulation Facilities. 19th International Congress on ICIASF 2001*, pp. 5–16, 2001. `http://ieeexplore.ieee.org/iel5/7597/20719/00960231.pdf?arnumber=960231`.

[6] J. B. Wachtman and R. A. H. (Editors), *Ceramic Films and Coatings*. William Andrew Publishing/Noyes, first ed., 1993.

[7] C. McDonagh, F. Sheridan, T. Butler, and B. MacCraith, "Characterisation of sol-gel-derived silica films," *J. Non-Cryst. Solids*, vol. 194, no. 1-2, pp. 72 – 77, 1996. `http://dx.doi.org/10.1016/0022-3093(95)00488-2`.

[8] P. Lavin, C. McDonagh, and B. MacCraith, "Optimization of ormosil films for optical sensor applications," *J. Sol-Gel Sci. Tech.*, vol. 13, no. 1-3, pp. 641 – 645, 1998. `http://dx.doi.org/10.1023/A:1008615932732`.

Chapter 7

Present and future directions for PSP

7.1 Introduction

In this chapter, the current usage of PSP systems by different groups worldwide along with recent developments in the area are reviewed. Some parameters of various PSP systems are summarised including the precision achieved. The issue of using an intensity versus lifetime approach are discussed again in the light of current knowledge and the specific requirements for PSP systems suitable for commercial airplane design are discussed. In addition, lifetime measurement strategies used in non-PSP contexts are evaluated for use in PSP. Finally, the objectives of this work are revisited and areas of future research are suggested.

7.2 Recent developments in PSP worldwide

PSP is used in many aerodynamic test centres worldwide, with the main activity located in the USA, Europe, Japan and Russia. The following is a brief summary of the regions and a slightly extended analysis follows:

- *Russia* – it appears that some of the developers of early PSP systems from Russia have moved to the west and the the research in Russia has been down-scaled, possibly due to a lack of funds.

- *USA* – the USA is the largest developer and user of PSP systems. The research is carried out primarily at the University of Washington, NASA and Boeing. The ma-

jority of the sensing material and equipment is commercially supplied by Innovative Scientific Solutions (ISSI) [1]. For industrial applications, single luminophore paints excited in the visible region of the spectrum are used almost exclusively. Therefore, most of the applications use in-situ calibration. The lifetime method is under extensive investigation and will be used in industrial tests in the near future.

- *Europe* – the main research activity is concentrated in three countries, which have developed their own PSP system: in France at ONERA (The French National Aerospace Research Establishment [2]), in Germany at DLR (German Aerospace Center [3]) and in the United Kingdom at BAE Systems [4].

- *Japan* – research in Japan is carried out within a very large project [5] involving many cooperating laboratories and coordinated by JAXA (Japan Aerospace Exploration Agency [6]). The research is dedicated to coatings for transonic and hypersonic flows as well as for cryogenic applications. Results for unsteady measurements (fast response PSP) were recently published [7].

7.2.1 Russia

The most significant recent research performed in Russia was presented at the first presentation of PSP in the West in 1991, where the Italian company INTECO publicly demonstrated the Russian system in a test on car model in a medium speed wind tunnel at wind speeds up to $40\,\mathrm{ms}^{-1}$. The intensity approach (I_{ref}/I) was used; the paint was excited by a laser and the images recorded using a CCD camera (512×512 pixels), with an experimental error of 745 Pa [8]. The German company OMT also distributes paints made by the Russian company Optrod [9].

7.2.2 Europe

BAE Systems (United Kingdom) developed their PSP system based on a scanning pulsed nitrogen laser beam and presented it at the 9^{th} PSP workshop [10] and other aerodynamic meetings. The exact operating principle is confidential. The system facilitates both pressure and temperature measurement, most likely obtained from multi-exponential temporal luminescence profiles. To our knowledge, apart from the demonstration of the system, any practical measurements using this equipment have not been published.

The second commercially available PSP system in the United Kingdom is developed and sold by Photonic Research Systems [11]. Only the hardware and software is supplied, the PSP paint itself must be acquired from the other source. This lifetime system, based on an interline transfer CCD chip, is not marketed specifically to the PSP industry and is very versatile in possible applications. Its predecessor, Imagex 2000, was used in this work.

In France, PSP research is carried out mainly by ONERA. Several systems were proposed and tested. A typical system consists of a dual luminophore paint excited in the UV by a 500 W mercury vapour lamp. The luminophore is pyrene-based for oxygen sensitivity and the second, oxygen insensitive, luminophore is rare-earth-based. The camera is equipped with a filter changer and acquires two spectrally filtered intensity images. This removes the need for a wind-off image, where the pressure is calculated from the ratio of two spectral images. Using such a system, a pressure error of 50 Pa with a car model (Peugeot 206) at a wind speed of $40\,\mathrm{ms}^{-1}$ was achieved. ONERA also cooperates with DLR, Germany on the research of new paint, where easy sublimation of pyrene is eliminated [12].

Another research focus at ONERA is focused on unsteady PSP (uPSP), where anodised aluminium is deployed. The signal is collected through a Cassegrain telescope and focused onto a photomultiplier with the full pressure profile being recovered using an xyz-bench upon which the full optical system is mounted [13]. In spite of the difficulties associated with the inhomogeneity of the anodised aluminium surface, an error of 2 kPa for a shock wave travelling at $480\,\mathrm{ms}^{-1}$ was reported.

7.2.3 USA

In the USA, the company Innovative Scientific Solutions (ISSI) is focusing on commercial support for PSP applications, selling PSP equipment (light sources, cameras and software) and also the paint itself. The standard paint in the USA is a single luminophore paint based on the polymer binder, Fluoro/Isopropyl/Butyl (FIB), and porphyrin (PtTFPP). This paint was first designed by the University of Washington and produced under licence by ISSI. A popular variation of the paint is one with an additional scattering agent (TiO_2), sold under the name uniFIB.

NASA tested the integration of several aerodynamic methods in a single experiment. This included PSP on a lambda wing configuration model made from resin materials, using

a stereolithography process. The model, coated with FIB paint, was illuminated by four blue LED arrays and the pressure was determined using intensity and lifetime approaches. For the intensity approach a 16-bit 512 × 512 CCD camera was used; for the lifetime measurement, a 1024 × 1024 interline transfer CCD chip collected the luminescence. At wind speeds of 30 to 60 ms^{-1}, the achieved rms pressure error was in the range of 0.2 and 2 kPa for intensity and lifetime-based results, respectively [14].

Other research has focused on to the environmental aspects of the usage of the pressure-sensitive paints [15]. A water-based PSP formulation of an oxygen permeable polymer (latex) and a platinum porphyrin luminescent dye was synthesised. Compared to the sol-gel-based paint presented here, such a formulation further reduces the content of volatile organic solvents in the paint and, therefore, reduces health risks to the user and simplifies the cleaning and disposal of the paint.

7.2.4 Japan

PSP research in Japan is associated mainly with the project MOSAIC (**MO**lecular **S**ensors for **A**erodynam**IC** research). This interdisciplinary project involves specialists from four different disciplines (chemistry, optical measurement, image processing and aero-thermodynamics) from several universities and research institutes [5].

The scope of the research is very wide and is focused on developing coatings for unsteady conditions where a fast response is required. Several papers have been published on the use of a $[Ru(dpp)_3]^{2+}$–based anodised aluminium PSP [7]. The pressure profile was first collected pointwise using a telescope to focus the luminescence onto a photomultiplier tube [16]. Later, using a Xenon lamp coupled into an optical fibre and equipped with a mechanical shutter (23 ms exposure time), luminescence was recorded by a CCD camera and an error of 160 Pa was achieved [17]. This year, results from an experiment using a high frame rate CMOS camera and an intensity approach were reported [18]. It was used to record the motion of a shock-wave. Using a frame rate of 5 kHz and an exposure time of 180 μs, a random error in images of ±40 kPa was achieved.

7.2.5 Dublin City University

The results presented in this paragraph were achieved using the image intensified DiCAM Pro camera with various data acquisition and processing systems, however with only single

point measurement using an in-situ calibration curve.

When the method described in chapter 4 (fitting the full exponential decay in order to recover the lifetime) is optimised it yields an error of 3.5 kPa under laboratory conditions, which includes binning both on the chip and during data processing, thereby largely reducing the spatial resolution of the lifetime images.

Using the in-phase/out-of-phase approach (Imagex-like approach) implemented with the same camera, where the internal timing system of the camera was disabled and the exposure was controlled externally, the achieved error was reduced to 0.35 kPa. While this reduction in the random error was significant (10×), it was achieved for full VGA resolution of the CCD chip, without the use of any binning in contrast to the first case. Therefore, the real improvement is effectively much larger.

7.2.6 Summary

Table 7.1 summarises the various experimental error values mentioned in the text above. It should be noted that some authors quote the achieved error explicitly, in some papers the error of the measurement can be easily calculated from the data presented, but the vast majority of authors do not quote experimental error at all.

As is seen from table 7.1, the spread of the achieved precision of measurements is large due to the various types of conditions under which the measurements were carried out. The errors achieved in this project lie in the mid-range, which demonstrates acceptable performance of the PSP system for single point measurements. The poor uptake of lifetime-based measurements in practical applications is relatively surprising given the potential advantages of such measurements.

7.3 Requirements for commercial PSP system for airplane design

Although PSP is not limited to this application, airplane design and testing is a primary focus for PSP products. Therefore, it is vital to improve PSP performance for this application. Any information provided by a PSP system is valuable but, for daily use, a commercial system must also provide quantitative information on the pressure distribution. Before a PSP system will be recognised as equivalent to standard pressure tap methods, it must comply with the following requirements (according to the Boeing civil aviation program [29]):

test subject	speed [ms^{-1}]	C_p† error	error [Pa]	reference
car model	40 ms^{-1}	0.8	745	[8]
flat plate	30	0.64	350	[19]
60° delta wing	25–35 ms^{-1}	0.09	50	[20]
swept half-wing	40–60 ms^{-1}	0.1	150	[21]
70° delta wing	25–50 ms^{-1}	0.46	250	[22]
NACA0012 wing	20 ms^{-1}	0.16	39	[23]
NACA0012 wing	50 ms^{-1}	0.04	61	[23]
–	300 ms^{-1}	0.02	0.2–1 kPa	[24]
car model	30, 40, 50 ms^{-1}	0.14	137	[25]
2-D model	3000 ms^{-1}	–	160	[17]
oscil. shock wave	480 ms^{-1}	–	2 kPa	[13]
Laval nozzle (unsteady)	steps 250 kPa	–	40 kPa	[18]
car model	94 ms^{-1}	0.05	250	[26]
double delta wing	150 ms^{-1}	0.1	1700	[27]
lambda wing	30-60 ms^{-1}	–	200 (intens.)	[14]
lambda wing	30-60 ms^{-1}	–	2000 (lifetime)	[14]
Peugeot 206	40 ms^{-1}	–	50	[12]
laboratory test (DCU)	single point	low resolution	3500	[28]
laboratory test (DCU)	single point	VGA resolution	350	–

† C_p is unit-less *pressure coefficient* defined in Equation 1.8

Table 7.1: Summary of achieved errors in pressure determination from literature

- **Traceability** – data generated must comply with the calibration and traceability requirements for such equipment as defined by the National Institute for Standards and Technology (NIST) or ISO 9000.
- **Preliminary data** – colour contours must be available in no more than 30 s after the test point data are acquired. C_p plots must be available on request in 2 minutes. Preliminary data quality must be the same as final data quality.
- **Final data** – final data must be available in 2 days after the test in appropriate industrial data format.

- **Aerodynamic non-intrusiveness** – the coating thickness must be < 3 mm, with a surface smoothness $< 8 - 32\,\mu$m rms.
- **Data acquisition time** – data acquisition time must be between 1–2 s; the interval between measurement is typically 5–8 s in continuous tunnels and 2–3 s in blow down tunnels.
- **Accuracy** – accuracy must be less than 0.02 C_p or 350 Pa, whichever is greater (at 2σ, assuming a normal distribution of error).
- **Temperature range** – the paint must support all temperature regimes of wind tunnel test from cryogenic wind tunnels to higher temperatures, from $-45\,°$C to $+70\,°$C.
- **Pressure range** – 0.35 to 6 atm (35 kPa — 600 kPa).

Some of these requirements are more difficult to achieve than others. The first three in the list are administrative or software-based, while the rest are of a more fundamental nature and must be considered from the experimental side.

Table 7.2 summarises the main challenges and compares the requirements and current status of commercial technology according to [30]:

	Requirement	**Status**
Preliminary data availability	2 minutes	20 minutes
Final data availability	2 days	4 weeks
Pressure accuracy (2σ)	0.05 psi	0.2 – 0.6 psi
	350 Pa	1.4 – 4.1 kPa

Table 7.2: Current status and requirements for PSP techniques.

7.3.1 Software for PSP data manipulation

Practical PSP applications require complex data manipulations. Primarily, the PSP data in the form of a 2D pressure image must be mapped onto a 3D grid of the model, where it can be compared with the results of other techniques, either experimental (e.g. projection moire interferometry (PMI), acoustic microphone array (AMA)) or numerical (CFD). All

transformations should happen ideally in real-time so that the results can be seen from any direction on a virtual 3D model [31]. For this purpose, almost every organisation involved in practical PSP usage has designed its own system.

NASA has developed software named Greenboot (running on the Linux operating system) and Legato (running on Windows), but sells neither of them. ONERA has designed the software Afix2 which is distributed as freeware [32]. Software originally developed by TsAGI is now distributed as part of a PSP system by OMT (Germany) and ISSI (USA).

7.3.2 Other areas for PSP applications

Other application of PSP typically include the aerodynamics of cars, turbines, compressors, rotor blades or jet engines. Such tests require slightly different ranges of pressures and temperatures than those necessary for the Boeing test. For some applications (e.g. turbines), the maximum temperature range is typically up to a few hundred degrees and occasionally up to 2000 °C [33]. In cryogenic wind tunnel experiments, the temperature range goes down to −156 °C [34]. Tests with rotating machinery bring another degree of complexity to the system, as the data acquisition must be synchronised with the evolution of the measured component [35].

Even when all these applications are included, the market for direct PSP application is relatively small and, therefore, it is worth investigating if PSP and TSP techniques could be employed in other areas. Application examples include the measurement of spatial oxygen distribution [36] or remote temperature sensing. Temperature can be sensed using TSP, or even a standard non-temperature-compensated PSP in an environment where no oxygen/pressure dependence is expected (for example temperature mapping of integrated circuits).

7.4 Lifetime approaches in other areas

Apart from the aerodynamic research area, fluorescence lifetime imaging (FLIM) has become very popular as a tool in other areas. Its use was reported, for example, in biological tissue autofluorescence monitoring [37], endoscopic cancer cell observation [38], many biomedical applications [39], spatial oxygen mapping in biologically active sediments [40], and for polymer semiconductor diagnostics [41]. Therefore it can be beneficial to utilise principles reported in other FLIM imaging systems in aerodynamic PSP systems, as the

task of measuring the lifetime is common to both of them and the expertise can be successfully applied across disciplines.

The main difference between aerodynamic tests and the applications above is the size of the imaged area, as FLIM measurements often capture images of biological tissues under a microscope or from an object on the scale of centimetres. The PSP systems deal with objects on a larger scale from a fraction of a meter to a full scale model of wingspan of several meters. The difference in the scale of the imaged areas is reflected in the necessary power of excitation sources, with a relatively large proportion of the luminescence light being collected for small tissue samples compared to the wind tunnel test, where the collection efficiency is relatively smaller.

Another promising setup presented for FLIM measurement, which may be compatible with PSP systems, is the Lambert Instruments Fluorescence Lifetime Attachment (LIFA) [42], which uses patented technology [43]. This system uses a harmonically-modulated light source in conjunction with a gain-modulated second generation image intensifier to measure the phase shift of the luminescence with respect to an excitation signal. Phase sensitive detection is a very reliable method for lifetime detection. In principle, this system employs lock-in amplification in every pixel. Typically, a single phase signal is processed in the lock-in amplifier but, in this case the "calculations" are carried out in an analog signal for all pixels in parallel.

The advantage of the LIFA system is that almost 50% of the light in the system is utilised in detection (and not blocked during out-of-gate intervals as in the case of gated lifetime systems). Higher efficiency in luminescence collection can cause lower random error as shown in Section 5.6.

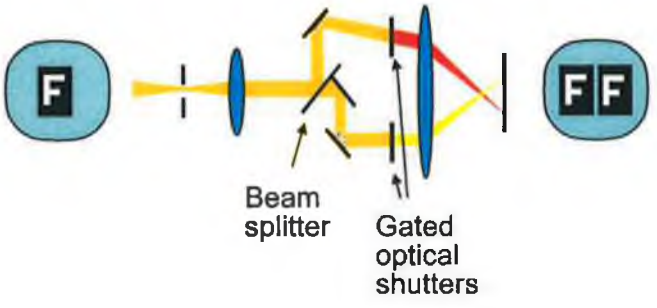

Figure 7.1: Schematics of the beam splitting system with parallel gating of two images [39].

Another interesting approach is a lifetime-based system designed for imaging living

cells under the microscope [39]. It uses 2-way objective optics to perform rapid lifetime determination and a schematic is shown in Figure 7.1. The observed object produces two images on the detecting CCD. Image intensifiers with different gates are inserted into the beam path of each image producing two lifetime images in parallel. Such a configuration can be beneficial for fast and unsteady PSP processes. However, for steady PSP measurements this introduces more complexity into the optical system and the total measurement time is not reduced if the same noise level per image is to be preserved.

In practical applications, for example in biomedicine, the absolute value of lifetime is again not crucial for the users. The important feature is the contrast in lifetime between different regions in the sample, a characteristic which is not visible under standard microscopy. Therefore, the issue of absolute error in lifetime is not addressed in many papers. An analysis of a system, compatible with a gated CCD camera, is reported by Sharman *et al.* [44]. The problem is approached from the theoretical side and reports that the maximum expected precision of lifetime limited by the Poisson noise is in region of 0.6–1.2% (for nanosecond lifetimes). A later paper from the same research group shows a modified phase-fluorometry method not exceeding 0.2% error in lifetime [45] (this method is not suitable for use with camera systems). In yet another case, a FLIM system imaging via an endoscope achieved a precision of 4–8% for lifetimes in the nanosecond range [38].

7.5 Lifetime versus intensity considerations

The majority of the work published about practical wind tunnel measurements is based on the intensity approach (I_{ref}/I), which involves relatively straightforward measurements. This contrasts with the relatively complex setup for data acquisition in a lifetime-based approach, which also yields larger absolute errors in the pressure. Moreover such systems are not yet commercially available. A practical comparison of intensity and lifetime approaches under otherwise identical conditions can be found in the review by Jordan *et al.* [14]. With his configuration, the error in lifetime-based measurement is 10× higher than the error in intensity-based measurement under identical conditions.

The superiority of the intensity systems over lifetime with regard to random error is understandable, because of the inherent complexity of the lifetime data acquisition protocol. Nevertheless, in some cases, the other advantages of the lifetime approach outweigh the small loss in precision.

Given this limit of precision in lifetime recovery, a key question is whether the lifetime precision can be improved in practical experiments.

In the last two years only two papers investigating the fundamentals of lifetime-based pressure-sensitive system were published in major journals [46, 47], indicating only minor interest in the lifetime approach from the aerodynamic community.

However, the PSP itself is still popular judging from the number of successful experiments published using this approach.

7.6 Objectives revisited and evaluation of the project

7.6.1 Objectives revisited

The major objectives of this project (Section 1.10) have been evaluated.

In the course of this project, the PSP technique was established for the first time in Ireland in Dublin City University. A pressure- and temperature-sensitive paint incorporating two luminophores in a porous sol-gel matrix was developed. The formulation is robust, does not suffer any significant damage during wind tunnel tests, has excellent adhesion to metal and other surfaces and is compatible with spray coating.

In parallel to the paint development, a complete data acquisition system and data acquisition protocol was designed to record 2D lifetime images. A commercially available pulsed LED light source and a gated CCD camera were used. The feasibility of the lifetime recovery from both luminophores during single measurement in laboratory conditions was shown. In addition, intrinsic temperature compensation of the pressure reading with a single paint and a single camera is possible. Single-point calibration curves over a range of oxygen concentrations and temperatures were obtained and the error of measurement was determined. Important features of the system are that it does not contain any mechanical components, can be remotely operated by PC and the two lifetimes are separated and recovered in the time domain. Both temperature and pressure maps are recorded at the same camera position, removing the need for image registration and completely eliminating wind-off images.

The optimisation of the system was considered with respect to the large relative error in recovered lifetime, which causes uncertainty in the pressure comparable to the maximum expected pressure difference during tests in a medium speed wind tunnel. An improved

data acquisition protocol was identified that reduced the error for pressure readings by a factor of 10 to ±350 Pa, which is an acceptable value when compared to recent reports in the literature.

Wind tunnel tests were carried out but the results were limited by spatial variations in the pressure profile, which are attributed to the influence of intensity fluctuations on the measured lifetime.

7.6.2 Project evaluation

As detailed above, the principal objectives of this project were achieved. The pressure and temperature errors achieved are comparable with recent literature values. However, a problem was identified with regard to the spatial variation of the pressure profile. This was correlated with the spatial variations in intensity of emitted light and this issue remains to be fully resolved. This in turn lead to unsatisfactory wind tunnel measurements.

If this issue can be resolved, the PSP&TSP system developed in this project has the potential for aerodynamic testing of surfaces in steady, medium speed wind tunnel conditions.

The project involved the successful combination of a range of diverse techniques, including sol-gel paint technology, optics, camera systems and complex data acquisition and analysis techniques.

Finally the project incorporated a number of novel features including:

- a sol-gel based paint,
- a high brightness phosphor, MFG,
- the combination of luminophores with lifetime separation enabling single camera and detector,
- the potential for filter free operation.

7.7 Suggestions for further work

Suggestions for future research in PSP at DCU are presented in this section.

It would be desirable to use FIB or other paint formulations used by other groups and test the current measurement protocol with them.

The known non-single exponential nature of luminescence decay of ruthenium-complexes could be used for both pressure and temperature determination from a 3-gate acquisition protocol, in the case where the decays exhibit different temperature dependences. A single luminophore paint might be then sufficient and the problem of background subtraction of the luminescence from the second luminophore could be avoided.

7.7.1 Alternative camera systems

Some authors [48] suggest that the image intensifier in intensified cameras is a major source of noise and, therefore, the use of image intensified CCD's should be abandoned. They could be replaced by interline transfer CCD's, which are also suitable for gated image acquisition.

In comparing both systems, we observed relatively lower random noise with the interline transfer CCD camera (as shown in Section 6.3.3). With the image-intensified DiCAM Pro camera, we experienced a limitation of the internal triggering system when the maximum number of accumulating loops (256 times) was the limiting factor for short exposure gates. The recorded images were around 10% of full well capacity of the CCD chip, thereby increasing Poissonian noise. Relatively small changes in the firmware would solve this issue. Therefore, an interline transfer CCD system with a two-channel programmable trigger generator for both the LED and CCD would be worth investigating.

7.7.2 Further temperature-sensitive paint tests

Although one of the objectives of this work was to develop a temperature sensitive paint, apart from establishing the feasibility of the approach and producing a calibration curve, the investigation was limited as intensive effort was focused on resolving issues with pressure errors and spatial variations. Further investigation into temperature-sensitive paint is needed to enable full compensation for small temperature variations.

7.8 References

[1] Innovative Scientific Solutions, Inc. (ISSI). `http://www.innssi.com/`.

[2] ONERA – Office National d'Etudes et de Recherches Aerospatiales (The French National Aerospace Research Establishment). `http://www.onera.fr/english.html`.

[3] DLR – Deutschen Zentrum für Luft- und Raumfahrt (German Aerospace Center) . http://www.dlr.de/as/institut/abteilungen/abt_ev/, http://www.dlr.de/.

[4] BAE – British Aerospace Systems. http://www.baesystems.com/.

[5] K. Asai, I. Okura, and H. Mizushima, "MOSAIC project – summary of phase one program," *ICIASF Record, International Congress on Instrumentation in Aerospace Simulation Facilities*, pp. 89 - 94, 2003. http://dx.doi.org/10.1109/ICIASF.2003.1274856.

[6] JAXA – Japan Aerospace Exploration Agency. http://www.jaxa.jp/index_e.html.

[7] M. Kameda, N. Tezuka, T. Hangai, K. Asai, K. Nakakita, and Y. Amao, "Adsorptive pressure-sensitive coatings on porous anodized aluminium," *Meas. Sci. Technol.*, vol. 15, no. 3, pp. 489–500, 2004.

[8] A. Vollan and L. Alati, "A new optical pressure measurement system (OPMS)," *ICIASF Record, 14th International Congress on Instrumentation in Aerospace Simulation Facilities*, pp. 10–16, 1991.

[9] OPTROD, Ltd. http://www.optrod.com/.

[10] A. Davies, "SUrface PRessure Measurement using Optics (SUPREMO)," tech. rep., Advanced Technology Centres (Sowerby), BAE Systems, 2000.

[11] Photonic Research Systems, Ltd. http://www.prsbio.com/.

[12] Y. Le Sant and M.-C. Merienne, "Surface pressure measurements by using pressure-sensitive paints," *Aerospace Science and Technology*, vol. 9, no. 4, pp. 285 – 299, 2005. http://dx.doi.org/10.1016/j.ast.2004.08.008.

[13] M.-C. Mérienne, Y. L. Sant, J. Ancelle, and D. Soulevant, "Unsteady pressure measurement instrumentation using anodized-aluminium PSP applied in a transonic wind tunnel," *Meas. Sci. Technol.*, vol. 15, no. 12, pp. 2349–2360, 2004.

[14] J. D. Jordan, A. Neal Watkins, G. A. Fleming, B. D. Leighty, R. J. Schwartz, J. L. Ingram, K. D. Grinstead Jr., D. M. Oglesby, and C. Tyler, "Rapid technology assessment via unified deployment of global optical and virtual diagnostics," *ICIASF*

Record, International Congress on Instrumentation in Aerospace Simulation Facilities, pp. 190 – 201, 2003. http://dx.doi.org/10.1109/ICIASF.2003.1274868.

[15] D. M. Oglesby, J. L. Ingram, D. Jordan, A. N. Watkins, and B. D. Leighty, "Water-based pressure sensitive paint," Tech. Rep. NASA/TM-2004-213268, NASA, 2004. http://techreports.larc.nasa.gov/ltrs/PDF/2004/tm/NASA-2004-tm213268.pdf.

[16] Y. Sakamura, T. Suzuki, M. Matsumoto, G. Masuya, and Y. Ikeda, "Optical measurements of high-frequency pressure fluctuations using a pressure-sensitive paint and cassegrain optics," *Meas. Sci. Technol.*, vol. 13, no. 10, pp. 1591–1598, 2002.

[17] K. Asai, K. Nakakita, M. Kameda, and K. Teduka, "Recent topics in fast-responding pressure-sensitive paint technology at national aerospace laboratory," *ICIASF Record, International Congress on Instrumentation in Aerospace Simulation Facilities*, pp. 25 – 36, 2001. http://dx.doi.org/10.1109/ICIASF.2001.960233.

[18] Y. Sakamura, M. Matsumoto, and T. Suzuki, "High frame-rate imaging of surface pressure distribution using a porous pressure-sensitive paint," *Meas. Sci. Technol.*, vol. 16, no. 3, pp. 759–765, 2005.

[19] V. S. Fonov, *Development and Analysis of Data Processing Methods Applied to Luminescent Coating Systems in Aerodynamics.* PhD. Thesis, Heriot Watt University (UK), 2003.

[20] Y. Shimbo, R. Mehta, and B. Cantwell, "Vortical flow field investigation using pressure sensitive paint technique at low speed," *AIAA Journal*, no. 97-0388, 1997.

[21] C. Klein, R. H. Engler, S. D. Fonov, and O. Trinks, "Pressure sensitive paint measurements on a wing model in a low-speed wind tunnel," *ICIASF Record, International Congress on Instrumentation in Aerospace Simulation Facilities*, pp. 22.1–22.6, 1999.

[22] M. Merienne and F. Bouvier, "Vortical flow field investigation using a two-component pressure sensitive paint at low speed," *ICIASF Record, International Congress on Instrumentation in Aerospace Simulation Facilities*, pp. 19.1–19.9, 1999.

[23] O. C. Brown, *Low-speed pressure measurements using a luminescent coating system.* PhD. Thesis, Stanford University, 2000.

[24] R. Engler, "Further developments of pressure sensitive paint for non flat models in steady transonic flow and unsteady conditions," in *16th ICIASF Congress, Dayton, Ohio, USA*, pp. 123–133, July 1995.

[25] "Joint experiment Ford, NASA Ames, Lockheed Martin, Aider, ONERA," 2001.

[26] M. Gouterman, J. Callis, L. Dalton, G. Khalil, Y. Mebarki, K. R. Cooper, and M. Grenier, "Dual luminophor pressure-sensitive paint: III. Application to automotive model testing," *Meas. Sci. Technol.*, vol. 15, no. 10, pp. 1986–1994, 2004.

[27] G. E. Erickson and H. A. Gonzalez, "Pressure-sensitive paint investigation of double-delta wing vortex flow manipulation," in *43rd AIAA Aerospace Sciences Meeting & Exhibit*, no. AIAA 2005-1059, (Reno, Nevada), pp. 1–59, 2005. `http://techreports.larc.nasa.gov/ltrs/PDF/2005/aiaa/NASA-aiaa-2005-1059.pdf`.

[28] J. Hradil, C. Davis, K. Mongey, C. McDonagh, and B. D. MacCraith, "Temperature-corrected pressure-sensitive paint measurements using a single camera and a dual-lifetime approach," *Meas. Sci. Technol.*, vol. 13, no. 10, pp. 1552–1557, 2002. `http://stacks.iop.org/0957-0233/13/1552`.

[29] D. Ball, "Technology development. where's the leverage now?," in 9th *Annual PSP Workshop*, (Washington DC, USA), Manager Enabling Technology and Research, Boeing Commercial Airplanes, 7 – 11 April 2002.

[30] M. Kammeyer, J. Donovan, C. Kelble, M. Benne, T. Kihlken, and J. A. Felter, "Accuracy assessment of a pressure-sensitive paint measurement system," in *40th AIAA Aerospace Sciences Meeting and Exhibit*, vol. AIAA-2002-0530, (Reno, Nevada), 2002.

[31] G. A. Fleming, S. M. Bartram, G. A. Fleming, W. M. Humphreys, Jr., L. N. Jenkins, J. D. Jordan, J. eph W. Lee, B. D. Leighty, J. F. Meyers, B. W. South, A. A. Cavone, J. L. Ingram, M. A. Kulick, D. M. Oglesby, R. J. Schwartz, and A. N. Watkins, "Unified instrumentation: examining the simultaneous application of advanced measurement techniques for increased wind tunnel testing capability," *AIAA Journal*, vol. AIAA-2002-3244, pp. 1–34, 2002. `http://techreports.larc.nasa.gov/ltrs/PDF/2002/aiaa/NASA-aiaa-2002-3244.pdf`.

[32] ONERA, "Resection software afix2." `http://www.onera.fr/dafe-en/afix2/`.

[33] S. W. Allison and G. T. Gillies, "Remote thermometry with thermographic phosphors: Instrumentation and applications," *Rev. Sci. Instrum.*, vol. 68, no. 7, pp. 2615–2650, 1997.

[34] A. N. Watkins, W. K. Goad, C. J. Obara, D. R. Sprinkle, R. L. Campbell, M. B. Carter, O. C. Pendergraft, Jr., J. H. Bell, J. L. Ingram, D. M. Oglesby, P. J. Underwood, and L. R. Humber, "Flow visualization at cryogenic conditions using a modified pressure sensitive paint approach," in *43rd AIAA Aerospace Sciences Meeting & Exhibit*, no. AIAA 2005-0456, (Reno, Nevada), p. 13, 2005. `http://techreports.larc.nasa.gov/ltrs/PDF/2005/aiaa/NASA-aiaa-2005-0456.pdf`.

[35] J. Gregory, "Unsteady pressure measurements in turbomachinery using porous pressure sensitive paint," in 9^{th} *Annual PSP Workshop*, (Washington DC, USA), 7 - 11 April 2002.

[36] G. Holst and B. Grunwald, "Luminescence lifetime imaging with transparent oxygen optodes," *Sens. and Act. B: Chemical*, vol. 74, no. 1-3, pp. 78–90, 2001.

[37] J. Siegel, K. Benny Lee, S. Webb, S. Leveque-Fort, M. Cole, R. Jones, K. Dowling, P. French, and M. Lever, "Application of the stretched exponential function to fluorescence lifetime imaging of biological tissue," *Proceedings of SPIE*, vol. 4431, pp. 99 – 107, 2001.

[38] J. Requejo-Isidro, J. McGinty, I. Munro, D. Elson, N. Galletly, M. Lever, M. Neil, G. Stamp, P. French, P. Kellett, J. Hares, and A. Dymoke-Bradshaw, "High-speed wide-field time-gated endoscopic fluorescence-lifetime imaging," *Optics Letters*, vol. 29, no. 19, pp. 2249 – 2251, 2004.

[39] D. Elson, S. Webb, J. Siegel, K. Suhling, D. Davis, J. Lever, D. Phillips, A. Wallace, and P. French, "Biomedical applications of fluorescence lifetime imaging," *Optics and Photonics News*, vol. 13, no. 11, pp. 26 – 32, 2002.

[40] G. Holst, O. Kohls, I. Klimant, B. Konig, M. Kuhl, and T. Richter, "A modular luminescence lifetime imaging system for mapping oxygen distribution in biological samples," *Sens. and Act. B: Chemical*, vol. 51, no. 1-3, pp. 163–170, 1998.

[41] E. Mendez, D. Elson, M. Koeberg, C. Dunsby, D. Bradley, and P. French, "Fluorescence lifetime imaging using a compact, low-cost, diode-based all-solid-state regenerative amplifier," *Review of Scientific Instruments*, vol. 75, no. 5 part 1, pp. 1264–1267, 2004.

[42] K. W. J. Stoop, L. K. van Geest, and C. J. R. van der Oord, "System for fluorescence lifetime imaging microscopy (FLIM)," 2002. Presented at EMBO Practical Course "Light Microscopy of Live Specimens", Heidelberg, May 2002, `http://www.tautec.com/LAMBERT/LIFA%20Application%20Note.pdf`.

[43] C. G. H. MORGAN, "Measurement of luminescence," 1992. European paten application – EP0519930B1, US patent application – US 5.459.323.

[44] K. K. Sharman, A. Periasamy, H. Ashworth, J. N. Demas, and N. H. Snow, "Error analysis of the rapid lifetime determination method for double-exponential decays and new windowing schemes," *Anal. Chem.*, vol. 71, no. 5, pp. 947–952, 1999.

[45] H. Rowe, S. P. Chan, J. Demas, and B. DeGraff, "Elimination of fluorescence and scattering backgrounds in luminescence lifetime measurements using gated-phase fluorometry," *Anal. Chem.*, vol. 74, no. 18, pp. 4821–4827, 2002.

[46] S. Grenoble, M. Gouterman, G. Khalil, J. Callis, and L. Dalton, "Pressure-sensitive paint (PSP): Concentration quenching of platinum and magnesium porphyrin dyes in polymeric films," *J. Lumin.*, vol. 113, no. 1-2, pp. 33–44, 2005.

[47] W. Ruyten, "Oxygen quenching of PtTFPP in FIB polymer: a sequential process?," *Chemical Physics Letters*, vol. 394, pp. 101–104, 2004. `http://www.sciencedirect.com/science/article/B6TFN-4CVV9VT-X/2/f7079c37f5a34c055800a5b2360c050b`.

[48] A. N. Watkins, J. D. Jordan, B. D. Leighty, J. L. Ingram, and D. M. Oglesby, "Development of next generation lifetime PSP imaging systems," *ICIASF Record, International Congress on Instrumentation in Aerospace Simulation Facilities*, pp. 372 – 382, 2003. `http://dx.doi.org/10.1109/ICIASF.2003.1274889`.

List of publications and conference presentations

Peer-Reviewed Publications

1. J. Hradil, C. Davis, K. Mongey, C. McDonagh, and B. D. MacCraith, "Temperature-corrected pressure-sensitive paint measurements using a single camera and a dual-lifetime approach," *Meas. Sci. Technol.*, vol. 13, no. 10, pp. 1552–1557, 2002, `http://stacks.iop.org/0957-0233/13/1552`.

Oral presentations

1. "Pressure Sensitive Paint (PSP) Measurements for Aerodynamic Applications", *Sensors and their Applications XII*, Limerick, 2003.

2. "Temperature-corrected pressure sensitive paint measurements for aerodynamic applications", *Opto Ireland*, Galway, 2002.

3. "Dual lifetime temperature-corrected PSP measurements using a single camera", 9^{th} *Annual PSP Workshop*, Washington, DC, 2002.

Poster presentations

1. "Surface pressure and temperature profile measurements for aerodynamic applications", Europt(r)ode IV, Manchester, U.K., 7–10 April 2002, presented by D. Gray.

Conference Proceedings

1. J. Hradil, C. Davis, K. Mongey, D. Gray, T. Dalton, C. McDonagh, B. D. MacCraith, "Temperature-corrected pressure sensitive paint measurements for aerodynamic applications", Opto-Ireland 2002: Optics and Photonics Technologies and Applications, *Proc. SPIE*, vol. 4876, p. 867–874, 2002.

2. J. Hradil, C. Davis, K. Mongey, D. Gray, T. Dalton, C. McDonagh, B. D. MacCraith, "Pressure Sensitive Paint (PSP) Measurements for Aerodynamic Applications", *Sensors and their Applications XII Conference Proceedings*, 2003.

Appendix A

List of abbreviations of chemical compounds

FIB	Fluoro/Isopropyl/Butyl, polymer binder used in sprayable paints
MTEOS	Methyl-triethoxy-silane, $CH_3(C_2H_5O)_3Si$
MFG	Manganese doped magnesium fluoro-germanate, $Mg_4(F)GeO_6$: Mn, $3.5MgO\,0.5MgF_2\,GeO_2$: Mn
$[Ru(dpp)_3]^{2+}$	Ruthenium complex, Ru(II) tris-(4,7-diphenyl-1,10-phenanthroline)
TEOS	Tetra-ethoxy-silane, $(C_2H_5O)_4Si$

Appendix B

Trigger circuit design

A computer controlled frequency generator based on an Epson SPG8640N (selectable-output crystal oscillator) was constructed. It is interfaced to the PC by a bidirectional parallel port and permits the frequencies from Table B.1. A schematic diagram is shown in Figure B.1.

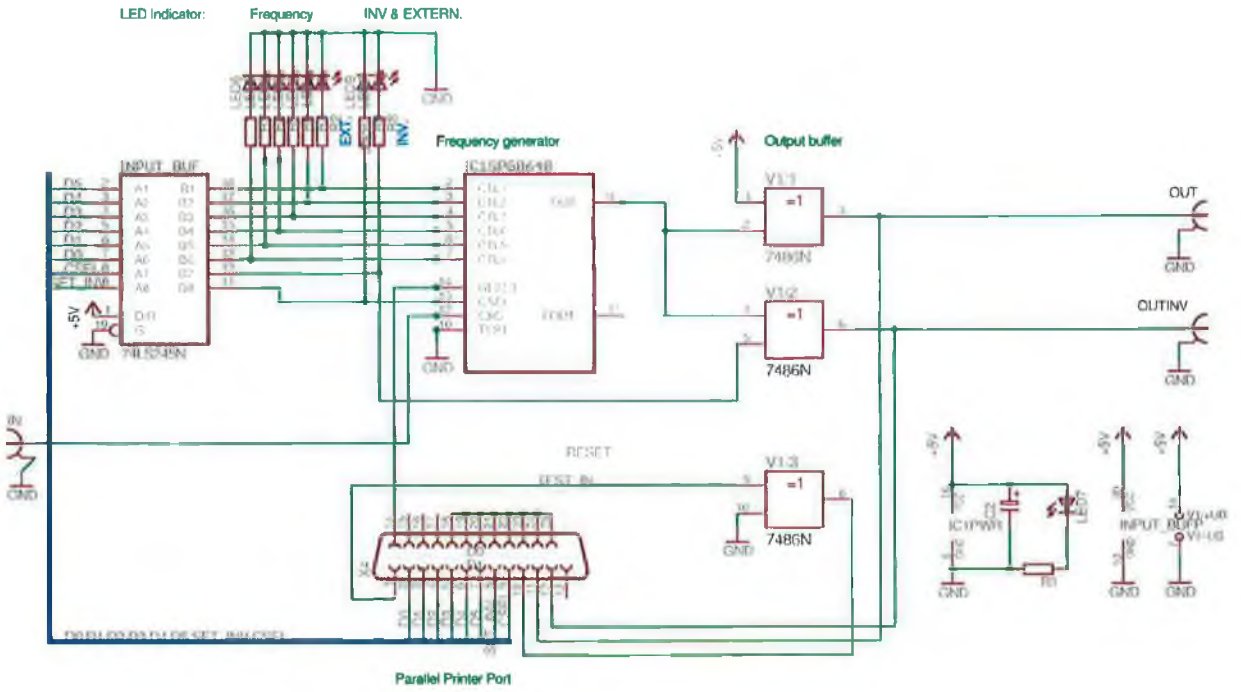

Figure B.1: Schematic diagram of trigger circuit.

Through the input buffer (74LS254), the six control bits are connected to the SPG8640

Set terminal		CTL4	0	0	0	0	1	1	1	1
		CTL5	0	0	1	1	0	0	1	1
CTL1	CTL2	CTL3/6	0	1	0	1	0	1	0	1
0	0	0	1M	100k	10k	1k	100	10	1	1/10
0	0	1	100k	10k	1k	100	10	1	1/10	1/100
0	1	0	500k	50k	5k	500	50	5	1/2	1/20
0	1	1	333.3k	33.3k	3.3k	333.3	33.3	3.33	1/3	1/30
1	0	0	250k	25k	2.5k	250	25	2.5	1/4	1/40
1	0	1	200k	20k	2k	200	20	2	1/5	1/50
1	1	0	166.6k	16.6k	1.6k	166.6	16.6	1.6	1/6	1/60
1	1	1	83.3k	8.3k	833.3	83.3	8.3	0.83	1/12	1/120

Table B.1: Possible output frequencies in Hz [1].

and the state of each bit is indicated by a set of LEDs on the side panel of the box. The SPG8640 circuit is an oscillator with a programmable divider. Through the CSEL, the oscillator or external source of frequency can be selected and the circuit serves as a divider only.

The output is connected to the two XOR gates which serve as external buffers. One of them facilitates the inversion of the output INVOUT, against the primary output, OUT.

In order to test the circuit connection, the remaining XOR gate is used as a feedback and inverts one bit, which can be read back to PC. If unexpected data are read, this means that the box is not connected, or that the power is disconnected. The circuit is powered by a 5V DC power supply.

A simple library in C++ (PPort.cpp) was written to control this circuit from a PC. It can test the connection, set the desired frequency according to the Table B.1, or set the outputs (OUT, INVOUT) constantly to HI or LO. When a alternating output at a particular frequency is selected, the duty cycle is approximately 50%.

B.1 References

[1] Seiko EPSON corporation, "Selectable-output crystal oscilator - SPG series," 2000.

Appendix C

Software

C.1 Data acquisition software – camera and frequency controller

For simple and automated camera control and image acquisition, control software operating in batch mode was designed. The program reads a configuration file (given as a parameter) and follows the instructions given in the configuration file. The instructions can consist of approximately 20 different commands whose full commented list is in the documentation for the `parse_file_avg.cpp`. The configuration file typically describes a sequence of commands for acquisition of the full pressure and temperature scan from 20 different images. Such an operation without user intervention allows for data acquisition to be run repeatedly for identical camera configurations and eliminates operator mistakes.

The first group of commands controls setting of the parameters of the DiCAM Pro camera and the start of the exposure of the image. The second set of command controls the frequency generator described in Appendix B. The program is run on Windows 98 and is written in C++. The commands are internally executed in two classes `cam.cpp` and `Pport.cpp`. The program makes use of the dynamic library, `sen95cam.dll`, supplied with the camera.

Images are stored in the internal 16-bit camera format B16 [1], which is similar to the standard 8-bit BMP format. It contains header information followed by the raw uncompressed image data. Such files can be read by the visual software supplied with the camera, but are not supported in standard image processing programs.

C.2 Data manipulation utilities

For simple manipulation with the B16 image format, a utility for point measurements was written in C++. This utility was tested on a PC running Linux , but can, be in principle, be compiled for Windows computers or other platforms. The program is called `b16tointensity LT_x LT_y RB_x RB_y *.b16` and extracts intensity information from all B16 files in the current directory. The first four parameters determine the region of interest (ROI) followed by a list of files to be processed. The average intensity of the area determined by the ROI is printed to the standard output. This is very useful for single-point measurements.

C.3 Matlab functions

A large amount of data processing was carried out in Matlab R12, in which the functions for import and export of B16 images were written. The function `read_b16(filename)` returns three matrices, the first containing raw pixel values, the second and third containing the dimensions of the image. The export function `write_b16(image,filename)` writes the image to the file `filename.b16`.

Previous functions can be used as part of complex data manipulation Matlab scripts (M-files). They are also used in a simple image browser whose outputs are presented in Chapter 6. The image browser can be accessed from within a Matlab program under `idisp(image)` function. The advantage of using Matlab for these scripts is the embedded cross-platform nature of the resulting programs (they run on all platforms where Matlab is available).

All the software mentioned here is freely available on Internet at `http://www.osl.dcu.ie/people/Honza/PSP/`.

C.4 References

[1] PCO, *DiCAM Pro - User manual.* PCO AG, Germany, 2000.

Index